Regulation of TLR-induced macrophage responses by cytoskeleton-associated phosphoproteins

Regulation der Antwort von Makrophagen auf TLR-Stimulation durch Zytoskelett-assoziierte Phosphoproteine

Dissertation zur Erlangung des

naturwissenschaftlichen Doktorgrades

der Julius-Maximilians-Universität Würzburg

vorgelegt von

Jens Wenzel

aus Sömmerda

Würzburg 2014

Eingereicht am: .....

Mitglieder der Promotionskommission:

Vorsitzender: .....

Gutachter : Prof. Dr. Roland Lang

Gutachter: Prof. Dr. Thomas Rudel

Tag des Promotionskolloquiums: .....

Doktorurkunde ausgehändigt am: .....

Table of content

Index of Figures

Index of Tables

Abbreviations

cursive / italic	gene symbols
capital letters	proteins

^{3}H	Tritium
ACTR3 (ARP3)	ARP3 actin-related protein 3, *Actr3*
ADP	Adenosine diphosphate
APC	Antigen presenting cell
APF	Actin polymerization factor
ARF	ADP-ribosylation factor, *Arf*
ATP	Adenosine triphosphate
BM	Bone marrow
BM2	Cell line
BMM	Bone marrow derived macrophages
C3bi	Complement receptor type 3
CaM	Calmodulin
cAMP	Cyclic adenosine monophosphate
CAPZB	Capping protein (actin filament) muscle Z-line, beta, *Capzb*
CARMIL	Leucine-rich repeat-containing protein, *carmil* (*Dictyostelium)*
CCL2 (MCP1)	Chemokine (C-C motif) ligand 2 or monocyte chemotactic protein-1, *Ccl2*
CCL3	Chemokine (C-C motif) ligand 3
CCL4	Chemokine (C-C motif) ligand 4
CD	Cluster of differentiation
CDC42	cell division cycle 42 protein, *Cdc42*
CIITa	Class II, major histocompatibility complex, transactivator, *Ciita*
CLIP-170	Cytoplasmic linker protein-170
CLRs	C-type lectin receptor
CORO1b	Coronin, actin binding protein 1B, *Coro1b*
CpG	CpG oligonucleotides
Cre	Cyclization recombination
CXCL12	Chemokine (C-X-C motif) ligand 12, *Cxcl12*
CytoD	Cytochalasin D

DAPI	4′,6-diamidin-2-phenylindol
DC	Dendritic cell
DD	Death domain
DNA	Deoxyribonucleic acid
dsRNA	Double-stranded RNA
DUSP	Dual specificity phosphatase
ECM	Extracellular matrix
EPS8	Epidermal growth factor receptor pathway substrate 8, *Eps8*
ERK 1/2	Extracellular-signal-regulated kinases 1/2, *Mapk2/Mapk3*
FACS	Fluorescence activated cell sorting
FAK	Focal adhesion kinase
FBS	Fetal bovine serum
FHOD1	Formin homology 2 domain containing 1, *Fhod1*
flox	Flanked by loxP
*f*MLP	N-formyl-methionine-leucine-phenylalanine
FMN1	Formin 1, *Fmn1*
GM-CSF	Granulocyte macrophage colony-stimulating factor,*Csf2*
GSK3	Glycogen synthase kinase 3, *Gsk3*
GTP	Guanosine triphosphate
GTPase	Guanosine triphosphate hydrolase enzyme
i.p.	Intra peritoneal
ICAM-1	Intercellular adhesion molecule 1, *Icam1*
IFNγ	Interferon gamma
IL	Interleukin
IQ	Isoleucine/glutamine motifs
IRAK-4	Interleukin-1 receptor-associated kinase 4, *Irak4*
IκB	Inhibitor of κB
KD	Knockdown
kDa	Kilo dalton
KO	Knockout
KSR	kinase suppressor of ras, *Ksr*
LBP	Lipopolysaccharide binding protein, *Lbp*
LFA-1	Lymphocyte function-associated antigen 1
LPS	Lipopolysaccharide

LRR	Leucin-rich repeat motifs
LSP1	Lymphocyte specific 1, *Lsp1*
LTA	Lipoteichoic acid from Gram positive bacteria
Mac-1	Macrophage-1 antigen
MAPK	Mitogen-activated protein kinase
MCP1 (CCL2)	Chemokine (C-C motif) ligand 2 or monocyte chemotactic protein-1, *Ccl2*
M-CSF	Macrophage colony-stimulating factor, *Csf1*
MD-2	Lymphocyte antigen 96, *Ly96*
MEK1	Mitogen-activated protein kinase kinase 1, *Map2k1*
MFI	Mean fluorescence intensity
MK2	MAP kinase-activated protein kinase 2, *Mapkapk2*
MMP-9	Matrix metalloproteinase-9
MØ	Macrophage
MSN	Moesin, *Msn*
MTSS1	Metastasis suppressor 1, *Mtss1*
Mx	Promoter for interferon-induced protein Mx (Myxovirus resistant)
MYD88	Myeloid differentiation primary-response protein 88, *Myd88*
MYO1e	Myosin IE, *Myo1e*
MYO1f	Myosin IF, *Myo1e*
MYO9b	Myosin IXb, *Myo9b*
NF-κB	Nuclear factor kappa-light-chain-enhancer of activated B cells
NK cells	Natural killer cells
NLR	Nucleotide-binding domain and leucine-rich repeat containing receptor NOD-like receptor
NPF	Nucleation-promoting factor
nsRNA	Non-silencing RNA (control siRNA)
N-WASP	neuronal Wiskott–Aldrich Syndrome protein
OVA	Ovalbumin
p38	p38 mitogen-activated protein kinases, *Mapk14*
PAK1	p21 protein (Cdc42/Rac)-activated kinase 1, *Pak1*
PAMP	Pathogen-associated molecular pattern
PCIP	Pentachloropseudilin
PDGF	Platelet-derived growth factor

PH	Pleckstrin homology domain
Pi	Inorganic phosphate
PI3K	Phosphatidylinositol-4,5-bisphosphate 3-kinase, *Pik3*
PIP_2	Phosphatidylinositol 4,5-bisphosphate
PIP_3	Phosphatidylinositol (3,4,5)-triphosphate
PMA	phorbol 12-myristate 13-acetate
poly I:C	Polyinosinic:polycytidylic acid
PP2	Kinase inhibitor, used as a Src-selective inhibitor
PRR	Pattern-recognition receptor
PXN	Paxillin, *Pxn*
PYK2	Proline-rich tyrosine kinase 2, *Pyk2*
qRT-PCR	Quantitative real-time polymerase chain reaction
RAC	GTPase subfamily
RAPL	GTPase subfamily
RAS	GTPase subfamily
RHO	GTPase subfamily
RLR	Retinoic acid inducible gene I (Rig-I)-like receptor
ROS	Reactive oxygen species
SH3	SRC homology 3 domain
siRNA	Small interfering RNA
SN	supernatant
SRC	Tyrosine kinase (cellular / sarcoma)
ssRNA	Single stranded RNA
TAK1	Tansforming growth factor-β-activated kinase 1
TCR	T-cell receptor
TH1	Tail homology domain 1
TH2	Tail homology domain 2
TIR	Intracellular Toll/IL-1R homology (TIR) domain
TLR	Toll-like receptor
TNF	tumor necrosis factor
TPA	12-*O*-Tetradecanoylphorbol-13-acetate
TRAF6	Tumor-necrosis factor (TNF)-receptor-associated factor 6
TRIF	TIR-domain-containing adapter-inducing interferon-β
WASP	Wiskott-Aldrich syndrome protein

WAVE	WASp and verprolin homologous protein
WB	Western blot
WIP	Wiskott-Aldrich syndrome protein interacting protein, *Waspip*
WIRE	WIP-related protein
WT	Wild type

Summary

Toll-like receptors (TLR) are pattern recognition receptors (PRR) by which macrophages (MØ) sense pathogen-associated molecular patterns (PAMPs). The recognition of lipopolysaccharide (LPS), the PAMP of gram negative bacteria, by TLR4 triggers signaling cascades and leads to the pro-inflammatory activation of the cells. A recent quantitative and kinetic analysis of the phosphoproteome of LPS-activated primary macrophages highlighted the cytoskeleton as a cell compartment with an enriched protein phosphorylation. In total 44 cytoskeleton-associated proteins were regulated by this post-translational modification and thus might be involved in the control and regulation of key macrophage functions like spreading, motility and phagocytosis.

To investigate the control of cytoskeleton-associated cell functions by TLR4 activation, we first developed a method to quantitatively measure the spreading response of bone marrow MØ after stimulation with LPS. Fluorescence microscopy was used for cell imaging and visualisation of the MØ contact area. In collaboration with the Fraunhofer Institute Erlangen, we developed and validated a software tool for the semi-automated segmentation and quantitation of MØ fluorescence microscopy data, which allowed fast, robust and objective image analysis. Using this method, we observed that LPS caused time-dependent spreading, which was detectable after 1-2 h and maximal after 24 h. Next, the impact of genetic or pharmacological inhibition of known TLR signaling components was investigated. Deficiency in the adapter protein MYD88 strongly reduced spreading activity at the late time points, but had no impact early after LPS-stimulation. A similar effect was observed upon pharmacological inhibition of ERK1/2 signaling, indicating that ERK1/2 mediates MYD88-dependent MØ spreading. In contrast, MØ lacking the MAPK p38 were impaired in the initial spreading response but responded normally 8-24 h after stimulation. The genetic deletion of the MAPK phosphatases DUSP1 and DUSP16 resulted in impaired late spreading, corroborating the essential role for functional MAPK signaling in TLR4-driven MØ spreading.

To identify the contribution of other cytoskeletal phosphoproteins to MØ spreading, siRNA knockdown of selected candidate genes in primary murine MØ was employed and combined with automated quantitative image analysis. These experiments revealed a functional role for the Myosins MYO1e and MYO1f in MØ spreading. These motor proteins are strongly phosphorylated in LPS-activated MØ. Because of their ability to simultaneously bind to actin filaments and cell membrane or other proteins, we investigated their role in phagocytosis,

cytokine production and antigen presentation. Phagocytosis and killing of bacteria were not affected in *Myo1e-/-* macrophages. However, MYO1e plays a role in chemokine secretion and antigen presentation processes. MCP1 (CCL2) release was selectively increased in *Myo1e*-deficient MØ and dendritic cells (DC), while cytokine secretion was unaffected. Furthermore, macrophages and DCs lacking MYO1e showed lower levels of MHC-II on the cell surface. However, mRNA levels of CCL2 and of MHC-II were unaltered. These data suggest a role for MYO1e in the transport of selected chemokines and of MHC-II molecules to the cell surface. MHC-II-restricted antigen presentation assays revealed an impaired capacity of macrophages and DC lacking MYO1e to stimulate antigen-specific T cells, suggesting that the reduced MHC-II expression is functionally relevant.

Taken together, in this study first a quantitative image analysis method was developed which allows the unbiased, robust and efficient investigation of the macrophage spreading response. Combination of this method with siRNA knockdown of selected cytoskeleton-associated phosphoproteins led to the identification of MYO1e and MYO1f as regulators of macrophage spreading. Furthermore, we identified MYO1e in MØ and DC to be essential for the intracellular transport of CCL2 and MHC-II to the cell surface and for optimal stimulation of antigen-specific CD4 T cells.

Zusammenfassung

Toll-like Rezeptoren (TLR) sind Mustererkennungsrezeptoren (PRR) durch die Makrophagen (MØ) pathogen-assoziierte molekulare Muster (PAMPs) erkennen. Die Erkennung von Lipopolysacchariden (LPS), dem PAMP gramnegativer Bakterien, durch TLR4 löst Signalkaskaden aus, die zu einer pro-inflammatorischen Aktivierung der Zellen führen. Eine quantitative und kinetische Analyse des Phosphoproteoms LPS-aktivierter primärer Makrophagen identifizierte das Zytoskelett als ein Zellkompartiment mit gesteigerter Proteinphosphorylierung. Insgesamt wurden 44 Zytoskelett-assoziierte Proteine identifiziert, die durch diese post-translationale Modifikation reguliert wurden und demzufolge an der Regulation wichtiger Zellfunktionen von Makrophagen wie Spreading, Motilität und Phagozytose beteiligt sein könnten.

Um die Kontrolle Zytoskelett-vermittelter Zellfunktionen nach TLR4 Aktivierung zu untersuchen, entwickelten wir zunächst eine Methode zur quantitativen Messung der Spreadingantwort von Knochenmarksmakrophagen nach LPS Stimulation. Die Visualisierung der Zellen sowie ihrer Kontaktfläche erfolgte hierbei mittels Fluoreszenzmikroskopie. Für eine schnelle, robuste und objektive Analyse der Fluoreszenzaufnahmen entwickelten und validierten wir in Kollaboration mit dem Fraunhofer Institut in Erlangen eine Software zur halbautomatischen Segmentierung und Quantifizierung der Kontaktfläche. Unter Verwendung dieser Methode konnte eine zeitabhängige LPS-induzierte Zunahme der Zellkontaktfläche beobachtet werden, die nach 1-2 Stunden detektierbar war und ein Maximum nach 24 Stunden erreichte. Durch den Einsatz pharmakologischer Inhibitoren sowie genetisch veränderter Zellen wurde anschließend der Einfluss bekannter TLR4-Signalwegkomponenten untersucht. Die genetische Defizienz des Adapterproteins MYD88 führte hierbei zu einer stark reduzierten Spreadingaktivität der Zellen während der späten LPS Stimulationsphase, wohingegen das initiale Spreading nicht beeinflusst wurde. Ein vergleichbarer Effekt konnte unter Verwendung eines pharmakologischen Inhibitors zur Hemmung des ERK1/2 Signalweges identifiziert werden. Diese Beobachtungen deuten darauf hin, dass ERK1/2 für die Weiterleitung des MYD88 vermittelten Spreading notwendig ist. Im Gegensatz dazu wurde in *p38*-defizienten Makrophagen ein beeinträchtigtes initiales Spreading beobachtet, wohingegen das späte Spreading nach 8 – 24 Stunden nicht beeinflusst war. Die genetische Deletion der MAPK Phosphatasen DUSP1 und DUSP16 resultierte ebenfalls in einer Minderung des späten Spreadings, ebenfalls ein Hinweis auf die essentielle Rolle funktioneller MAPK Signalwege.

Um die Beteiligung weiter Zytoskelett-Phosphoproteine am Zellspreading zu identifizieren, wurde die Expression ausgewählter Kandidatengene in primären Makrophagen mittels spezifischer siRNA unterdrückt und das Zellspreading mit Hilfe der entwickelten Software quantifiziert. Diese Versuche zeigten eine funktionelle Rolle der Myosine MYO1e und MYO1f. Diese Motorproteine weisen ebenfalls eine starke Phosphorylierung nach LPS Stimulation auf. Aufgrund ihrer Eigenschaft simultan mit Aktinfilamenten und Zellmembranen sowie anderen Proteinen zu interagieren, untersuchten wir ihre Rolle während der Phagozytose, Zytokinfreisetzung und Antigenpräsentation. Obwohl *Myo1e* defiziente Makrophagen keine Beeinträchtigung der Phagozytose oder Abtötung von Bakterien aufwiesen, spielte das Motorprotein eine wichtige Rolle in der Chemokinfreisetzung und Antigenpräsentation. Interessanterweise war die Sekretion des Chemokins MCP1 (CCL2) in *Myo1e*-defizienten Makrophagen und dendritischen Zellen (DC) selektiv erhöht, während die Zytokinfreisetzung unbeeinträchtigt war. Des Weiteren wiesen *Myo1e* KO Makrophagen und DC eine reduzierte MHC-II Oberflächen-Expression auf, obwohl die MHC-II als auch die CCL2 Transkription auf mRNA Ebene nicht beeinflusst war. Diese Daten legen nahe, dass MYO1e während des Transports bestimmter Chemokine, sowie von MHC-II zur Zelloberfläche eine wichtige Rolle spielt. Zudem zeigten *Myo1e* KO Makrophagen und DC in einem MHC-II-abhängigen Antigenpräsentationsassay eine abgeschwächte Fähigkeit zur Antigen-spezifischen T-Zell Aktivierung, was die funktionelle Relevanz der reduzierten Expression von MHC-II nahelegt.

Zusammenfassend wurde in dieser Studie zunächst eine Methode zur quantitativen Bildanalyse entwickelt, welche eine unvoreingenommene, robuste und effiziente Untersuchung des Spreadings von Makrophagen erlaubte. Die Kombination dieser Methode mit dem spezifischen siRNA Knockdown ausgewählter Zytoskelett-assoziierter Phosphoproteine führte zur Identifizierung von MYO1e und MYO1f als wichtige Regulatoren dieser Zellfunktion. Darüber hinaus konnte in Makrophagen und DC eine essentielle Rolle für MYO1e im intrazellulären Transport von CCL2 und MHC-II an die Zelloberfläche identifiziert werden, sowie dessen Notwendigkeit für eine vollständige Aktivierung antigen-spezifischer CD4 T Zellen.

1 Introduction

1.1 The immune system

The immune system is a complex, sensible and well-rehearsed system developed during evolution to protect multicellular organisms from infection with pathogens like bacteria, viruses, parasites or fungi. The first defense line against foreign organisms for instance are the skin and the mucosal surface of the respiratory, gastrointestinal and urogenital tracts [1]. Once the invaders overcome these barriers they are immediately recognized by resident or recruited cells of the innate immune system. This non-specific part of the immune system engage cells like macrophages, dendritic cells, neutrophils, eosinophils, natural killer (NK) cells, basophils, mast cells, gamma/delta (γδ) T-cells and epithelial cells, which are continually disposed to rapidly act against pathogens. Upon activation, innate immune cells mediate the response to prime cells of the adaptive immune system and thereby activate a pathogen specific immunity. This protection is arranged by B- and T-cells which finally induce a spectrum of specific effector mechanisms to eliminate the pathogen [2].

1.2 Macrophages and dendritic cells

Macrophages (MØ) were first recognized and described as “big-eaters” by Ilya Metchnikoff more than 130 years ago [3]. Blood circulating monocytes, which themselves develop from hematopoietic stem cells of the bone marrow are the progenitor cells, competent to differentiate into macrophages. In response to a wide range of stimuli, including chemokines and cytokines, monocytes transmigrate from the blood vessels into the peripheral tissue and differentiate into macrophages [2]. Dependent on the colonized tissue, MØ can differentiate into a specialized phenotype termed as Kupffer cells in the liver, microglia in brain, osteoclasts on bones or alveolar MØ in the lung. In general macrophages serve as scavenger cells by uptake and clearance of apoptotic cells and cell debris or wound healing to maintain tissue homeostasis [4]. Beside their role in homeostasis, they have important functions in immune response. These relatively long-living cells are able to phagocytose and degrade foreign materials like invading pathogens and other macromolecular agents. This process causes a phenotypical switch from the “silent” to the pro-inflammatory state, resulting in the release of cytokines and chemokines to activate surrounding cells, interfere with the threat and induce an adaptive immune response [2].

Dendritic cells (DCs) belong to the myeloid cell linage and originate from hematopoietic progenitor cells. DCs exhibit long dendrite extensions resulting in their nomenclature. Compared to macrophages, DCs also exist in different tissues resulting in phenotypical difference and therefore termed Langerhans cells in the skin or lamina propria DCs in the intestine [4]. Immature DCs migrate through the blood vessels and the tissue, while tacking up pathogenic material and additionally extracellular liquids with their dissolved substances by phagocytosis and macropinocytosis. Their main task in the immune response is the activation of T-lymphocytes after recognition of pathogenic material. Both cell types are essential in the induction and mediation of an inflammation to trigger a successful immune response [2].

1.2.1 Immunological functions of macrophages and DCs

In response to invading pathogens and tissue injury MØ and DCs are necessary to avoid immunopathology and to tissue repair. Both cell types are found under homeostatic condition in several organs and share certain functions such as recognition of pathogens, phagocytosis and antigen presentation via the major histocompatibility complex (MHC) [2, 5]. Upon recognition of infectious material immature DCs and resident tissue macrophages undergo a genetic reprogramming resulting in a change of their activation state and expression of a broad repertoire of anti-microbial agents and functions. Maturated DCs lose their phagocytosis capacity and actively migrate from the tissue to the lymph nodes and the spleen to activate T-cells by antigen presentation. Macrophages switch to a pro-inflammatory “M1” phenotype responsible for a local host defense within the affected tissue [5]. M1-macrophages and mature DCs express several pro-inflammatory cytokines like TNFα, IL-1, IL-6 or IL-12 and chemokines like CCL2, CCL3 or CCL4 which are released for an intercellular communication. Upon biosynthesis, these produced molecules are guided through the cytoplasm towards the cell membrane by a complex trafficking machinery including cytoskeleton structures and are finally released in a controlled manner [6-10]. In response to these secreted mediators, endothelial cells from peripheral vessels become activated resulting in an up-regulation of adhesion molecules and loosening of cell-cell junctions to enable immune cell invasion towards chemokine gradients into the tissue. To initiate tissue infiltration, immune cells attach by integrin binding to the vessel walls and migrate through the endothelium accompanied by morphological changes. Subsequent to transmigration the adherence and spreading of immune cells, facilitated and affected through controlled cytoskeleton dynamics, is essential to accumulate cells at the site of infection. Among a broad

spectrum of immune cells including neutrophils, NK-cells, B- and T-cells also monocytes migrate to the site of infection. Dependent on the cytokine signal the monocytes can further differentiate into tissue macrophages or into DCs. To restore homeostatic tissue conditions MØ and DCs also produce suppressive cytokines and balance the immune response [2]. Anti-inflammatory macrophages, described as "M2" phenotype excessively phagocytose apoptotic neutrophils and secret the cytokines IL-10 and TGF-β [5, 11]. Both molecules are able to down-regulate TNFα, IL-1, IL-6 and MHC expression, thus leading to a reduction in immune response. Aside IL-10 and TGF-β tissue DCs produce pentraxin-3, a protein able to block adhesion molecules on endothelial cells, which prevent further immune cell recruitment into the tissue [5, 12].

1.2.1.1 Phagocytosis and killing of intracellular pathogens

Recognition and binding of pathogens to surface receptors of immature DCs and resident tissue macrophages like Fcγ-, scavenger-, mannose- and glucose- or lipid receptors stimulates an engulfment of the foreign organism. This uptake, called phagocytosis, leads to formation of intracellular vesicles known as phagosomes [2, 13]. The whole internalization process is caused by active deformation of the cell membrane triggered in response to the surface receptor activation. The forces required for this mechanism are produced by the underlying actin cytoskeleton, involving a variety of proteins known from analysis on phagocytes [14, 15]. The maturation of the phagosomes and the subsequent fusion with acidic and protease containing lysosomes form the phagolysosomes, responsible for intracellular pathogens killing [16]. Furthermore, the V-ATPase proton pump lowers the pH to 4-5, toxic substances for instance nitric oxide (NO) are produced by the inducible nitric oxide synthase (iNOS) and reactive oxygen species (ROS) are generated by a membrane associated nicotinamide adenine dinucleotide phosphate (NADPH) oxidase in the cytoplasm and diffuse across the membrane [17]. These mechanisms inhibit bacterial replication and kill most of the pathogens

1.2.1.2 Antigen presentation via MHC-II

An important capability of MØ and DCs to induce an adaptive immune response is the antigen presentation via MHC. Two different classes of this molecule are expressed in vertebrates [2]. While MHC-I is responsible to present antigens (AG) from intracellular origins such as virus, MHC-II expressed by MØ, DCs and B-cells present AG from exogenous origin like bacteria. Antigens presented by MHC-I are recognized by cytotoxic CD8 T-cells, which in turn induce a programmed cell death of the infected cell and thus

mediate cellular immunity to primary combat intracellular pathogens. In contrast, MHC-II-presented antigens are recognized by CD4 helper T-cells to mediate a humoral immunity. B-cells primed by activated T helper cells produce specific antibodies and thus allows an adapted defense against extracellular pathogens [2, 18]. Prior to MHC-II restricted AG-presentation the proteins of phagocytosed pathogens need to be processed into smaller peptides by proteolytical cleavage within the phagolysosomes. Subsequently the peptides are loaded onto MHC-II molecules which in turn are transported by the cytoskeleton machinery to the cell surface and present the AG to CD4 T cells [19]. The AG-loaded MHC-II alone is not sufficient to induce an effective T-cell activation. Thus, a second antigen nonspecific signal is provided by co-stimulatory molecules required to become fully activated T-cells. In addition to MHC-II, these molecules like CD40, CD68 and CD80 are up-regulated on the surface of DCs and MØ in response to their activation [2, 5].

1.3 Recognition of pathogens

Recognition of pathogens occurs via pattern recognition receptors (PRR) expressed on cells of the innate immune system, allows them to discriminate between self and non-self material and if necessary to induce an adequate immune response. These receptors specifically bind to conserved microbial structures described as pathogen associated molecular patterns (PAMP). Dependent on their structure and cellular localization the PRR are classified into different families including transmembrane C-type lectins (CLRs), and Toll-like receptors (TLRs) on the cell surface and cytosolic retinoic acid inducible gene I (Rig-I)-like helicases (RLRs) and nucleotide-binding leucine-rich receptors (NLRs). Interaction of these PRRs with their specific ligands induces an activation of MØ and DCs, resulting in phagocytosis, expression of cytokines and chemokines, antigen presentation and co-stimulatory molecules, cell migration and maturation [2, 20, 21].

1.3.1 TLRs and their ligands

Toll-like receptors (TLRs) are an evolutionary old pattern recognition and signaling system which was first described in development of *Drosophila melanogaster*. Later TLRs were identified to play an important role in immunity in adult flies [22]. Today 10 and 12 functional TLRs are known in human and mice, but only TLR1-9 are conserved in both organisms. However, murine TLR10 is not functional because of a retroviral insertion and human TLR11-13 have been lost from the genome. Each TLR recognizes a specific PAMP

derived from bacteria, virus, parasites and fungi and induces a rapid and massive transcriptional response of the stimulated cell [23]. TLRs are transmembrane receptors which consist of an extracellular domain with leucin-rich repeat motifs (LRR) and an intracellular Toll/IL-1R homology (TIR) domain. The TIR domain is also found in members of IL-1 receptor family like IL-1R, IL-18R and IL-33R and is necessary to recruit intracellular TIR-containing adapter molecules to induce signaling [24, 25]. On the one hand, TLR1, TLR2, TLR4, TLR5, TLR6 and TLR11 are expressed on cell surfaces and mainly recognize microbial membrane components like lipids, lipoproteins and proteins. For instance lipoteichoic acid from Gram positive bacteria (LTA) is bound by a heterodimer of TLR2/6, flagellin of flagellated bacteria is recognized by TLR5 and lipopolysaccharide from Gram negative bacteria (LPS) is bound by a complex of TLR4/CD14/MD-2. On the other hand, TLR3, TLR7, TLR8 and TLR9 are only expressed intracellularly on vesicular structures like endosomes, lysosomes or endolysosomes where they recognize microbial nucleic acids after degradation of the pathogens. TLR9 binds to unmethylated CpG motifs within bacterial and viral DNA while TLR3 interacts with viral dsRNA. In contrast TLR7 and TLR8 become activated in response to viral ssRNA [2, 23, 26].

1.3.2 TLR4-induced intracellular signaling

Activation of TLR4-driven signaling (Fig. 1) requires oligomerization of several proteins including LPS binding protein (LBP), CD14 and MD-2. The soluble shuttle protein LBP directly binds to LPS and facilitates the interaction with CD14. This membrane-anchored protein transfers LPS to TLR4 which interacts with the soluble protein MD-2 [27]. Subsequent to the receptor complex formation and ligand binding, TLR4 dimerizes and undergoes conformational changes on its cytoplasmic TIR domain, required for the recruitment of downstream signaling molecules. An essential adaptor molecule in TLR-mediated signaling pathways is the myeloid differentiation primary-response protein 88 (MYD88). MYD88 contains a C-terminal TIR domain and an N-terminal death domain (DD). TLR4/MYD88 TIR-TIR domain interactions subsequently recruit and activate the DD domain containing IL-1 receptor-associated kinase-4 (IRAK-4). Phosphorylated IRAK4 recruits tumor-necrosis factor (TNF)-receptor-associated factor 6 (TRAF6) followed by the activation of the transforming growth factor-β-activated kinase 1 (TAK1). TAK1 in turn stimulates mitogen-activated protein kinase (MAPK) pathways and mediates the activation of NF-κB and AP-1. The transcription factor NF-kB kept inactive under basal conditions by its inhibitor IκB, is essential to induce a pro-inflammatory immune response through expression of target

genes [2, 24, 27]. In addition to the MYD88-dependent pathways a MYD88-independent signal transduction in MØ and DCs exists. TLR4 engages the TIR-domain-containing adapter-inducing interferon-β (TRIF) pathway to induce MAPK and NF-κB activation as well as IFN-β expression through IRF3 activation. However, both signaling pathways are required for a rapid and full pro-inflammatory immune response to LPS. Experiments with MYD88-deficient mice revealed a reduced and delayed LPS response compared to wild-type mice [26, 28]. Activation of TLR4 finally results in expression of pro-inflammatory cytokines, up-regulation of co-stimulatory molecules and DC maturation [2, 29, 30].

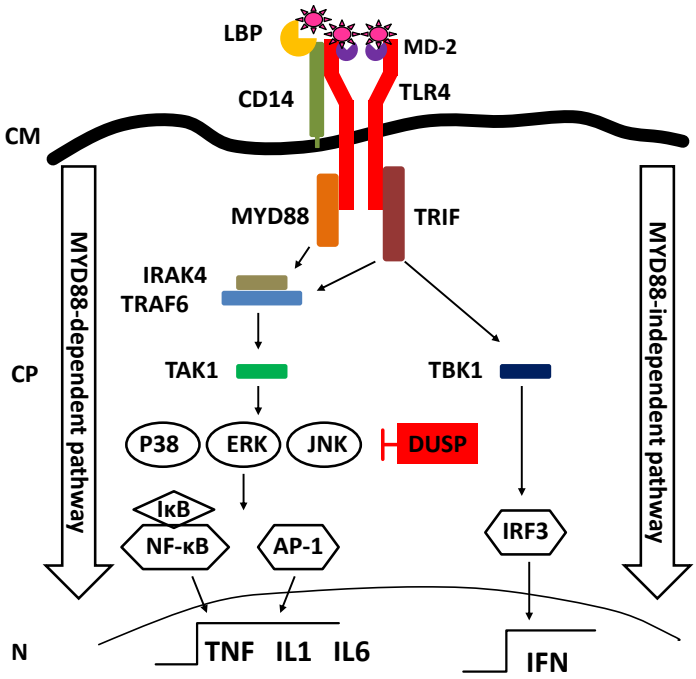

Figure 1. TLR4 signaling. Schematic illustration of intracellular signaling triggered by LPS induced TLR4 activation. For details, see text. Cell membrane (CM), cytoplasm (CP), nucleus (N), TRL4 (red), CD14 (green), LBP (yellow), MD-2 (dark purple), LPS (bright purple), MYD88 (bright brown), TRIF (dark brown), IRAK4 (grey), TRAF6 (bright blue), TAK1 (green), TBK1 (dark blue), MAPKs (oval symbols), NF-κB inhibitor (rhomb), transcription factors (hexagons). Intracellular regulation of MAPK activity by DUSPs (red box) described in chapter 1.3.3.

1.3.3 Regulation of MAPK signaling by dual-specificity phosphatases (DUSP)

A major role in TLR4-driven signal transduction is played by mitogen-activated protein kinases (MAPK) including the extracellular signal-regulated kinase (ERK), c-jun N-terminal or stress-activated protein kinase (JNK) and the p38 group of protein kinases (p38). These serine/threonine kinases are activated through rapid threonine/tyrosine phosphorylation by their upstream kinases. In response to receptor activation MAPKs activate specific substrate proteins, e.g. transcription factors leading to pro-inflammatory gene expression. However, MAPKs are responsible in regulation of many other cell functions like differentiation, proliferation and apoptosis, cell repair, as well as chemotaxis and actin organization [31-33]. To avoid an over-response, MAPK activity has to be controlled and regulated by dephosphorylation of the threonine-X-tyrosine motif. Eukaryotic cells express a variety of

MAKP phosphatases including dual-specificity phosphatases (DUSP) as endogenous regulators (Fig. 1). DUSP MAPK phosphatases possess a MAPK-binding domain mediating selective binding with individual MAPK family members. Interaction of the catalytical DUSP domain with phosphorylated threonine/thyrosine residues on MAPK mediates the dephosphorylation [34]. DUSPs differ in their tissue distribution, substrate specificity, cellular localization and inducibility by extracellular stimuli [35]. One important family member is DUSP1, expressed in response to TLR stimulation through the MYD88-dependent or -independent pathway and additionally enhanced in response to anti-inflammatory IL-10 [36]. Increased expression of DUSP1 leads to a deactivation of MAPK in order p38 > JNK >>ERK and thus decrease the amount of released IL-6 and TNF [37]. DUSP1 knock out (KO) MØ cultured in medium containing 10% fetal bovine serum (FBS) showed defects in spreading and an impaired ERK activation. Furthermore, a reduced MØ migration into the peritoneum was observed after injection of KO mice with thioglycolate [38]. DUSP16, an additional MAPK phosphatase functional in mouse, dephosphorylates JNK and p38 [39], and its stability is controlled by ERK-dependent phosphorylation [40]. Mice lacking DUSP16 died shortly after birth and their bone marrow cells poorly proliferate in response to GM-CSF [41]. Macrophages deficient in DUSP16 produce increased amounts of the pro-inflammatory cytokine TNF and IL-12 [41]. Hence, this MAPK phosphatase plays an important role in myeloid cell differentiation and effector function.

1.4 The cytoskeleton

The cytoskeleton is a system of intracellular filaments with scaffolding properties present in all pro- and eukaryotic cells [42]. This cell organelle together with its specific associated proteins is organized in microtubules, intermediate filaments and microfilaments, which are distributed through the whole cell and differ in their molecular composition and function.

Research on the cytoskeleton revealed its involvement in almost all immune system functions, starting from immune cell maturation, to cell recruitment, inter- and intracellular signaling and transport processes as well as activation triggered by of innate and adaptive immune receptors. Defects in this sensible and complex system can cause immune deficiencies like the Wiskott-Aldrich syndrome (WAS) induced by mutations within the WAS-protein [43, 44]. Furthermore, even bacterial and viral pathogens developed strategies to manipulate the cytoskeleton and subvert immune cells [45-47]. For a better understanding of this complex

system it is essential to further investigate which cytoskeletal processes and components contribute to the control and regulation of immune cell responses.

1.4.1 Microtubules and intermediate filaments

Microtubules are essential cytoskeletal polymers forming hollow tubes with approximately 25 nm in diameter. These structures participate in distribution of organelles during cell division and affect cell shape, motility and other intracellular transport processes. Microtubules are highly dynamic and build by heterodimerization of the small monomers α- and β-tubulin forming the functional α-/β-tubulin [48, 49]. The regulation of the microtubule system occurs by transcription of different tubulin isotypes, folding of α-/β-tubulin heterodimers and post-translational modification of tubulin. The microtubule dynamic is based on binding and hydrolysis of guanosine triphosphate (GTP) by tubulin subunits inducing microtubule assembly and disassembly [48, 50]. From resident peritoneal macrophages it is known that IFNγ/LPS stimulation stabilizes microtubules via the CLIP-170 protein resulting in an enhanced cell spreading and FcγR-mediated phagocytosis [51]. Recent studies on primary bone-marrow macrophages (BMM) revealed the requirement of microtubules in IFNγ/LPS induced matrix metalloproteinase (MMP)-9 secretion. Vesicles loaded with the proteinase were selectively guided through the cell by the motor protein kinesin along stabilized and acetylated microtubules [52]. In the microtubule system the proteins kinesin and dynein are well described essential motors for a directional cargo transport [49, 53].

Intermediate filaments are found in the nucleo- and the cytoplasm of metazoan cells [54]; they are built by fibrous proteins which consist of long, un-interrupted segments forming multistranded coils. This protein family consist of ~65 distinct proteins which assemble in very flexible filaments approximately 10 nm in diameter. Intermediate filaments are the "stress-buffering" elements of the cytoskeleton becoming more viscoelastic under shear stress compared to microtubules and microfilaments, thus they play an important role e.g. in migration processes. [55-57]. The best described proteins of this superfamily are the nuclear lamin, with an important role in nuclear membrane stabilization during mitosis and keratin as well as vimentin [55]. In circulating human $CD4^+$ T-lymphocytes vimentin forms an intracellular cage that provides protection against deformation. Upon activation of the cells by the chemokine C-X-C motif ligand (CXCL)12, the vimentin cage collapses and facilitates transendothelial migration [58]. Furthermore, the expression of vimentin during myeloid cell maturation seems to be important for the differentiation into fully active macrophage-like

cells. Vimentin knockdown experiments with phorbol 12-myristate 13-acetate (PMA) - treated BM2 cells resulted in macrophage-like cells with a suppressed phagocytosis capability and ROS production [59]. In addition to microtubules and intermediate filaments, the actin cytoskeleton is required to complete the function of this complex cell compartment.

1.4.2 Cytoskeleton and actin dynamic

Microfilaments are also known as actin cytoskeleton composed of superfine filamentous actin (F-actin) structures with 7-9 nm in diameter. It builds a dense layer in the cortical region of the cell but is also found distributed in the cytoplasm and even localized within the nucleus [60, 61]. This highly dynamic filament system with its related proteins contributes e.g. in the cell cycle, membrane deformation during endo- and exocytosis, intracellular transport, signal transduction, regulation of cell shape, motility and spreading as well as in chromatin remodeling and gene expression [60, 62-66]. F-actin is build by polymerized monomers of globular actin (G-actin), while its adenosine triphosphate (ATP)-dependent assembling and disassembling is controlled by actin polymerization and depolymerization factors which themselves are regulated by many associated proteins [65, 67, 68]. Actin filaments are highly dynamic structures undergoing constant changes described as dendritic nucleation or treadmill model (Fig. 2). An actin filament can be subdivided in a polymerizing *barbed end* and a depolymerizing *pointed end.* This filament polarity allows a directed elongation of actin filaments inducing e.g. membrane deformations. ATP-bound G-actin is recruited by an activated polymerization factor to a free *barbed end* or already existing actin filament and biochemically linked to initiate filament growth and elongation. To control the direction of filament assembling capping-proteins interact with dispensable filaments and terminate its elongation. Filaments mature by hydrolysis of ATP bound to each actin subunits and are disassembled by depolymerization factors at the *pointed end.* Released ADP-bound G-actin gets subsequently reloaded with ATP by nucleotide exchange factors to be re-used for F-actin assembling. Under steady state conditions these changes occurs slowly but cells can accelerate this process very quickly by activation of various surface receptors in response to extracellular stimuli [64, 65, 68]. The fast reorganization of microfilaments in macrophages within 1-6 min upon LPS stimulation was already described in 1991 [69]. This process as well as the functionality of the actin cytoskeleton is regulated by associated proteins, which are focus of the next chapter.

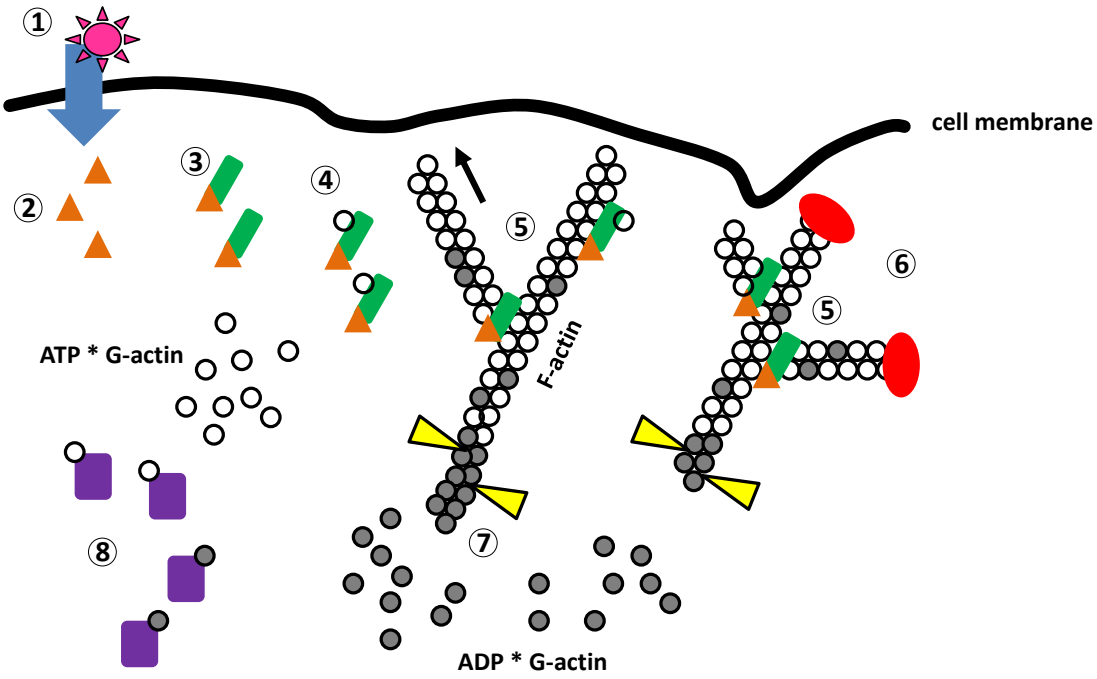

Figure 2. Dendritic nucleation / treadmill model for membrane protrusion. (1) Activation of surface receptor (blue) by extracellular stimuli (purple). **(2)** Recruitment and activation of cytoskeletal signal mediators (orange). **(3)** Interaction of signal mediators (orange) with actin polymerization factors (green) induces **(4)** binding to monomeric ATP coupled G-actin (white circle). **(5)** The activated complex attaches to preexisting filaments and induce a rapid growth at the *barbed end* of the new branch, pushing the membrane forward. **(6)** Capping proteins terminate filament elongation (red). **(7)** Actin filaments age by hydrolysis of ATP bound to each actin subunit (white circles > grey). Actin depolymerization factors (yellow) dissect ADP-actin filaments and facilitate dissociation of ADP-actin (grey circles). **(8)** Nucleotide exchange factors (dark purple) recycles ATP loading of monomeric G-actin (grey circles > white) to provide a new pool of monomeric ATP-actin for F-actin assembling. Modified scheme from Pollard, TD *et al.* Cell 2003 [64]

1.4.2.1 Signal transduction and cytoskeleton-associated proteins

Dynamic and function of the actin cytoskeleton are controlled by a large group of associated proteins. More than 150 are already identified containing actin binding domains [66]. They control the monomer-polymer balance of actin and its organization, which is regulated through a number of co- and post-translational modifications e.g. acetylation, phosphorylation, ubiquitinylation, methylation and oxidation [70-72]. Trigger-induced actin modifications are mediated by cytoskeletal proteins which themselves requires activation in response to extracellular stimuli. One essential mechanism is protein phosphorylation. In a quantitative phosphoproteome analysis of LPS activated primary macrophages our group identified the cytoskeleton as a hotspot of TLR4-induced protein modification. A group of 44 cytoskeletal associated proteins were detected, including e.g. signal mediators like PXN, LSP1, MSN, EPS8; the actin polymerization factor subunit ARP3; the formins FHOD1 and FMN1; the capping protein CAPZB and motor proteins like MYO1e, MYO1f and MYO9b

[30]. These results are supported by investigations on the macrophage cell line J774 [73]. The researchers identified LPS triggered cell motility and assembly of actin filaments leading to the formation of a lamella protrusion and accumulation of phosphorylated actin–regulatory proteins paxillin (PXN) and N-WASP at the leading edge. This whole process was accompanied by a redistribution and transient co-localization of TLR4 and CD14 at the leading lamella where the receptors triggered local enrichment of actin filaments and transient phosphorylation of paxillin on tyrosine 118 and N-WASP on serine 484/485 within 30 min [73]. A comparable actin-dependent receptor clustering is also described in RAW 264.7 cells [74]. The mutual control of TLR4 signaling and the actin cytoskeleton in immune response has become a focus of investigations. Several studies described a cytoskeletal-dependent regulation of the transcription factor NF-κB in response to LPS. In myelomonocytic cell lines and human monocytes the inhibition of actin polymerization through Cytochalasin D (CyotD) induces a significant activation of NF-κB through an IKK-dependent pathway [75, 76]. In J774 cells a TLR4-driven transient phosphorylation of paxillin and N-WASP is followed by phosphorylation of the NF-κB inhibitor IκB on Ser32/35 (30-60 min) mediated by Src kinase [73]. However, CytoD does not affect LPS induced NF-κB activation in murine macrophages, but is critical for a post-translational regulation of iNOS and ROS production [77]. To understand the cause of the events, the identification of responsible signal cascades is essential. Many cytoskeletal signal pathways are regulated by small GTPases of the RHO, RAS, RAC and ARF family in response to TLR4 stimulation [78]. Dynamics in TLR4-induced B-cell polarization and migration are dependent on MYD88 and correlates with enhanced RAC activation, but were independent on ERK1/2 and p38 [79]. In macrophages the RHO GTPases RAC1 and CDC42 contribute to LPS-induced lamellipodia and fillopodia formation and are essential for intracellular TNF trafficking to the membrane [80]. Furthermore, in RAW cells a MYD88-independent TLR4 activation of CDC42 and RAC1 was shown. Stimulation of both kinases was induced through actin polymerization itself, with an important role in phagocytosis [81]. Further studies also link the classical MAPK ERK1/2 and p38 to the regulation of actin cytoskeletal cell functions. In M-CSF-stimulated macrophages the p21-activated kinase (PAK1) affects lamellipodial dynamics by regulating ERK1/2 activity. MØ lacking PAK1 showed an enhanced spreading in response to adherence, forming less stable lamellipodia [82], and in smooth muscle cells p38 is involved in lamellipodia formation [83]. Literature analysis of cytoskeletal phospho-proteins detected in our own study [30] partially linked them to known TLR4-associated signal pathways or rather to important immunological cell functions while their regulation is still unclear. The

actin polymerization factor FHOD1, a formin responsible to build bundled actin structures important in stress fibers and fillopodia formation [84, 85], was described to specifically interact with RAF-1 and ERK but not with p38 and JNK [86]. The phosphorylation of FHOD1 on C-terminal residues S1131, S1137 and T1141 in endothelial cells is necessary for stress fiber formation [87]. The best described actin polymerization factor ARP2/3, a multi protein complex composed of seven subunits including ARP2, ARP3 and ARPC1-5 is responsible for formation of actin filament branches, and is regulated through interaction with nucleation-promoting factors (NPFs) of the WASP and WAVE family [88]. In *Drosophila* and *Dictyostelium* cells binding of NPFs to ARP2/3 is not sufficient for its activation. Mass spectrometry analysis and experiments with ARP2 phospho-mutant constructs identified an important role of ARP2 phosphorylation on Y200 and T235/6 in membrane protrusion and cAMP chemotaxis [89, 90]. Furthermore, ARP2/3 is indirectly regulated by ERK through the activation of the NPF WAVE2 by this MAPK in human epithelial cells [91]. In addition, the phosphosite S77 within the ARPC5 subunit in human neutrophils was identified as a p38-mediated MK2 substrate [92]. An additional example is LSP1, the lymphocyte-specific protein 1 expressed in human and murine myeloid and lymphoid cell lines [93]. The signal transducer with actin binding capacity was shown to be a substrate of p38/MK2 in human neutrophils [94]. Furthermore, LSP1 was identified to target MAPK scaffold proteins KSR, MEK1 and ERK2 to the actin cytoskeleton [95].

Interestingly, 18 of 44 LPS regulated cytoskeletal phosphoproteins detected in our own phosphoproteome analysis contain phosphorylation sites with a MAPK sequence motif (Tab.1), identifying them as probable kinase substrates regulated by these essential pathways. Literature knowledge in combination with our results highlights the essential role of cytoskeletal reorganization as well as a mutual control of TLR4-induced signaling.

Cytoskeletal phosphoproteins containing MAPK substrate motifs
Add1 (Alpha-adducin 1)
Epb4.1/1 (erythrocyte protein band 4.1- protein 1)
Fhod1 (formin homology 2 domain containing protein 1)
Flna (Filamin-A)
Frmd4b (FERM domain containing protein 4B)
Hdac6 (Histone deacetylase 6)
Lima1 (LIM domain and actin-binding protein 1)
Lsp1 (Lymphocyte specific protein 1)
Marcks (Myristoylated alanine-rich C-kinase substrate)
Mkl1 (megakaryoblastic leukemia/myocardin-like 1)
Mprip (Myosin phosphatases Rho interacting protein)
Mtss1 (Metastasis suppressor 1)
Myo9b (Myosin-9b)
Plec1 (Plectin-1)
Pxn (Paxillin)
Snta1 (Alpha-1-syntrophin)
Spnb2 (Spectrin beta 2)
Svil (Supervillin)

Table 1. Cytoskeletal phosphoproteins with MAPK substrate motifs. Cytoskeletal phosphoproteins with LPS-induced phosphorylation of one or more sites within a MAPK substrate motifs, detected in phosphoproteome analysis of primary macrophages [30].

1.4.3 Myosins

Myosins are actin-based motor proteins functional in cell migration and adhesion, signal transduction, membrane traffic, vesicle transport as well as protein, RNA and organelle localization [96, 97]. Phylogenetic analysis of these molecular motors from different organisms divided this superfamily into 35 classes [98, 99]. These molecules can heterodimerize through interaction of one or two heavy chains and a variable number of light chains, resulting in formation of two-headed or single-headed motors [96, 98]. The heavy

chain can be divided in the motor, the neck and the tail domains. The neck domain consists of a isoleucine/glutamine (IQ) motifs, allows binding of light chains and functions as lever arm which enables motor domain movement [96, 98, 100]. Myosin light chains play an important role in the regulation of ATPase and contractile activity of the motor protein [101]. They are controlled by phosphorylation through myosin light chain phosphates [102] and Ca^{2+} dependent interaction with calmodulin [103, 104]. The myosin tail harbors domains responsible for interaction with proteins, membranes or other cargos (Fig. 3a). The motor domain allows attachment and detachment to actin filaments through binding and hydrolysis of ATP, resulting in a movement along actin tracks and production of mechanical forces through conformational changes (Fig. 3b). Differences in motor properties of myosins define their specific intracellular function. Important characteristics are the force which is produced during an ATPase cycle as well as the velocity and direction of the movement along actin filaments [96]. A further critical aspect is the duty ratio of these molecular motors. It is defined as the fraction of the ATPase cycle that a motor spends strongly attached to a filament, resulting in low-duty-ratio or high-duty-ration classification. The main factors controlling the kinetic of the ATPase cycle is the rate of inorganic phosphate (Pi) or ADP release [105, 106] (Fig. 3c). Myosins with high-duty-ratio, called processive motors, are thought to act as effective cargo transporters because of the minimal risk of detaching and falling off the actin track. In contrast, low-duty-ratio motors are presumably better to induce rapid contraction or participate in signal transduction [96, 99, 106]. The direction of myosin movement is given by the structure of actin filaments resulting in the discrimination as plus-end-directed (towards the *barbed end*) or minus-end-directed (towards the *pointed end*) motor [96].

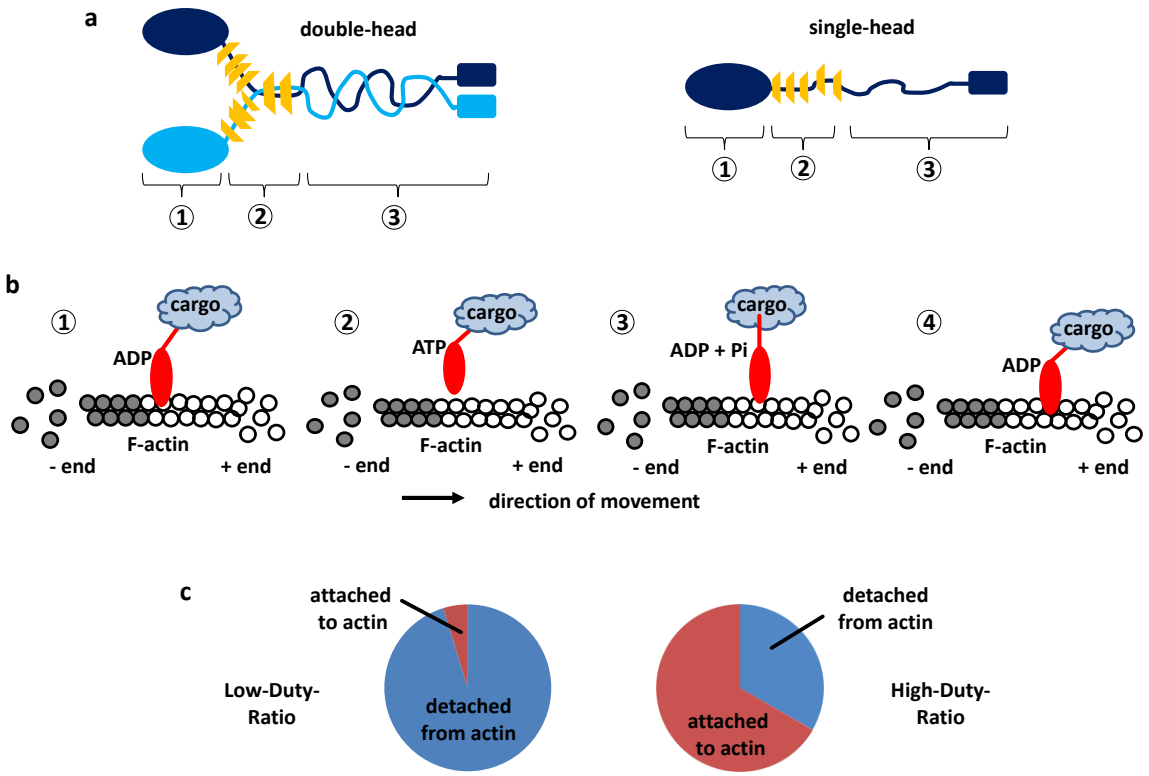

Figure 3. Scheme of myosin structure and actin-based movement. (a) Illustration of single- and double-head myosin built by heterodimerization of two heavy chains (blue) with its distinct domains. (1) Head- or motor-domain containing actin- and nucleotide-binding-pocket. (2) Neck region with bound light chains (yellow). (3) Tail region with cargo binding domain (square). **(b)** Directed movement of myosin along actin filament by hydrolysis of ATP (1-4 ATPase cycle). (1) ADP bound myosin is coupled to actin filament. (2) Binding of ATP leads to dissociation from actin polymer. (3) Hydrolysis of ATP into ADP + Pi induce a +end directed conformational change of the myosin. (4) Dissociation of Pi is followed by myosin head binding to a new filament site and rearrangement of the initial conformation. Repetition of ATPase cycle can occur. **(c)** Duty ratio is a measure how long a myosin is attached to actin filaments during an ATPase cycle. Useful to estimate myosin function and mechanism. *Duty ratio* = $time_{on}/(time_{on}+time_{off})$ [99, 105, 106].

1.4.3.1 Class I myosins

Class I myosins (MYO1) are monomeric and single-headed myosins expressed in many species from yeast to human, in a molecular weight range of 110-130 kDa [107]. In humans and mice this myosin class is represented by eight members MYO1a-h, subdivided with regard to differences in the tail domain. They all share the common myosin structure expressing an N-terminal motor domain, the neck domain containing several regulatory light chain binding sites and the C-terminal tail domain. The tail regions comprise tail homology (TH)1 domains responsible for membrane interaction and a pleckstrin homology (PH) domain which is a putative lipid-binding motif. MYO1e and MYO1f are termed ‘long-tail’ myosins according to the expression of an additional TH2 and SRC homology (SH)3 domain (Fig.4) TH2 mediates an ATP independent actin interaction and SH3 a direct interaction with other

proteins [99, 108]. The functional activity and subcellular localization of the proteins depends on the regulation of these domains. Related investigations have been mainly done in lower eukaryotes like yeasts, *Acanthamoeba*, *Dictyostelium*, or *Aspergillus*. Here, ATPase activity of the motor region is stimulated through a kinase induced phosphorylation of conserved phospho-sites within the catalytic myosin I heads, called 'TEDS rule' (threonine or serine, aspartyl or glutamyl residues). Higher eukaryotes do not require TEDS phosphorylation because they have a negatively charged aspartate or a glutamate at this site, which seems to be important for the activity of this region [103, 109]. In addition to heavy chain phosphorylation, the change in Mg^{2+} ion concentration regulates MYO1 motor activity [110]. IQ motifs of the neck region have a higher affinity to Ca^{2+} free calmodulin (CaM), assumed to have a function in controlling the length of the myosin lever arm and regulation of the power stroke. Interaction with Ca^{2+} bound calmodulin inhibits myosin 1 kinase activity and seems to prevent lever arm movement [103, 104, 111, 112]. The tail region with its binding domains is responsible for the subcelluar distribution and function of the respective MYO1 [103].

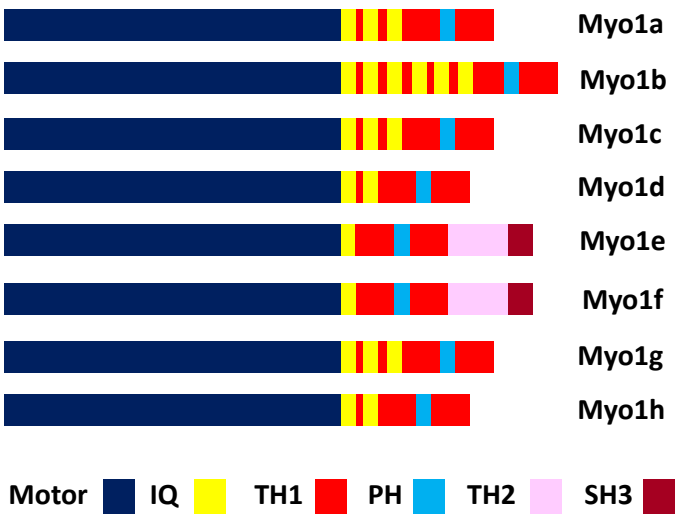

Figure 4 Schematic overview of the class I myosin family with respective domain structure. Based on tail domain comparison this group is subdivided into 8 members. MYO1e and f are called 'long-tailed' myosins regarding the expression of an additional TH2 and SH3 domain. The other members termed 'short-tail' myosins. The N-terminal motor domain (blue) is followed by the neck-region containing 1-6 regulatory CaM light chain binding sites (yellow) and ending in the C-terminal tail domain (red). Modified scheme from McConnell *et al.* Trends Cell Biol 2010 [99].

These myosins are described as membrane – cytoskeleton crosslinkers and thus may contribute in the control of plasma membrane tension, vesicle shedding and transport as well as endo- and exocytosis [99]. The role of this myosin class in vertebrate cells, especially immune cells, has moved into the focus of research. In macrophages, phagocytosis of foreign material is a very important mechanism which depends on cytoskeletal rearrangements. A recruitment of MYO1c in primary MØ [113] and MYO1g in J774 cells was observed in Fcγ-receptor mediated phagocytosis. The recruitment of MYO1g to the phagocytic cup and even

the whole engulfment process downstream of Fcγ-receptor was dependent on its PH domain [114].

In B-cells MYO1c is necessary for cell spreading and also accumulates within the immunological synapse. Cells lacking MYO1c lost the ability to cluster MHC-II molecules on their surface resulting in an impaired T-cell activation [115, 116]. Furthermore, MYO1g was shown to regulate B-cell migration, endo- and exocytosis as well as cytoskeletal plasticity [116, 117].

1.4.3.2 Myosin1e and Myosin1f

MYO1e and MYO1f are termed 'long-tailed' myosins because of the expression of an additional C-terminal TH2 and SH3 domain. Sequence alignments of both proteins show a 71% homology on amino acid level, and a strikingly high sequence analogy of 94-96% between mice and human species. Both myosins are differently expressed in cells of the innate and adaptive immune system. While MYO1f is predominantly expressed in immune cells, MYO1e can be found ubiquitously [98, 118]. Long-tailed myosins are plus-end directed, low-duty ratio motor molecules which accumulate in actin rich regions, mainly known from investigations of their homologues in lower eukaryotes [106, 109, 119]. They are able to crosslink actin filaments via their TH2 domain, and even an interaction with microtubules by TH1-TH2 domain binding was observed [109, 120]. In vertebrate cells the TH2 domain is important for myosin1 recruitment to endocytic structures [121, 122]. In rat liver cells, an auto-inhibition of the long-tailed myosin I (MYR3) by its own tail domain and by Ca^{2+} binding to its light chain calmodulin is described. Experiments with MYR3 tail domain mutant constructs revealed an intramolecular self binding of the SH3 domain to prolin-rich motifs present in MYR3 and thereby inhibit the ATPase activity [120].

First immunologically relevant observations for MYO1f were obtained from neutrophils lacking this long-tailed myosin. The cells exhibited a reduced motility and increased adhesion to fibronection and ICAM-1, resulting from an enhanced exocytosis of β2-integrin (CD18) containing granules. Localization of MYO1f in the cortical region of neutrophils was observed by fluorescence microscopy [118]. Experiments with a human neutrophils cell line (HL-60) revealed a PIP_3-mediated MYO1f recruitment to the plasma membrane in response to chemoattractant *f*MLP. Substitution of the positively charged lysine (position 770) and arginine (position 780) residues to alanine within the TH1 domain prevented the PIP_3 binding and the MYO1f recruitment [123]. Comparable results were obtained from experiments with human T-lymphocyte cell lines (Jurkat cells) were MYO1f also localized at the plasma

membrane [124]. These results suggest a possible role for long-tailed myosins in exocytosis processes. The closely related MYO1e was found to interact via its SH3 domain with the prolin-rich proteins dynamin and synaptojanin-1, known for their contribution in clathrin-mediated endocytosis. However, removal of the TH1 and TH2 domain suppressed localization to clathrin-coated vesicles indicated that the interaction of the SH3 domain alone was not sufficient [121]. Further investigations identified an additional nonspecific electrostatic interaction of the MYO1e tail with vesicles containing negatively charged phospholipids and thus confirmed a contribution of long-tailed myosins in endocytosis [125, 126]. An important role of MYO1e in regulation of granules exocytosis was detected by experiments with *Xenopus oocytes*. Here, the localization of MYO1e to the surface of lectin-containing granules in the cortex of PMA treated cells was observed. Interfering with either overexpression or inhibition of MYO1e influenced the lectin secretion [127-129]. Furthermore, recent studies on fibroblasts provide evidence for a role of MYO1e in coordination of actin assembly during clathrin-mediated endocytosis. It was shown that MYO1e interacts via its SH3 domain with actin-regulatory and -binding proteins WIP/WIRE and N-WASP and target them to the endocytic site for ARP2/3 complex activation and formation of vesicles [122]. Gupta and co-workers could show an active movement of MYO1e to the tips of active lamellipodia as well as a SH3 domain dependent co-localization with CARMIL, FHOD1, ARP3 and β3-integrins. Deletion of SH3 resulted in a decreased stable adhesion of the cells [130]. The knowledge about the regulation and functionality of MYO1e in primary immune cells is more limited. The class I myosin seems to be important during B-lymphocyte development and is expressed as one target of the Bruton's tyrosine kinase (Btk) during differentiation [131]. In human DCs MYO1e was shown to control movement of MHC-II vesicles along actin filaments. Here the MHC-II transport was regulated by the GTPase ARF7 which interacts with MYO1e via its effector protein ARF7EP [19, 132]. Furthermore, MYO1e was also found to be expressed in podocytes of the kidney where it plays an important role in the formation of cell-cell junctions and is crucial for the filter function of the blood-urine barrier [133-135].

1.4.4 Integrins

Integrins are important molecules responsible to link the extracellular matrix (ECM) to the actin cytoskeleton and transmit biochemical signals across the cell membrane [136]. These transmembrane receptors are essential for cell attachment, spreading, phagocytosis, signal transduction, cell-cell interaction, cell shape, motility and regulation of actin dynamics. Each integrin is build by a non-covalent heterodimerization of a α- and β-subunit. 8 α-subunit and 8

β-subunit are known in vertebrates characterized to form 24 different integrins partially specific or redundant in their ligand interaction [137]. Not all of these molecules are constitutively active and thus require an activation by an inside-out signaling mediated in response to other receptors e.g. chemokine receptors, T- or- B-cell receptors or activation of TLRs. The activation by an inside-out signal leads to a conformational change of the integrin and allows binding to extracellular ligand. In contrast the ligand binding generates an outside-in signal of the integrin which in turn induces intracellular signal cascades to regulate required cell functions [138]. An important β_2-subunit expressed on MØ is CD18 which forms the functional integrin Mac-1 through interaction with α_M-subunit CD11b or by interaction with α_L-subunit CD11a the integrin LFA-1. Both heterodimers play essential roles in MØ immunity. In J774.A1 cells it was found that LPS activated CD11b/CD18 via MYD88, IRAK, p38 and RAP1 GTPase signaling is responsible for effective cell spreading. Furthermore, the RAP1 GTPase mediated activation of the αMβ2-integrin after LPS stimulation was required to effectively phagocytose C3bi-opsonized target [139, 140]. Inhibition of integrin signaling or culturing RAW cells in low-adherence plates reduced TLR4-driven ERK and JNK phosphorylation and resulted in a decreased TNF production. This demonstrates that TLR4 requires the cooperation of integrin receptors for a full response [136]. Moreover it was shown that TLR4 rapidly activated CD11b through inside-out signaling via PI3K, RAPL GTPase pathway in murine macrophages and subsequently down-regulated the TLR4 response via outside-in signaling through SRC and SYK. Activation of these tyrosine kinases leads to degradation of phosphorylated MYD88 and TRIF to dampen the TLR4 signaling and prevent a hyper-response [141].

2 Aim of the Study

The cytoskeleton is a highly dynamic structure of intracellular filaments present in all pro- and eukaryotic cells [42]. This cell compartment and its specific associated proteins possess scaffolding properties and serve as important regulators in immune cell functions starting from cell maturation, to cell recruitment and adherence, inter- and intracellular signaling and transport processes. Defects in this sensible and complex system can cause immune deficiencies like the Wiskott-Aldrich syndrome (WAS) induced by mutations within the WAS-protein [43, 44]. Furthermore, bacterial and viral pathogens developed strategies to manipulate the cytoskeleton and subvert immune cells [45-47]. Thus, for a better understanding of this structure it is essential to further investigate which cytoskeletal processes and components contribute to the control and regulation of immune cell responses.

The regulation of the cytoskeleton, as well as of individual cytoskeletal proteins, are well described in fibroblasts, stable cell lines and lower eukaryotes, but less is known about their function and regulation in primary cells of the immune system. The starting point for this study was a phosphoproteome analysis of TLR4-activated bone-marrow derived macrophages, which highlighted the cytoskeleton as a hotspot of LPS-induced protein phosphorylation [30]. This finding stressed the potential impact of TLR activation on the cytoskeleton and associated macrophage functions like phagocytosis and motility. In addition, the identification of a large number of cytoskeletal proteins with LPS-regulated phosphorylation provides molecular candidates whose individual regulation and contribution to TLR-induced macrophage responses are yet mostly unknown.

To investigate these questions generates a need to measure and manipulate cytoskeleton-dependent macrophage functions in a quantitative manner. We therefore first aimed to develop and validate a microscopy-based quantitative method to determine the macrophage spreading response as a readout system with potential to apply as high or middle throughput screen. Furthermore, through utilization of specific KO mice, pharmacological inhibitors and specific siRNA knockdown the role of known TLR4 signal components and newly identified phosphoproteins should be revealed in this context. As a consequence of the screen interesting and contributing candidate proteins should became the focus of more detailed investigations to reveal further involvement and regulation of important TLR4-driven immune cell functions.

3 Material and Methods

3.1 Material

3.1.1 Chemicals and reagents

Acetic acid glacial ($C_2H_4O_2$)	# 3738.1	Roth
Acrylamide/Bis-acrylamide Gel 40 %, Rotiphorese	# A515.1	Roth
Ammoniumchloride (NH_4Cl)	# 1.01145	Merck
Ammoniumpersulfate (APS, $(NH_4)_2S_2O_8$)	# 31117	Fluka
Bovine Serum Albumin (BSA)	# K45-001	PAA
Bromphenol blue ($C_{19}H_9Br_4NaO_5S$)	# B-5525	Sigma-Aldrich
Carboxyfluorescein succinimidyl ester (CFSE)	# 422701	BioLedgend
Chloroform ($CHCl_3$)	# 102445	Sigma-Aldrich
Deoxycholic acid ($C_{24}H_{40}O_4$)	# D6750	Sigma-Aldrich
DEPC water (PCR grade)	# T143.3	Roth
Dimethylsulfoxide (DMSO, C_2H_6OS)	# D-5879	Sigma-Aldrich
Ethidiumbromide solution ($C_{21}H_{20}BrN_3$)	# E15-10	Sigma-Aldrich
Ethylenediaminetetraacetic acid (EDTA) disodium salt	# 8043-2	Roth
Ethanol (for analysis, denatured, C_2H_6O)	# 1.00974	Merck
β-glycerophosphate disodium salt ($C_3H_7Na_2O_6P$)	# 35675	Calbiochem
Glycine ($C_8H_9NO_3$)	# 3790.3	Roth
Glycerine ($C_3H_8O_3$)	# 49767	Fluka
Glycogen ($(C_6H_{12}O_6)_{n=7-11}$)	# AM9510	Ambion
Hydrochloric acid (HCl)	# 6331.3	Roth
[^{3}H]-Thymidin	PerkinElmer, Rodgau, Germany	
β-mercaptoethanol (C_2H_6OS)	# M-7154	Sigma-Aldrich
Methanol (MeOH, CH_4O)	# 20847.307	VWR
Mounting medium (DAPI containing)	# SCR-38448	Dianova
Phosphate buffered saline (PBS)	# 1.15925	Biochrom & in house
Phosphoric acid (H_3PO_4)	# 21510-4	Sigma-Aldrich
Polybrene (Hexadimethrine bromide, 6 mg/ml in PBS)	# 107689	Sigma-Aldrich
Ponceau S $C_{22}H_{16}N_4Na_4O_{13}S_4$)	# P-3504	Sigma-Aldrich
2-propanol (C_3H_7OH)	# 109634	Merck
FProtease inhibitor cocktail cOmplete	# 11697498001	Roche

Sodium chloride (NaCl)	# 3957.1	Roth
Sodium fluoride (NaF)	# S7920	Sigma-Aldrich
Sodium hydroxide (NaOH)	# 1.06498	Merck
Sodium nitrite ($NaNO_2$)	# 1065490100	Merck
Sodium orthovanadate (Na_3VO_4)	# S6508	Sigma-Aldrich
Substrate for ELISA, OptiEIA	# 555214	BD Biosciences
Substrate for WB, Immobilon Western	# WBKLS0500	BD Biosciences
Sulfanilamide (4-aminobenzenesulfonamide, $C_6H_8N_2O_2S$)	# 86060	Fluka
Sulphuric acid (H_2SO_4)	# 4623.4	Roth
Tetramethylethylenediamine (TEMED, $C_6H_{16}N_2$)	# 87689	Fluka
Trifast	# 30-2030	Peqlab
Tris base ($C_4H_{11}NO_3$)	# 5429.2	Roth
Trypan blue ($C_{34}H_{28}N_6O_{14}S_4$)	# T-8154	Sigma-Aldrich
Tween 20 (Polysorbat 20, $C_{58}H_{114}O_{26}$)	# 8.22184	Merck

3.1.2 Kits and enzymes

Accutase	# L11-007	PAA
DuoSet ELISA Development System		R&D
TNF-α	# DY410	
IL-10	# DY417	
IL-12p40	# DY499	
IL-6	# DY406	
IL-2	# DY402	
IFN-γ	# DY485	
CCL3	# DY450	
CCL4	# DY451	
IP-10	# DY466	
ELISA MAX™ Standard Set		BioLedgend
CCL2/MCP-1	#432703	
High Capacity cDNA Reverse Transcription Kit	# 4368813	Applied Biosystems
peqGold dNTP Mix (10 mM each nucleotide)	# 20-3011	Peqlab
peqGold Taq DNA-Polymerase ‘all inclusive’	# 0191411-1	Peqlab
RNeasy Micro Kit	# 74004	Quiagen

3.1.3 Western blot antibodies and protein ladder

3.1.3.1 Western blot antibodies

All antibodies (Table 2) required for protein detection by Western blot (WB) analysis were diluted in 3%BSA in TBS-T. The respective secondary horseradish peroxidase (HRP)-conjugated anti- antibodies were purchased from Jackson ImmunoResearch (#711-036-152, #115-036-068) and applied in a 1:10.000 dilution. To determine protein size the PageRuler Prestained protein ladder purchased from Fermentas (# 26616) was utilized.

Table 2. Primary antibodies (recognizing mouse proteins) for WB

Antibody	Source	Dilution	Expected band size	Catalog number	Company
anti-ERK1/2	Rabbit	1:1000	42/44 kDa	# 4695	Cell Signaling
anti-pERK (Thr202/Tyr204)	Rabbit	1:2000	42/44 kDa	# 4370	Cell signalling
anti-p38	Rabbit	1:1000	43 kDa	# 9212	Cell signalling
anti-pp38 (Thr180/Tyr182)	Rabbit	1:1000	43 kDa	# 9211	Cell signalling
anti-GRB2	Mouse	1:10.000	24 kDa	# 610112	BD
anti-pMK2 (Thr334)	Rabbit	1:1000	49 kDa	# 3007	Cell Signaling
anti- MYO1e	Rabbit	1:800	127 kDa	17768-1-AP	Proteintech Europe

3.1.4 Primers and probes

Genotyping of mice was done by Barbara Bodendorfer. In case of *Myo1e* KO mice the screen was done by Sharon Chase (Department Cell and Developmental Biology, SUNY Upstate Medical University, Syracuse, NY, USA). Conditional p38 KO mice [142] were screened and obtained after polyI:C treatment from the group of Jean Pierre David in Erlangen.

Table 3. Genotyping primers

Tagret	Name	Primer pairs	Band size
Dusp1-/-	RL 300	caggtactgtgtgtcggtggtgctaatg	300 & 301 : wt ~300 bp 302 & 301 : ko ~250 bp
	RL 301	ctatatcctcctggcacaatcctcctag	
	RL 302	aaatgtgtcagtttcatagcctgaagaacg	
Dusp16-/- *(gene trap)*	RL 528	cgctcttaccaaagggcaaaccc	536 & 535 : wt ~450 bp 528 & 535 : ko ~650 bp
	RL 535	ccatctcatggcagaggagtgact	
	RL 536	gacctgtgcataactggccctactac	
Myd88-/-	RL 665	agacaggctgagtgcaaacttgtgctg	665 & 667 : wt ~1000 bp 666 & 667 : ko ~1000 bp
	RL 666	agcctctacaccttctcttctccaca	
	RL 667	atcgccttctatcgccttcttgacgag	
Myo1e-/-	#1	ttccgcttacggtggaaatg	#1 & #3: - wt --, ko ~250bp #3 & #4: -wt ~150bp, ko --
	#3	tcatgtgtagcccaagctcacc	
	#4	actcattctgtcatctgactccacc	
Rag1-/-	RL984	gaggttccgctacgactctg	984 & 985 : wt 474bp 985 &986 : ko 530bp
	RL985	ccggacaagtttttcatcgt	
	RL986	tggatgtggaatgtgtgcgag	

The quantitative Real-time polymerase chain reaction (qRT-PCR) analysis to determine gene expression was performed using specific primers and probes (Table 4) designed by the Universal ProbeLibrary (UPL, Roche) and employment of the FastStart Universal Probe Mastermix (Roche).

Table 4. Primer and probe combinations used for quantitative Real-time PCR

Gene of interest	Primer number	primer sequence	UPL
Actr3 (ARP3)	RL1049	gactttggacgtcgtttgc	# 64
	RL1050	catcaataggcttgggcttc	
Ccl2/Mcp-1	RL473	tcactgaagccagctctctct	# 22
	RL474	gtggggcgttaactgcat	
Ciita (CIITA)	RL822	gatgtggaagacctggatcg	# 110
	RL823	tgcatcttctgaggggtttc	
Coro1b	RL1055	ttcagccgcatgagtgaac	# 17
	RL1056	gtagagccccattgcttgaa	
Eps8	RL1053	cactgggagatagttgggtga	# 108
	RL1054	ggacgtaaggtgggatgaac	
Fhod1	RL1043	gctctgcaccgactcctg	# 78
	RL1044	atccggagggagacacttg	

Fmn1	RL1045	ttccacattgctgttcatcc	# 4
	RL1046	cagcgggaaaacactcttgt	
Hprt	RL415	tcctcctcagaccgctttt	# 95
	RL416	cctggttcatcatcgctaatc	
Lsp1	RL1220	acccacaccgaagacacc	# 75
	RL1221	ttcctcgtcttcttctctcca	
I-Ab1 (MHC-II)	RL824	gtggtgctgatggtgctg	# 26
	RL825	ccatgaactggtacacgaaatg	
Mtss1	RL1222	cttcataaacaaagccggaaa	# 33
	RL1223	gctgctgctactactgttgtcc	
Myo1e	RL1183	ccaaggagcgcacagtatgag	RL1228 (5'-FAM-3'BHQ) acccgcctcatatctatgccct
	RL1184	tctctgtcgatcgatcatgtttctgta	
Myo1f	RL1017	cctacataccatccctcacca	# 53
	RL1018	tccactctgcttcacgttgt	

All primers were purchased from Metabion. *Myo1e* probe and primer were designed by SDS 2.4.1 software from Applied Biosystems and ordered from Metabion.

3.1.5 siRNA

Small interfering RNA oligonucleotides (siRNA) for selective gene silencing were purchased from Dharmacon (Thermo Fisher Scientific) using Dharmacon's pre-validated ON-TARGET*plus* siRNA database. Each specific siRNA set composed of a pool of four specifically directed siRNAs. Lyophilized siRNAs samples were resuspend in 1-fold siRNA buffer from Dharmacon to a final concentration of 20 µM, heated for 1 min to 90°C and incubate at 37°C for 60 min on a thermo shaker. Dissolved samples were stored in aliquots at -80°C.

Table 5. siRNAs for selected gene silencing

Target gene	Gene ID	siRNA catalog number
Actr3 (Arp3)	74117	# L-046642-01-0005
Coro1b	23789	# L-048421-01-0005
Eps8	13860	# L-045154-01-0005
Fhod1	234686	# L-057380-01-0005
Fmn1	14260	# L-042798-01-0005
Lsp1	NM_019391	# L-043955-01-0005
Mtss1	211401	# L-041040-01-0005
Myo1f	17916	# L-050897-01-0005
non-silencing siRNA (nsRNA) (control)	---	# D-001810-01-20

3.1.6 Antibodies for immunofluorescence analysis

Antibodies for FACS analysis and fluorescence microscopy imaging (Table 6) were diluted in 0,2%BSA/PBS. Stained FACS samples were stored up to 5 days in 2% PFA/PBS at 4°C. Specimens for fluorescence microscopy were covered with DAPI containing mounting medium (Dianova SCR-38448), sealed with nail polish and stored at 4°C.

Table 6. Conjugated primary antibodies for immunofluorescence

Antibody	Conjugated fluorophore	Dilution	Clone	Catalog number	Company
B220	PE	1:400	RA3-6B2	553089	BD
CD11a	PerCP	1:400	M17/4	46-0111-82	eBioscience
CD11b	Violet421	1:400	M1/70	101235	BioLegend
CD11b	APC	1:400	M1/70	101212	BioLegend
CD11c	PE-Cy7	1:400	N418	25-0114-82	eBioscience
CD16/CD32 (Fc-block)	-	1:1000	93	14-0161-86	eBioscience
CD18	PE	1:400	M18/2	12-0181-81	eBioscience
CD19	PE	1:400	6D5	115508	BioLegend
CD29	APC	1:200	eBioHMb1-1	17-0291-80	eBioscience
CD3	PerCP	1:100	145-2C11	100326	BioLegend
CD4	FITC	1:800	GK1.5	100406	BioLegend

CD40	APC	1:400	3/23	558695	BD
CD45.1	APC	1:300	A20	110720	BioLegend
CD61	FITC	1:200	2C9.G3	11-0611-81	eBioscience
CD8a	eFluor450	1:400	53-6.7	48-0081-82	eBioscience
CD80	PE	1:200	16-10A1	104707	BioLegend
CD86	FITC	1:200	B7-2 (GL1)	553691	BD
F4/80	FITC	1:200	BM8	123108	BioLegend
Ly6C	FITC	1:400	AL-21	553104	BD
Ly6G	PE	1:400	1A8	551461	BD
MHC-II (I-A/I-E)	PerCP	1:1000	M5/114.15.2	107623	BioLegend
MHC-II (I-A/I-E)	eFluor450	1:400	M5/114.15.2	48-5321-82	eBioscience
NK1.1	PE-Cy7	1:100	PK136	25-5941-82	eBioscience
PDCA	PE	1:400	eBio927	12-3172-81	eBioscience

3.1.7 Buffers

Buffers and water-soluble reagents were prepared with high-purity water (HPW) from the in-house Milli-Q purification system.

3.1.7.1 ELISA

Buffers listed in Table 7 were used for Enzyme-linked-Immunosorbent Assay (ELISA).

Table 7. Buffers for ELISA

Coating buffer (only for CCL2 ELISA BioLedgend)	8,4 g sodium bicarbonate ($NaHCO_3$); 3,56 g sodium carbonate (Na_2CO_3), pH9,5 in 1L HPW (according to manufacturer's instructions)
Blocking buffer	1% BSA in 1x PBS
Stop solution	2 N sulphuric acid (H_2SO_4) in HPW
Wash buffer	0.05% Tween 20 in 1x PBS

3.1.7.2 SDS Page and Western Blot

Recipes for sodium dodecyl sulfate-polyacrylamide gel electrophoresis (SDS-PAGE) buffers and Western blot are shown in Table 8.

In all cases, 10% SDS gels were prepared for protein separation as described in Table 8.

Table 8. Buffers for SDS-PAGE and Western blot

Buffer	Compostion
4x Lämmli	6.25 ml 1 M Tris base/HCl (pH 6.8; 62,5 mM final)); 2 g SDS (2% final); 20 ml glycerol (20% final); 400 µl 0.5 M EDTA (2 mM); 100 mg Bromphenol blue; add HPW to a final volume of 100 ml. Add 70 µl β-mercaptoethanol to 1 ml Lämmli buffer freshly before use.
Ponceau staining	0.5 g Ponceau S (0.1 %) dissolved in 500 ml 5 % glacial acetic acid.
Ripa	Add to 150 ml 1x PBS (keep order as listed): 2 g sodium deoxycholate (25.5 mM final); 2 ml 10% SDS (0.1% final); 0.8 ml 0.5 M EDTA (2 mM final); 0.42 g sodium fluoride (50 mM); 2 ml NP40 (1 % final); add 1x PBS to a final volume of 200 ml. Add freshly before use: 1:50 sodium fluoride (0.5 M); 1:50 Roche Complete (1 tablet in 1 ml); 1:100 β -glycerophosphate (1 M); 1:200 sodium orthovanadate (200 mM)
4x Resolving gel	36,3 g Tris base (1.5 M) in 200 ml HPW adjust to pH 8.8 with HCl, store at 4°C
4x Stacking gel	12 g Tris base (0.5 M) in 200 ml HPW adjust to pH 6.8 with HCl, store at 4°C
Stripping	0.2 N NaOH in HPW
10x Tank	60.56 g Tris base (250 mM); 288 g glycine (1.9 M); 200 ml 10% SDS (1%) Adjust to a final volume of 2 l with HPW, store at RT
1x Tank	Dilute 10x tank buffer 1:10 with HPW.
10x TBS	48.4 g Tris base (200 mM); 160 g sodium chloride (1.4 M) Adjust to pH 7.6 with HCl and add HPW to a final volume of 2 l.
TBS-T	Dilute 10x TBS 1:10 and add 0.1% Tween 20.
10x Transfer	48.4 g Tris base (200 mM); 216.4 g glycine (1.44 M); 100 ml 10% SDS (0.5 %) Adjust to a final volume of 2 L with HPW, store at RT.
1x Transfer	1x transfer buffer consists of 10x transfer buffer (1:10) and 10% Methanol in HPW

Table 9. SDS-PAGE gel composition

Calculated for two 20 cm x 10 cm gels, *add directly before casting

Reagents	Resolving gel 10%	Stacking gel 4%
Acrylamide	12.6 ml	1.5 ml
Resolving gel buffer	12.6 ml	-
Stacking gel buffer	-	4 ml
10 % SDS	0.5 ml	160 µl
HPW	24.4 ml	10.4 ml
10 % APS*	300 µl	80 µl
TEMED*	70 µl	16 µl

3.1.7.3 Cell culture

Buffers applied for cell culture:

Table 10. Buffers for cell culture

Erylysis buffer	9.1 g ammonium chloride (0.17 N) in 1 L HPW + 20 ml 1 M Hepes in HPW (20 mM final); ~pH 7.0 pH is not adjusted, sterile filtered, store at RT
PBS	37 mM NaCl; 2.7 mM KCl; 80 mM Na_2HPO_4 pH 7.4, autoclave, store at 4°C
Trypan blue	0.04% in PBS

3.1.8 Bacteria and medium

E.coli (E550 ATCC 25922) was stored in glycerol stocks at -80°C. 24 h prior to intra peritoneal (i.p.) injection into mice the bacteria were cultured at 37°C in autoclaved lysogeny broth (LB) media (without antibiotics). LB media contains 5 g/l yeast extract, 10 g/l tryptone and 10 g/l NaCl (pH 7.0). Bacteria number was adjusted to $4*10^8$/ml by measurement of the optical density (OD_{600}) and dilution in sterile PBS. *E.coli* were inactivated by incubation at 65°C for 20 minutes.

3.1.9 Cell culture media, supplements and stimulatory agents

3.1.9.1 Media

Dulbeco's modified Eagle's Medium (DMEM)		
High Glucose (4.5 g/l)	# E15-810	PAA
RPMI 1640	# E15-840	PAA
Opti-MEM	# 11058-021	Invitrogen

3.1.9.2 Supplements

β-mercaptoethanol	# M-7522	Sigma-Aldrich
(10 mM Stock in 1x PBS, sterile filtered, stored at 4 °C, 50 µM final)		
Penicillin/Streptomycin (100x)	# P11-010	PAA
Foetal Bovine Serum (FBS)	# F7524	Sigma
Foetal Bovine Serum (FBS)	# S0115	Biochrome
Donor Horse Serum (HRS)	# S-HEU03-I	CellConcepts
Non-essential amino acids	# M7145	Sigma-Aldrich
Hank's Balanced Salt Solution (HBSS)	# H15-008	PAA

3.1.9.3 Complete DMEM (cDMEM) and complete RPMI (cRPMI)

Preparation of complete cell culture media DMEM High glucose or RPMI was done by supplementation with 10% FBS, 1x Penicilin (100 U/ml) / Streptomycin (1 mg/ml), 2,5 ml β-Mercaptoethanol (0.05 mM). Medium for macrophage differentiation in hydrophobic Teflon bags were complete by addition of 10% FBS, 5% HRS, 2,5 ml β-Mercaptoethanol (0.05 mM), 1:100 non-essential amino acids (Sigma, M7145, stock 100x).

3.1.9.4 Stimulatory agents

LPS (*E. coli* 055:B5)	# L-6529	Sigma-Aldrich
Stock 10 µg/ml in media (4°C), final 100 ng/ml		
Interferon γ (murine, recombinant, source: *E. coli*)	# 315-05	Peprotech
Stock 1 mg/ml in PBS (-20°C), Stock 1 µg/ml in media (4°C), 50 ng/ml final		
OVA (Albumin from chicken egg white)	# A5503	Sigma-Aldrich
Stock 100 mg/ml in PBS (-20°C), 2 mg/ml final		
DQ-OVA (OVA; heavily labeled with BODIPY® dye)	#D12053	Lifetechnologies
Stock 1 mg/ml in PBS (-20°C), 20 µg/ml final		

3.1.9.5 Inhibitors

Cytochalasin D	# C8273	Sigma-Aldrich
Stock 4mM in DMSO (-20°C), final 5µM		
PD184352 (MEK1 inhibitor)	#S1020	Selleck Chemicals.
Stock 10 mM in DMSO (-20°C), final 10 µM		

3.1.10 Consumable items

Blotting paper	# GB-40	Hartenstein
Cell culture dishes		
Nunclon delta (Ø 10 cm)	# 150350	Nunc
Tissue culture polystyrene dish, 150 x 25 mm style	# 353025	BD Falcon
Cell culture plates		
96-well Nunclon (F bottom)	# 167008	Nunc
24-well Nunclon	# 662160	Greiner bio-one
12-well Nunclon	# 3512	Costar
CD4 (L3T4) MicroBeads, mouse	#130-049-201	MiltenyBiotec
CD45R (B220) MicroBeads, mouse	#130-049-501	MiltenyBiotec
Cell Strainer 70 µM	# 352350	BD Falcon
Cryotube Vials (1 ml)	# 366656	Nunc
ELISA plates MaxiSorp	# 442404	Nunce
Electroporation chambers	# 71-2030	Peqlab
MACSiMAG Seperator	#130-092-168	MiltenyBiotec
MACS Separation columns (LS)	#130-042-401	MiltenyBiotec
Needles (sterile)		
27G x ¾'', Nr. 20 (0.4 mm x 19 mm)	# 302200	BD Microlance 3
22G x 1 ¼'', Nr. 12 (0.7 mm x 30 mm)	# 300900	BD Microlance 3
14G x 2'', IV indwelling cannula (2.2 x 50 mm)	# 4252217B	Henke Sass Wolf
Nitrocellulose transfer membrane Protran	# 10 401 396	Whatman
Petri Dishes	# 82.1473.001	Sarstedt
Permanox chamber slides	# 177445	Nagle Nunc
Pipets Stripette (5 ml / 10 ml / 25 ml)	# 4487/88/89	Costar
Pipet tips		
0.1 - 20 µl, epT.I.P.S	# 022492012	Eppendorf
2 - 200 µl, epT.I.P.S	# 0030000.870	Eppendorf
200 - 1000 µl,	# 729065	Biozym
2.5 ml (PD-tips, multistep pipet)	# 702388	Plastibrandrand
5 ml (PD-tips, multistep pipet)	# 702390	Plastibrandrand
Filter tips		
0.5 – 20 µl, Biosphere filter tips	# 70.1116.210	Sarstedt
20 µl, Biosphere filter tips	# 70.760.213	Sarstedt
2 – 200 µl, Biosphere filter tips	# 70.760.211	Sarstedt
100 - 1000 µl, Biosphere filter tips	# 70.762.211	Sarstedt
Polypropylene Conical Tubes 15 ml	# 352096	BD Falcon
Polypropylene Conical Tubes 50 ml	# 352070	BD Falcon
Reaction plates		
384 well reaction plate	# 4343370	Applied Biosystems
Reaction plate covers		
QPCR adhesive clear seal	# 4ti-0560	4titude
Reaction tubes		
PCR tubes, 0.5 ml	# 0030124537	Eppendorf
Safe-lock, 1.5 ml	# 0030120.086	Eppendorf
Safe-lock, 2.0 ml	# 0030120.094	Eppendorf
1.5 ml PP	# 421-800	J. Peske GmbH
Steritop filter 0.22 µm	# SCGPT05RE	Millipore
Syringes		
1 ml, Soft-JECT Tuberculin	# 5010-200V0	Braun

10 ml, Discartid	# 309110	BD Biosciences
50 ml	# 300866	BD Plastipak
Teflon foil for bag preparation	DuPont, purchased via Cadillac Plastic, Karlsruhe, Germany	

3.1.11 Laboratory equipment

1450 microplate scintillation counter	Wallac, Turku, Finland
Analytical Balance Acculab (max. 210 g)	Satorius group
AxioCam MRm camera	Carl Zeiss Microscopy
Balance Scout Pro (max. 600 g)	Ohaus
Biophotometer	Eppendorf
Bioruptor	Diagenode
Centrifuge Heraeus Pico 17	Thermo Scientific
Centrifuge Heraeus Fresco 17	Thermo Scientific
Centrifuge Heraeus Multifuge 3SR+	Thermo Scientific
ChemiLux Imager, incl. CCD camera (WB documentation)	INTAS
Electrophoresis Power Supply EV261 / EV243	Peqlab
SPECTRAmax 340PC ELISA Reader	Molecular Devices
Flow Cytometer FACS Canto II	BD
Freezer (-20°C)	Liebherr
Freezer (-80°C)	Thermo Scientific
Fridge (4°C)	Liebherr / Siemens
GenePulser Xcell	Bio-Rad
Ice machine	Ziegra Eismaschienen
IH-110 harvester for 96-well deep unifilter plates	Inotech
Incubator Hera Cell 240	Thermo Scientific
Laboratory Water Bath Aqualine AL12	LAUDA
Laminar Flow HeraSafe	Thermo Scientific
Liquid Nitrogen Tank (N_2), 35VHC	Union Carbide
Microscope Axiovert 40C	Zeiss
Microwave	Severin
Milli-Q Biocel, Q-Guard2, Ultrapure Organex Cartridge (# QTUM000EX)	Millipore
Multichannel pipets Finnpipette (5-50 µl / 50-300 µl)	Thermo Scientific
Multistep pipet Handystep S	Brand
Neubauer counting chamber Improved	Brand
PerfectBlue Gelsystem Mini S & Mini L	Peqlab
Just Cast (adjustable casting chamber)	Peqlab
Perfect Blue Tank Electroblotter Web M	Peqlab
Fiber mat	Peqlab
Perfect Blue Doppelgelsystem Twin ExW S	Peqlab
Pipetboy acu	Integra Biosciences
Pipets (1000 µl, 200 µl, 20 µl, 10 µl, 2 µl)	Gilson
Rocking Platform (RT)	VWR
Shaker Polymax 2040 (4°C)	Heidolph Instruments
Spectrophotometer Nanodrop 1000	Peqlab
Taqman 7900 HT Fast Real-Time PCR System	Applied Biosystems
Thermocycler T3000	Biometra
Thermocycler TGradient	Biometra
Thermomixer compact / comfort	Eppendorf
Vacuum pump BVC21	Vacuubrand

Vortex-Genie 2	Scientific Industries
Zeiss AxioVert 200M	Carl Zeiss Microscopy

3.1.12 Software

Adobe Acrobat Reader X	Adobe Systems
Adobe Photoshop CS2 / CS5	Adobe Systems
AxioVision Rel 4.8	Zeiss
Endnote X4	Thomson Reuters
ChemoStar Imager V.0.1.25	INTAS
FACSDiva Software V6.12	BD
FlowJo 7.6.5	TreeStar, Inc
Gel documentation system GDS V3.28	INTAS
Graph Pad Prism 4	Graph Pad Software
MS Office Professional Plus 2010 Version 14.0.6106.5005	Microsoft
NanoDrop ND1000 Version 3.6.0	Thermo Scientific
Probe finder	Roche Applied Science
SDS RQ Manager 1.2	Applied Biosystems
Sequence Detection System 7900 HT SDS 2.3	Applied Biosystems
SoftMax Pro 5.4	Molecular Device
VectroNTI 9.1.0	Invitrogen

3.2 Methods

3.2.1 Molecular biology

3.2.1.1 RNA isolation

The isolation of RNA from cell lysates was mainly performed by a phenol/choroform extraction method. $5*10^5$ – $1*10^6$ stimulated or unstimulated cells were directly lysed by adding 500µl TriFast™ to each well and RNA preparation was performed according to the manufacture's protocol. Subsequently the RNA pellet was resuspended in 15µl PCR-grade water. In case of siRNA treatment $2*10^5$ cells were used for RNA extraction and RNA isolation was performed using RNeasy Mini Kit (Qiagen) according to the manufacture's protocol. The RNA concentration and purity was determined by using the Nanodrop ND-1000 UV/Vis-spectrophotometer. Finally the extracted RNA was stored at -20°C or directly prepared for cDNA synthesis.

3.2.1.2 cDNA synthesis

Conversion of extracted RNA into random-primed single-stranded cDNA for qRT-PCR was performed by using the High Capacity cDNA Reverse Transcription Kit (Applied Biosystems) according to the manufacture's protocol. For reverse transcription 200 ng - 1 µg

total RNA was add in 10 µl RNAse free water and complete with 10 µl master mix to a total reaction volume of 20 µl. The master mix composition and the used thermocycler program are shown in Table 11.

Table 11. cDNA synthesis master mix and program

cDNA synthesis master mix		cDNA synthesis program		
Component	Volume			
10x RT buffer	2 µl		Temperature	Time
10x Random Primers	2 µl	Step 1	25 °C	10 min.
25x dNTPs (10 mM)	0.8 µl	Step 2	37 °C	120 min.
Reverse Transcriptase	1 µl	Step 3	85 °C	5 min.
PCR grade water	4.2 µl	Step 4	4 °C	∞

3.2.1.3 Quantitative real-time PCR and calculation of fold changes

To identify the relative expression levels of different genes a quantitative real-time PCR (qRT-PCR) was performed based on the Universal ProbeLibrary System from Roche. The primer-probe combinations required for specific mRNA detection were designed by an online software provided on the Roche homepage. An intron-spanning assay was applied to minimize the risk of false positive signals arise from genomic DNA contamination in the RNA samples. The following PCR reactions occurred in a total volume of 12 µl (5µl cDNA dilution plus 7µl mastermix) and were performed in 384-well plates (15-50 ng cDNA per well) on the 7900HT Fast Real-Time PCR System. For the mastermix recipe see Table 12.

To allow the comparison of target gene expression between different samples the deltadeltaCT (ΔΔCT) method was utilized to calculate the fold changes [143]. Therefore, the CT value (number of PCR cycles required to rise the fluorescence intensity significantly above the background signal) from the gene of interest was normalized to the CT value of the house-keeping gene *Hprt* and subsequently calculated to the untreated control used as calibrator. In case of siRNA treatment the unstimulated and non-targeting siRNA (nsRNA) challenged condition was used as calibrator.

$$\Delta CT = CT_{Hprt} - CT_{gene\ of\ interest}$$

$$\Delta\Delta CT = \Delta CT_{treated\ sample} - \Delta CT_{untreated\ sample\ (average)}$$

$$\text{fold change} = 2^{\Delta\Delta CT}$$

Each condition was analyzed as single biological sample and each sample was assayed in technical duplicates.

Table 12. Mastermix for qRT-PCR

Component	Volume	Final concentration
FastStart Universal Probe Master (ROX) (2x)	6 µl	1 x
Forward / reverse primer (100 µM)	0.1 µl	~ 800 nM
Probe (10 µM)	0.1 µl	~ 80 nM
PCR grade water	0.7 µl	

Before PCR, the plates were centrifuged for 10 minutes at 900 x g and covered with an adhesive seal to avoid evaporation of the sample during PCR reaction (see Table 13).

Table 13. Taqman program for qRT-PCR

	Temperature	Time	Cycles
Step 1	50°C	2 min.	
Step 2	95°C	10 min.	
Step 3	95°C	15 sec.	40
	60°C	1 min.	

3.2.1.4 Polymerase chain reaction

The polymerase chain reaction was used to amplify specific DNA sequences for mouse genotyping. The peqGOLD Taq-DNA-Ploymerase system from Peqlab was applied with respective primers listed in Table 3. Cycling conditions for each PCR reaction were adapted to the product size.

3.2.2 Immunoassays

3.2.2.1 ELISA

An enzyme-linked-immunosorbent assay (ELISA) was performed to determine cytokines and chemokines in the supernatant of activated macrophages and DCs. The R&D and BioLedgend sandwich ELISA were accomplished according to the manufacture's protocol.

3.2.3 Biochemical analysis

Total or phosphorylated proteins in cell lysates were detected by SDS-PAGE and subsequent Western blot analysis [144].

3.2.3.1 SDS-PAGE

Buffers and gel preparation was performed according to recipes listed in section 3.1.7.2. At

least $1*10^6$ cells were lysed in 150 µl RIPA buffer and mixed with 50 µl Lämmli buffer before heated at 95°C for 10 min. A final sonication step was performed to complete the protein denaturation. Samples were stored at -20°C or directly loaded onto the polyacrylamide gel. To separate the proteins the electrophoresis was done at 100 – 120 mA in 1x Tank buffer.

3.2.3.2 Western Blot

Prior to immunovisualization of the proteins their immobilization on a membrane was performed by the wet blot method. For this the polyacrylamide gel was applied on a nitrocellulose membrane and covered on both sites with Whatman papers and two sponges. After assembling the complete setup in the transfer chamber, it was filled up with transfer puffer and the blotting was performed at 300 - 500 mA (1.5 mA/cm^2) for 3h. Afterwards the membrane was blocked for 30 min – 1 h in 1x TBS-T with 3% BSA to avoid unspecific binding. Incubation with the respective primary antibody (Table 2) occurs at 4°C overnight. On the next day the membrane was washed in TBS-T and incubated with the HRP-conjugated secondary antibody for 1 – 2 h at room temperature. Finally the proteins were detected using Immobilon Western HRP substrate and a ChemoCam Imager.

3.2.4 Cell culture

Solutions and buffers required for preparation, culture or stimulation of cells lines or primary cells were prepared with LPS-free reagents. Cell culture reagents were tested for endotoxin content by the quantitative chromogenic limulus amebocyte (LAL) lysate endpoint assay QCL-1000 (# 50-6470, Cambrex). Cells were incubated at 37°C, 85% humidity and 5% CO2. Centrifugation of cells was performed at 1,400 rpm for 5 minutes at 4 °C.

3.2.4.1 Cell lines

As a source of macrophage colony stimulating factor (M-CSF) L-cell-conditioned medium (LCCM) produced by the mouse fibroblast cell line L929 (ATCC # CCL-1) was used for macrophage differentiation. Granulocyte macrophage colony-stimulating factor (GM-CSF) required for dendritic cells differentiation was obtained from the murine myeloma cell line (X63 Ag8), which contains with the cDNA of granulocyte macrophage-colony stimulating factor gene *(Csf2)* and were generated by Brigitta Stockinger in the lab of David Gray [145].

3.2.4.2 L-cell conditioned medium (LCCM)

L-cell-conditioned medium (LCCM) was used as a source of macrophage colony stimulating factor (M-CSF). L929 cells ($5x10^6$ cells/tube) were cultured on 15 cm cell culture dishes to a

nearly confluent stage, trypsinized and splitted 1:5. The M-CSF containing supernatant was collected from cells grown again to confluence, fresh cDMEM was added, and the procedure was repeated without splitting every other day for three weeks until the cells started detaching. The collected LCCM was sterile filtered and stored in 50 mL aliquots at 4 °C.

3.2.4.3 Preparation of GM-CSF containing media

To obtain GM-CSF containing supernatant the *Csf2* expressing, non-adherent, murine, myeloma cell line X63 [145] was cultured in cRPMI with 1 mg/ml G-418 under selective pressure. After cell expansion the geneticin was removed and the supernatant was collected every five days by centrifugation at 4,000 rpm for 10 minutes at 4°C. Cells were transferred back to the culture flask to continue the supernatant production. Collected SNs were sterile filtered and aliquoted for storage at – 20°C.

3.2.4.4 Macrophage differentiation

Primary macrophages were differentiated from murine bone-marrow. Thus mice were sacrificed by cervical dislocation, the skin was disinfected with 70% ethanol and femur and tibias were isolated. The bones were opened with sterile scissors under the laminar flow and the bone marrow was flushed out with 10 ml ice cold PBS using a 10 ml syringe and a 22-gauge needle. The bone-marrow was incubated for 5 min in 5ml erylysis buffer at room temperature to eliminate co-isolated erythrocytes, centrifuged and subsequently resuspended in cDMEM containing 10% LCCM. The cells were incubated overnight in a 10 cm Petri dish for fibroblast depletion. Non-adherent cells were collected, counted and replated at a density of $5*10^6$ cells per dish in 10 ml cDMEM containing 10% LCCM. At day four, 5 mL of fresh cDMEM with 10 % LCCM was added. After six to seven days of differentiation, cultures were nearly confluent. Non-adherent cells were removed, the remaining cells washed once with 1xPBS and then incubated with 4-5 mL accutase at 37°C for 5 min to detach the cells. The accutase was inhibited by adding 5 ml cDMEM. Subsequently cells were counted with a Neubauer chamber using tryphan blue do identify death cells, centrifuged and resuspended in cDMEM to adjust the required cell concentration. Cells were replated and rest overnight at 37°C before they were used for experiments.

Differentiation of macrophages for siRNA knockdown (KD) occurred in hydrophobic Teflon bags according to the protocol from Wiese M. *et al* [146]. 6 to 10 million cells were cultured 8 days at 37°C, 10% CO_2 and 90% humidity in 50 ml cDMEM (described in 3.1.8) containing

15% LCCM. Cells were harvested with a 50 ml syringe using a 14-gauge needle and prepared for siRNA KD described in 3.2.4.6.

3.2.4.5 DC differentiation

Bone-marrow was prepared as described in 3.2.4.4. After erythrocyte lysis $6*10^6$ bone-marrow cells were plated in 10 cm cell culture dishes in 10 ml cRPMI containing 10 % GM-CSF. Every three days the cells were feed by adding 10 ml of fresh medium including 10% of the differentiation factor. Non-adherent cells were harvested on day 8 and prepared for stimulation.

3.2.4.6 Specific siRNA Knockdown

Delivery of siRNA into primary MØ was done by electroporation as described in Wiese M. *et al* [146]. Prior to electroporation cells were harvested from Teflon bags, washed once in 10 ml of ice cold Opti-MEM, centrifuged and resuspend in Opti-MEM in a concentration of $2*10^6$cells / 50µl. Afterwards, 20 µl of the 20 µM siRNA stock were transferred into 4-mm electroporation chambers and filled up to a volume 50 µl with Opti-MEM. 50 µl of the cell suspension were added, incubated 5 min on ice and subsequently pulsed in a GenePulser Xcell electroporation device. Pulse conditions were 400 V, 150 µF, and 100 Ω. Electroporated cells were diluted in pure RPMI, transferred into required well plates and incubated at 37°C. 1-2 hours upon siRNA delivery pure RPMI was aspirated and exchanged by addition of cRPMI. Cells were incubated 48h at 37°C, 5% CO_2 prior to LPS stimulation. The KD efficiency on mRNA level was determined by qRT-PCR as described in 3.2.1.4.

3.2.4.7 Stimulation of cells

LPS and IFN-γ stocks were dissolved in the cell culture media. For LPS stimulation 100 ng/ml was used as final concentrations. In case of IFN-γ 50 ng/ml was applied.
For stimulation of macrophages and DCs, cell suspensions were usually adjusted to 1 - $2*10^6$ cells/ml and plated as listed in Table 14.

Table 14. Stimulation of macrophages and DCs: cell numbers and assays

Plate format	Number of cells/well	Final volume/well	Assay
8 Well chamber slides	25.000	0,3 ml	cell spreading and SN for ELISA
12 well	1.500.000	1 ml	WB (lysis in 150 µl Ripa buffer)
24 Well	500.000	0,5 ml	RNA for qRT-PCR of WT and KO cells (lysis in 500µl Trifast), SN for ELISA
48 Well	200.000	0,5 ml	RNA for qRT-PCR of siRNA treated cells (RNA extraction by kit)
96 Well	300.000	0,2 ml	FACS staining for surface molecules

3.2.4.8 Measurement of cell spreading

To measure TLR4-driven cell spreading $2,5*10^4$ WT and KO cells were transferred to 8-well Permanox chamber slides 24 h prior to LPS stimulation. In case of siRNA treatment, cells were plated 48 h before activation. Cells were fixed at indicated time points in pre-warmed 2% PFA/PBS for 20 min, followed by CD11b/APC surface staining. Therefore, the fluorochrome conjugated antibody was diluted 1:200 in 0,2% BSA/PBS added to the cells and incubated 30 minutes at 4°C. Subsequently samples were washed twice with PBS, covered in DAPI containing mounting medium. and stored at 4°C. Fluorescence images were obtained using a Zeiss AxioVert 200M (Germany) widefield microscopy. Contact areas of activated macrophages were semi-automatically determined with the developed two-step segmentation software described in 4.1.1 and Wenzel J. *et al* 2011[147].

3.2.4.9 FACS analysis for surface molecule expression

FACS staining was performed according to standard protocols with antibodies listed in Table 6. Data were record on a FACSCanto II (BD Bioscience) and analyzed by FACSDiva Software V6.12 and FlowJo 7.6.5 software.

3.2.4.10 OT-II stimulation assay

Differentiated bone-marrow MØ or DC were cultured for 24 h in the presences or absence of 2 mg/ml ovalbumin. The APCs were washed at least 5 times with pure RPMI before co-cultivation with purified CD4+ cells from OT-II mice. Numbers of APCs were titrated from $1*10^5$ to $1*10^3$ while constant numbers of $3*10^5$ CD4+ T cells were added to the suspension. CD4+ T cells were purified from spleen and lymph nodes of OT-II mice by magnetic cell

sorting (Miltenyi Biotec) and their purity was determined by FACS to be >93%. Supernatants were collected 72 h after co-cultivation and analyzed for the presence of IFNγ and IL-2, as described in 3.2.2. To analyze proliferation capacity, cells were subsequently pulsed with [^{3}H]-thymidine (1 µC/well) for 20 hours. Culture supernatants were harvested onto glassfiber filtermates using an ICH-110 harvester and filters were counted in a 1450 microplate scintillation counter.

3.2.4.11 CFSE dilution assay and T-cell activation marker

Antigen-presenting cells (APCs) and CD4+ T cells were prepared as described in 3.2.4.10. In advance to co-cultivation the initial CD4+ T cell population was stained with CFSE according to the standard protocol. In separated approaches for 24 h and 72 h time points the cell culture was stained for CD4 and CD25. T cell activation and division was determined by FACS analysis.

3.2.4.12 DQ-OVA assay

To analyze the antigen processing capacity of APCs, $4*10^5$ bone-marrow derived MØ or DC were incubated in 24 well plates under presence of 20 µg/ml DQ-OVA. To stop DQ-OVA cleavade, cells were washed twice with PBS and fixed in 2% PFA/PBS for at least 30 minutes. To determine antigen processing increased fluorescence of cleaved DQ-OVA was analyzed by FACS. To prevent DQ-OVA endocytosis and processing, control cells were incubated at 4°C under constant ovalbumin presence.

3.2.5 Mice

All mice were used on a C57BL/6 background and bred under SPF conditions in the animal facilities of the 'FAU Erlangen-Nürnberg' ('Franz-Penzholdt-Zentrum' and 'Biotechnologisches Entwicklungszentrum'). Experiments were performed in the animal house of the 'Institut für klinische Mikrobiologie, Immunologie und Hygiene'. All animal work was conducted according to relevant national and international guidelines and approved by the 'Regierung von Mittelfranken'.

Mice lacking Myo1e and respective control animals were maintained at the Department of Laboratory Animal Resources, SUNY Upstate Medical University (Syracuse, NY). All protocols for animal studies and cell collection using these mice were approved by the SUNY Upstate Medical University IACUC. Bone marrow of C57BL/6 and, Myo1e -/- mice was controlled deep-frozen in FCS containing 10% DMSO, shipped on dry ice from USA to Germany and stored in liquid nitrogen until usage.

3.2.5.1 Starins

C57BL/6 wild-type (wt) mice were purchased from Charles River periodically and bred in the barrier area of the FPZ.

Mice deficient in the myeloid differentiation primary response gene 88 (*Myd88-/-*, [148]) were generated by Osamu Adachi in the lab of Shizuo Akira. Mice deficient in MAPK *p38* were kindly provided by Jean Pierre David [142]. Blastocysts from mice deficient in the dual-specificity phosphatase 1 (MKP-1; *Dusp1-/-*) were generated by the R. Bravo laboratory at Bristol-Myers Squibb Pharmaceutical Research Institute [149] and kindly provided Andrew C.B. Cato [150]. Mice with a gene trap insertion in the locus encoding dual-specificity phosphatase 16 (MKP-7; *Dusp16tp mice*) were generated in the laboratory of Roland Lang [41]. Breeding colonies of mice lacking B- and T-cells (RAG1 KO) and mice expressing the congenic marker CD45.1 (B6.Ptprc) were maintained at the Franz Penzoldt Center of the Medical Faculty at the University Erlangen-Nuremberg. Bone–marrow and mice deficient in Myosin1e (*Myo1e-/-*) were generated and kindly provided by the laboratory of Mira Krendel [133].

3.2.5.2 Generation of bone marrow chimeras

Bone-marrow chimeras were generated to examine the MYO1e-dependent immune cell recruitment *in vivo* and its function in B-cells.

Prior to radiation the mice were pre-treated 7 days with antibiotics (Neomycinsulfat, Polymyxin B-sulfat) administered orally by the drinking water. RAG1 KO mice for B-cell experiments were sublethally irradiated with a dose of 4 Gray (Gy) and PTPRC mice for *in vivo* immune cell recruitment with a lethal dose of 9 Gy. The reconstitution of mice with either WT or *Myo1e* KO bone marrow occurred 24 h upon treatment. In advance, the deep-frozen bone marrow from femur and tibias of one mouse per genotype was rapidly thawed at 37°C, washed in 20 ml ice cold HBSS, centrifuged and resuspended in 2 ml ice cold HBSS. Independent of the cell number 200 µl of the bone marrow was injected intravenously (i.v.) into each recipient mouse. 6-8 week upon bone-marrow transplantation mice were ready for experiments. During the whole process mice were kept under antibiotic treatment.

3.2.5.3 Utilization of bone-marrow chimeras

B-cells from RAG1 KO chimeras were isolated from spleen by a B220+ positive selection via magnetic cell sorting (MACS). Their purity was determined by FACS to be >93%.

Immune cell recruitment to the site of injection was examined in PTPRC chimeras using the congenic CD45.1/.2 marker to distinguish between donor and recipient cells. $4*10^7$ heat inactivated (20 min, 65°C) *E.coli* were injected intraperitoneal (i.p.). After 24 h mice were sacrificed and cells within the peritoneum were flushed out with 2 ml ice cold PBS. The total cell number in the lavage fluid was determined to finally calculate the number of migrated immune cell populations. Donor immune cell subsets were discriminate by FACS as CD45.1 negative and analyzed as listed in Table 15.

Table 15. FACS staining for immune cell subsets

immune cell subset	marker
monocytes	$Ly6G^{neg}$; $Ly6C^{pos}$; $CD11b^{pos}$
neutrophils	$Ly6G^{pos}$; $Ly6C^{pos}$; $CD11b^{pos}$
macrophages	$F4/80^{pos}$; $CD11b^{pos}$
pDCs	$CD11c^{pos}$; $PDCA^{pos}$; $MHC\text{-}II^{pos}$
NK cells	lymphocyte gate; $NK1.1^{pos}$
B-cells	lymphocyte gate; $B220^{pos}$
CD4 T-cells	lymphocyte gate; $CD3^{pos}$; $CD4^{pos}$
CD8 T-cells	lymphocyte gate; $CD3^{pos}$; $CD8^{pos}$

3.2.6 Statistical evaluation

For statistical evaluation Student's T test was performed with the parameters "2-tailed" (Seiten 2) and "unpaired with heterogeneous variances" (Typ 3). p-values below 0.05 were regarded as significant (*), below 0.01 (**) and 0.001 (***) were regarded as highly significant.

4 Results

A global and quantitative phosphoproteome analysis of TLR4 activated primary macrophages, done in our lab, identified more than 1800 phosphoproteins containing around 7000 phosphorylation sites. Further bioinformatic analysis pointed out the cytoskeleton as one cell organelle with enhanced protein phosphorylation [151]. In total, 44 cytoskeletal or associated proteins were reproducibly regulated by this post translational modification after LPS. A remarkable fast and strong phosphorylation of the actin polymerization factors ARP3 and FHOD1 was detected simultaneously to the regulation of capping and motor proteins like CAPZB or MYO18a and MYO1e (Fig. 5). Many of these proteins are described in fibroblasts, stable cell lines or model organisms like yeast, but their task in primary immune cells is mainly unknown. Based on these data, we started to investigate the role and function of TLR4-induced changes in cytoskeleton remodeling and related immune cell responses.

	LPS [100ng/ml]	
	15min	4h
Actr3 (Arp3)	88	95
Add1	6	5
Capzb	10	8
Coro1b	6	0
Dbn1	11	2
Epb4.1l1	5	5
Epb4.1l2	2	1
Eps8	6	5
Fhod1	55	10
Flna	2	8
Fmn1	19	0
Frmd4b	1	2
Hdac6	3	1
Inf2	1	1
Inppl1	13	0
Lcp1	10	9
Lima1	17	10
Lsp1	24	6
Marcks	6	5
Mib2	2	1
Mkl1	17	7
Mkl2	15	8

	LPS [100ng/ml]	
	15min	4h
Msn	1	4
Mtss1	9	5
Myh9	1	2
Myo18a	13	1
Myo1c	1	1
Myo1e	10	8
Myo1f	3	3
Myo5a	2	2
Myo9b	8	6
Palld	6	2
Phactr4	8	2
Plec1	1	2
Ppp1r9b	10	6
Pxn	3	5
Snta1	2	1
Spnb2	1	1
Svil	2	1
Tln1	2	2
Tmod3	6	9
Twf1	6	0
Vasp	8	4
Wipf1	6	3

Figure 5. Phosphorylated cytoskeleton-associated proteins detected in the phosphoproteome analysis of LPS treated primary MØ. Shown are intensities of the most strongly regulated phosphorylation site of each detected protein in response to 15 min and 4 h LPS stimulation Intensities are calculated by the ratio of stimulated to unstimulated condition. Listed are only proteins with the GO annotation “actin binding” or “cytoskeletal protein binding” and at least a 1,5-fold increase in any phosphosite by LPS. Detailed information with respect to multiple phosphorylation sites is publicly accessible at www.phosida.com. Numbers indicates the fold induction, additionally illustrated as heat map (red = strong; blue = weak induction).

4.1 TLR4 induced-cytoskeleton remodeling

4.1.1 Quantification of LPS-induced macrophage spreading

In order to investigate the control of TLR4-driven changes in cytoskeleton remodeling a quantitative readout system was needed. Therefore, we validated the spreading response of primary macrophages as measurable readout. Cell spreading was defined as the change in contact area of macrophages to the support material. To define the cell boarders against the background of the slide we visualized the cells by fluorescence microscopy. Therefore, CD11b staining of the macrophage cell surface was used to define the contact area to the slide and combined with DAPI staining of the nuclei to identify individual cells on the microscopy image (Fig. 6a-c). The spreading response of macrophages to LPS was examined in a kinetic analysis using time points between 1 h and 24 h. The stimulation was performed on Permanox slides with 100 ng/ml LPS. A first significant increase of the contact area was already observed 1h after cell treatment. The macrophages continued to spread and increased their contact size to roughly twice of their initial size after 24h. This was also observed to be the maximum in most of the experiments. To confirm that the spreading of primary macrophages was dependent on actin cytoskeleton and its LPS induced polymerization we used the actin polymerization inhibitor Cytochalasin D (CytoD). The cells were treated 1h prior to stimulation with 5 µg/ml of the inhibitor. The inhibitor treatment completely prevented macrophage spreading in response to LPS (Fig. 6d, e). These data confirmed that the activation of TLR4 by its antagonist LPS induces an actin polymerization-dependent remodeling of the cytoskeleton that finally results in macrophage spreading. Furthermore this experimental setup provided us the possibility to use the spreading readout for a more detailed analysis in order to investigate which of the cytoskeletal phosphoproteins and TLR4 signal cascades contributes in this context.

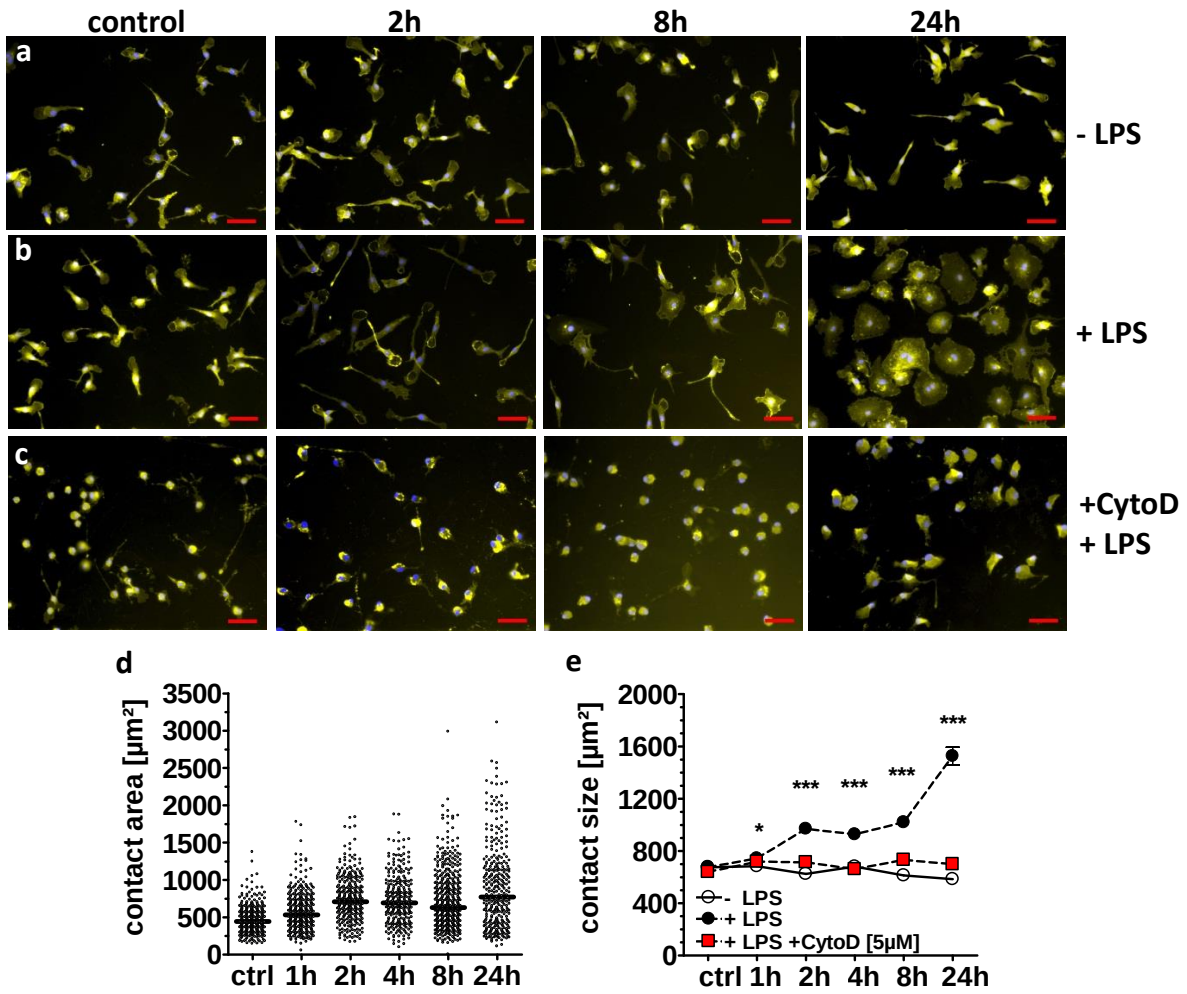

Figure 6. LPS induced spreading of primary macrophages. BMM were plated in eight-well chamber slides and rested over night before addition of LPS (100 ng/ml) .The inhibitor of actin polymerization Cytochalasin D (5 µg/ml) was added 1 h prior to LPS-stimulation. At the indicated time points after addition of LPS, slides were processed for staining of CD11b and nuclei, followed by fluorescence microscopy. **(a-c)** Representative images from control, 2 h, 8 h, and 24 h time points. Cells were imaged at 20x magnification. Scale bar = 50 µm. **(d)** Detailed quantification of cell spreading by manual annotation of CD11b staining. Each dot represents one single cell per condition. Black bars within the scatter plots show median contact area. **(e)** Comparative spreading representation. Shown are mean + SEM of at least 300 cells per condition. Media control (open circles), LPS (closed circles) and LPS in the presence of CytoD (red closed squares). Statistical significance refers to LPS-treated compared to untreated condition. Representative of 2 independent experiments with similar results * $p < 0.05$, *** $p < 0.0001$.

Manual annotation of contact areas from the fluorescence microscopy images is a very time consuming process. To perform experiments with multiple conditions in a feasible time frame and a less biased analysis it was necessary to develop an annotation software. In collaboration with the group of PD Dr. Thomas Wittenberg (Fraunhofer Institut Erlangen) a two-step segmentation algorithm was established and specifically adapted to this issue [152]. In a first step, the software annotates the DAPI stained nuclei of the imported images (Fig. 7a-c) by a watershed transform-based segmentation routine [153, 154]. Subsequently, this information is

used as an initialization point to annotate in a second step the cell boarder by a gradient magnitude based fast marching level set method [154, 155] (Fig. 7d-f). The results of the annotated cell boarder are highlighted, allowing quality control and manual editing by the user. For most cells the obtained automatic segmentation was found to be correct, but in case of overlapping cells some manual editing was required (arrows in Fig. 7e and f).

To test the accuracy and reliability of the automatic segmentation algorithm, we compared the distribution of contact areas of macrophages under resting and LPS-stimulated condition using automated tool segmentation versus manual annotation. Comparing image data from one single experiment we obtained very similar distribution of contact areas and median values in resting and early LPS-stimulated cells. At later time points the segmentation algorithm generated smaller values (Fig. 7g). To test whether this "shrinkage effect" was generic at later time points we extended the comparison analysis to a series of six experiments (Fig. 7h). Contact area values of resting cells and early (2 h) time points showed a consistently high agreement between software and manual annotation. At later time points the annotation difference got more striking and also "blow-up effects" were observed. Overall we observed a good agreement between results obtained by automated segmentation and manual annotation. Convinced that we had obtained an annotation software with capacity for high throughput analysis we used this system to investigate TLR4 driven macrophage spreading and its control by MAPK signaling as well as selected phosphoproteins.

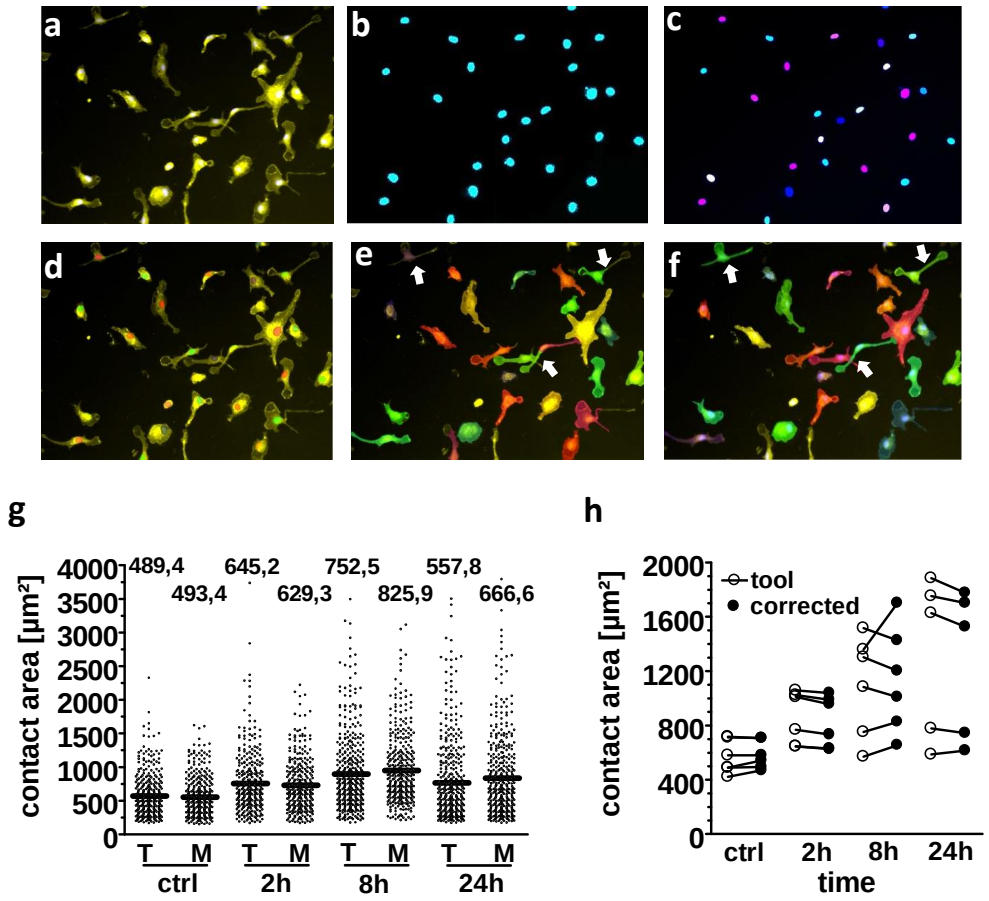

Figure 7. Validation of a semi-automatic quantification software. Segmentation and annotation of macrophages with two-step segmentation software. Fluorescence microscopy images of CD11b-APC and DAPI stained macrophages were uploaded into the software **(a)**, nuclear segmentation **(b-c)** and contact area annotation was performed by the tool **(d-e)** and finally checked and corrected by the user **(f)**. Arrowheads indicate shrinkage and blow-up effects requiring manual editing of the annotation. **(g)** Comparison of cell contact area measured automatically by the tool (T) versus manual annotation (M). Data are from one experiment. Each dot represents one cell. Black bars within the scatter blot show median contact area (numerical value indicated above). **(h)** Comparison of data obtained by annotation with tool (open circle) versus combination of tool and manual correction (closed circle) from six independent experiments. Each dot represents the median of at least 300 annotated cells.

4.1.2 MyD88 is required for macrophage adhesion after TLR4 activation

TLR4 requires adapter protein recruitment at its intracellular domain to induce signal mediation upon activation. One universal adapter protein is MYD88 that binds to almost all TLR family members leading to a change in gene expression and cytokine secretion. We employed macrophages with genetic deletions of *Myd88* to determine the control of LPS-induced cell spreading by this molecule. In comparison of *Myd88* knockout to heterozygous macrophages, we observed that the spreading response at the late 8 and 24 h time points was severely impaired in the absence of MYD88 (Fig. 8a) indicating that the adapter protein is essential for a late phase spreading response to LPS and to maintain cell shape. However, *Myd88* KO macrophages respond comparably to heterozygous control cells at the early 2 h

time point. This indicates that other signaling molecules (e.g. the adapter TRIF) may play an important role in cytoskeletal rearrangement after LPS. The effect of *Myd88*-deficiency on cytokine responses to LPS was examined using supernatants from the cultures used for cell spreading analysis. In the absence of MYD88, secretion of the pro-inflammatory cytokines TNF, IL-6 and IL-12p40 as well as of anti-inflammatory IL-10 was almost absent (Fig. 8b). The results revealed not only the requirement of the adapter protein in TLR4-driven cytokine response but also a contribution of MYD88 in LPS induced macrophage spreading.

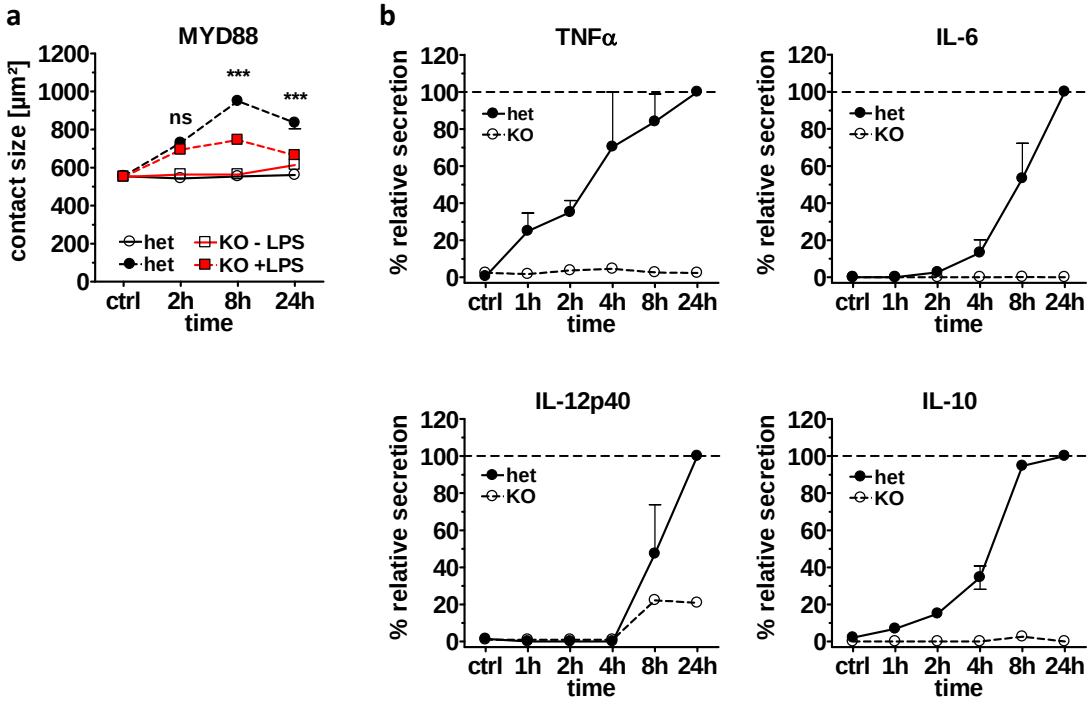

Figure 8. Contribution of MYD88 in MØ spreading and control of LPS induced cytokine secretion. (a) Phenotype of *Myd88* KO macrophages in cell spreading**.** Shown are mean and SEM from one representative experiment of two performed. LPS (closed symbols), media control (open symbol), *Myd88*± (circles), *Myd88*−/− (red squares). Statistical significance refers to *Myd88*± compared to *Myd88*−/− genotypes. **(b)** Supernatants of the cultures used for macrophage spreading analysis were analyzed by ELISA for the presence of the cytokines TNF, IL-6, IL-12p40, and IL-10. To normalize for differences between experiments in the absolute amount of cytokines produced, the maximum level of the LPS-treated WT or control macrophage in each experiment was set to 100% (shown as - - - -). Shown are mean + SD values from two independent experiments. ns=not significant;*** p <0.0001 n=2.

4.1.3 MAPK signaling in early and late phase spreading

MAPK pathways are some of the major and best described signal cascades in innate immune cells. Initiated by adapter protein recruitment to the transmembrane domain of the activated cell surface receptor, they mediate the signal in a hierarchical manner from the membrane through the cell, resulting in a change in gene expression and substrate protein activation. We

used primary macrophages with genetic deletion of p38 and pharmacological inhibition of the ERK1/2 kinase MEK1 to examine their role in macrophage spreading.

A possible contribution of the p38 MAPK was investigated using macrophages derived from the bone marrow of conditional *p38*-flox/flox; Mx-Cre mice [142] treated with poly I:C to induce deletion of *p38* (Fig. 9b). Deletion of p38 was very efficient in mice expressing Cre, p38 was undetectable. The conditional KO of p38 resulted in a strongly reduced phosphorylation of MK2, a substrate kinase downstream of p38. Initiation of ERK1/2 phosphorylation which appears very fast within 1 h after LPS stimulation is not influenced by the *p38* KO but a prolonged activation of ERK1/2 was apparent (Fig. 9b). The spreading response of primary macrophages was only weakly affected by the *p38* KO. Deficient macrophages showed a significantly, but moderately reduced initial spreading at 2 h after LPS stimulation. However, there was no difference detected between *p38* WT and KO cells at the late spreading phase 8 h and 24 h post stimulation (Fig. 9a). Examination of the TLR4-driven cytokine secretion in the supernatant of these cells showed that TNF was secreted simultaneous to IL-10 rapidly after LPS-stimulation, while the release of IL-6 and IL-12p40 was first measurable 8 hours upon macrophage activation. In absence of p38 TNF and IL-10 levels were decreased 40-60% during the time course, while in contrast IL-12p40 release was strongly increased. Secretion of IL-6 was not altered by p38 deletion (Fig. 9c). Taken together, the MAPK p38 appeared to be required for maximal initial spreading, but in contrast to the strong effects observed for *Myd88* deficiency, p38 was not involved at later time points. Furthermore, p38 MAPK signaling was necessary for an efficient TNF and IL-10 production but inhibited IL-12p40 secretion.

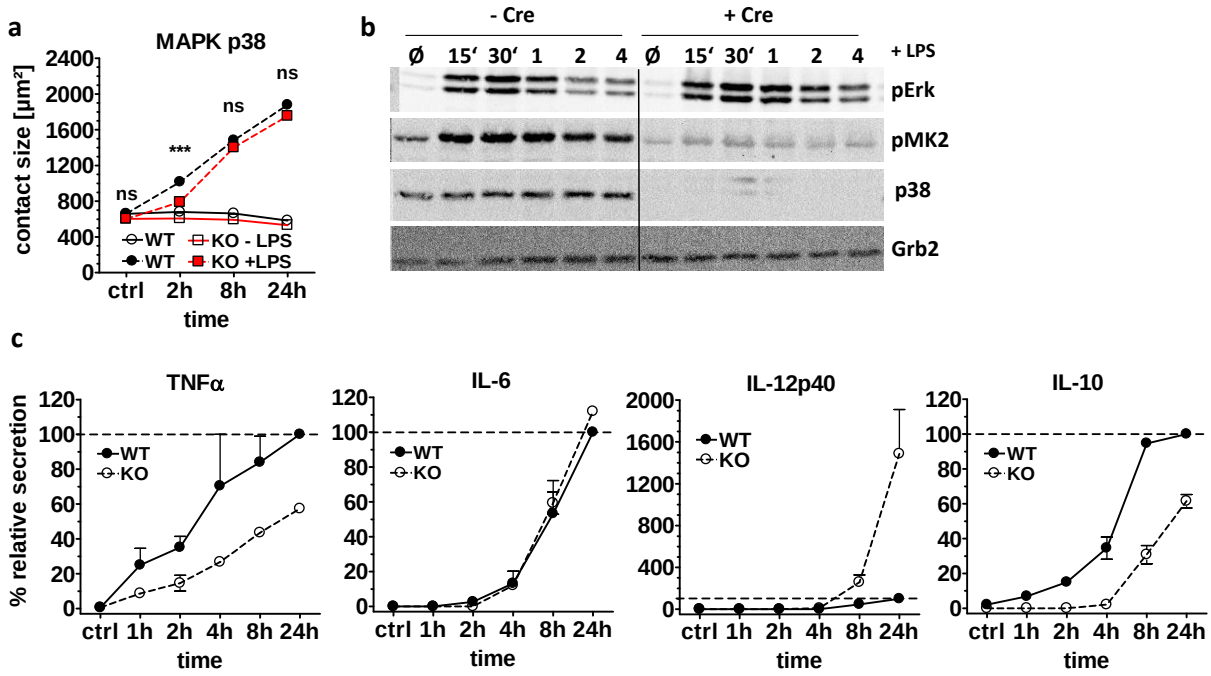

Figure 9. Reduced early spreading response and altered cytokine release of *p38* KO MØ. **(a)** Phenotype of *p38* KO macrophages in cell spreading**.** Shown are mean and SEM from one representative experiment of two performed. LPS (closed symbols), media control (open symbol), *p38* WT (circles), *p38*−/− (red squares). Statistical significance refers to *p38* WT compared to *p38* KO genotypes. **(b)** Western blot control for p38 protein levels and phosphorylation of MK2 and ERK1/2. Cell lysates were taken at indicated time points (15 min to 4 h) after LPS stimulation (100 ng/ml). Grb2: loading control. **(c)** Supernatants of the cultures used for macrophage spreading analysis were analyzed by ELISA for the presence of the cytokines TNF, IL-6, IL-12p40, and IL-10. To normalize for differences between experiments in the absolute amount of cytokines produced, the maximum level of the LPS-treated WT cells in each experiment was set to 100% (shown as - - - -). Shown are mean+SD values from two independent experiments. ns=not significant;*** p <0.0001 n=2

To address the role of ERK1/2 MAPK signaling in LPS-induced macrophage spreading, the second generation MEK1 inhibitor PD184352 was used. It has been reported to have a higher specificity than older reagents [156]. The pharmacological inhibitor PD184352 was added one hour prior LPS-stimulation to the culture, interfering with the up-stream kinase MEK1 to block ERK1/2 phosphorylation and signal mediation *via* this MAPK. Pretreatment of macrophages with PD184352 strongly reduced basal and LPS-induced phosphorylation of ERK1/2. An impact on p38 MAPK phosphorylation could not be observed (Fig. 10b). MEK1 inhibition had no effect on basal macrophage spreading compared to untreated cells, and did not show a significant difference in early spreading (2 h) after TLR4 activation. However, the further increase in the contact area at 8 h and 24 h time points was prevented (Fig. 10a). We also determined the cytokine release of PD184352 treated macrophages, indicating that MEK1 inhibition resulted in a 40-50% reduction of TNF and nearly blocked the IL-10 secretion. Also in the supernatant we determined strongly increased amounts of IL-6 and IL-

12p40 at the late 24 h time point (Fig. 10c). In summary, blocking ERK1/2 signaling caused a reduction of the macrophage spreading 8 h and 24 h after LPS-simulation, similar to the effect of *Myd88* deficiency, and showed also important contribution in cytokine response of TLR4 activated macrophages.

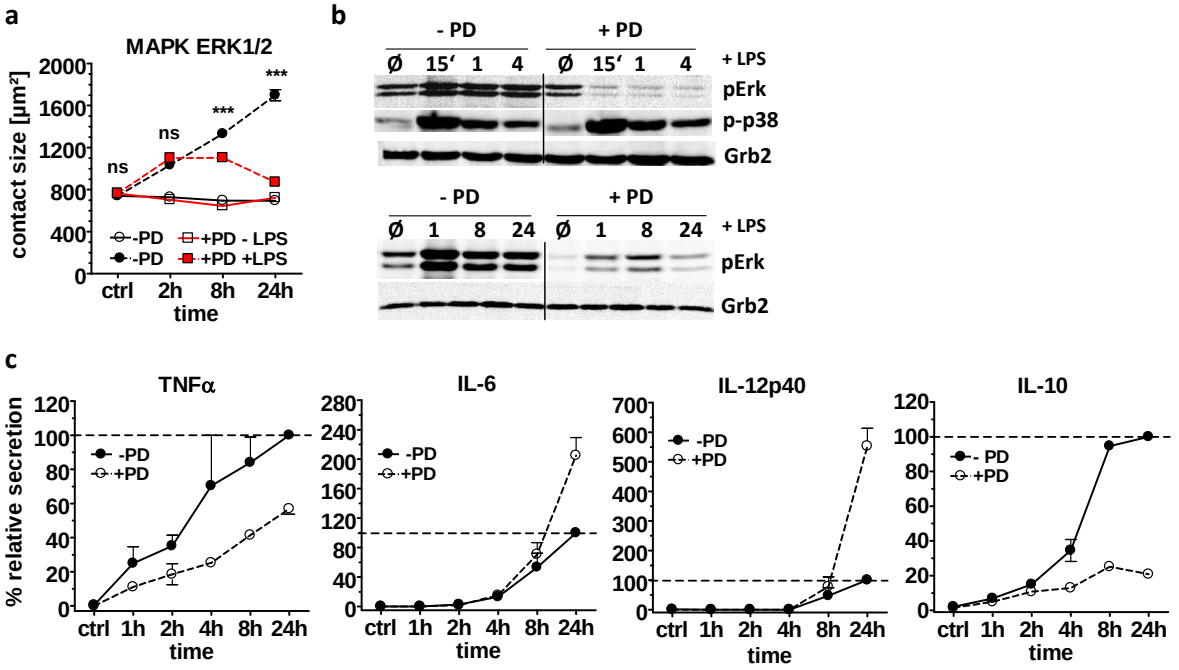

Figure 10. ERK1/2 signaling is essential for late phase spreading response. (a) Effect of pharmacological blockade of ERK1/2 activation on macrophages spreading. Cells were pre-treated with MEK1 inhibitor PD184352 (10 µM, squares) or not (circles) 1 h prior to LPS addition (closed symbols) or media control (open symbols). Shown are mean+SEM of at least 300 cells per condition. Statistical significance refers to PD184352 treated compared to no inhibitor. **(b)** Western blot control for ERK1/2 and p38 phosphorylation. Cell lysates were taken at indicated time points (15 min to 24 h) after LPS stimulation (100 ng/ml). Grb2: loading control. **(c)** Supernatants of the cultures used for macrophage spreading analysis were analyzed by ELISA for the presence of the cytokines TNF, IL-6, IL-12p40, and IL-10. To normalize for differences between experiments in the absolute amount of cytokines produced, the maximum level of the LPS-treated non inhibitor control macrophage in each experiment was set to 100% (shown as - - - -). Shown are mean + SD values from two independent experiments. ns=not significant;*** p <0.0001 n=2.

4.1.4 DUSP1 and DUSP16 in LPS induced cytoskeleton remodeling

Dual-specific phosphatases (DUSP) are endogenous negative regulators of intracellular signal pathways. Eleven DUSP gene family members are MAPK phosphatases (MKP) because they habor a MAPK binding domain allowing them to interact with one or more members of the MAPK family (p38, ERK1/2 and JNK) [37, 157]. DUSP1 and DUSP16 are both MKP and show preference for binding to and inactivating p38 and JNK, respectively. We previously observed an essential and time dependent contribution of ERK1/2 and p38 signaling in cytoskeletal remodeling as well as cytokine secretion in TLR4-activated macrophages. Whether these processes are possibly regulated by DUSPs has not been studied. To address

this issue we employed primary macrophages deficient either for *Dusp1* or *Dusp16*, determining the LPS-induced spreading response and cytokine secretion. Both genotypes showed a similar TLR4-driven early spreading response (2 h) comparable to the WT and control cells. However, KO macrophage spreading was significantly affected throughout the late phase, 8 to 24 hours. While *Dusp*1 as well as *Dusp*16 KO cells showed a similar 20% reduction in the contact areas 8 h after stimulation, the difference was more striking in *Dusp*16 KO macrophages at the 24 h time point (Fig. 11a and c). Compared to WT macrophages, *Dusp*16 KO cells showed a 40-50% decrease in contact size indicating a more crucial contribution of DUSP16 in LPS induced spreading (Fig. 11c). Observation on cytokine secretion revealed a divergence of both DUSPs in IL-10 and IL-12p40 release. Macrophages deficient for *Dusp*1 showed an increased IL-10 secretion and a severely reduced IL-12p40 release in response to TLR4 activation (Fig. 11b). Contrary results were obtained under *Dusp*16 deficient conditions. These macrophages secreted 40% less IL-10, however strikingly more IL-12p40 after LPS stimulation (Fig. 11d). In case of TNF and IL-6 secretion no difference in the KO cells compared to the WT situation was detected. Taken together, the results indicated a contribution of DUSP1 and DUSP16 in TRL4-driven macrophage spreading as well as IL-10 and IL-12p40 production, possibly caused by dysregulation of MAPKs signaling.

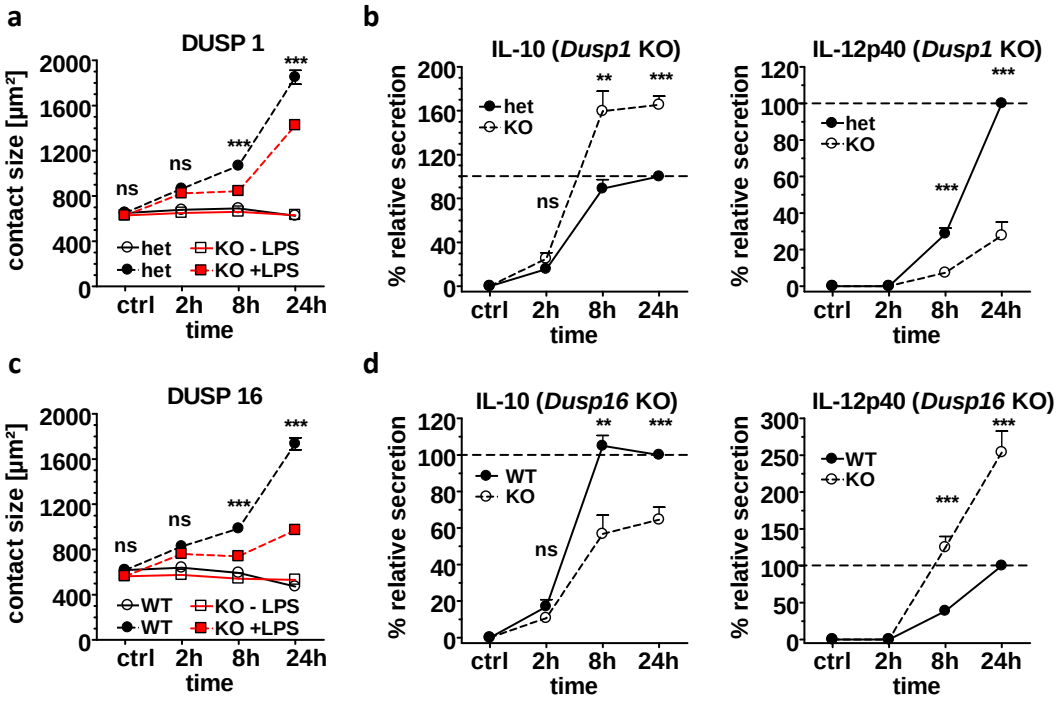

Figure 11. A role of Dual-specificity phosphatases (DUSP) in MØ spreading and cytokine secretion. (a) Phenotype of *Dusp1* KO macrophages in cell spreading**.** Shown are mean and SEM from one representative experiment of three performed. LPS (closed symbols), media control (open symbol), *Dusp1*+/− (circles), *Dusp1*−/− (red squares). Statistical significance refers to KO compared to *Dusp1* heterozygous genotypes. **(b)** Supernatants of the cultures used for macrophage spreading analysis were analyzed by ELISA for the presence of the cytokines IL-10 and IL-12p40. To normalize for differences between experiments in the absolute amount of cytokines produced, the 24h time point of the LPS-treated control cells in each experiment was set to 100% (shown as - - - -). **(c, d)** Phenotype of *Dusp16* KO macrophages in cell spreading and cytokine secretion. Legends and statistical analysis as described for (a) and (b). ns=not significant; ** p <0.001, *** p <0.0001 n=3.

4.1.5 Validation of siRNA KD to investigate cytoskeletal phosphoprotein function

We next were interested to functionally analyze the role of LPS-regulated phosphoproteins associated with the cytoskeleton in macrophage spreading. We therefore combined our previously developed automatic quantification software with a specific siRNA knock down of selected cytoskeletal proteins in primary macrophages. This approach allowed us to determine the function of candidate proteins in LPS-induced cytoskeleton remodeling by measuring the cell spreading response. Based on three criteria, candidate proteins were selected. First, the intensity of the detected phosphorylation in the phosphoproteome analysis, meaning the fold induction of a phosphosite after LPS stimulation compared to the unstimulated condition. Second, the reproducible detection of a phosphosite in repeated experiments, and third whether the detected phosphoproteins have already been described in the literature or not. For a first screen we chose seven proteins ACTR3 (ARP3), FMN1, FHOD1, CORO1b, MTSS1, LSP1, EPS8 and performed specific siRNA knockdown, with an efficiency of 50 – 85%

reduction in their mRNA levels. As positive control we used ACTR3 (ARP3) which was strongly phosphorylated in response to TLR4 activation. Interacting with ARP2 it builds the actin polymerization factor ARP2/3 which is one of the best described in a broad variety of cell types. Knockdown (KD) of ACTR3 (ARP3) with an efficiency of 85% on mRNA level resulted in an initially smaller contact size between cells and the supported material as well as a strikingly reduced spreading throughout the whole time course compared to LPS-stimulated macrophages treated with an unspecific non-targeting control RNA (Fig. 12a). KD of FMN1 and FHOD1, actin polymerization factors of the formin family, did not result in an altered spreading phenotype although a good KD efficiency with 85% for FMN1 and 60% for FHOD1 were reached (Fig. 12b and c). The Knockdown of the ARP2/3 antagonist CORO1b, which induces actin disassembly and inhibition of the ARP2/3 complex known in mast cells, fibroblasts and yeast [158-161], resulted in altered and finally increased contact size at the very late spreading phase 24 h post LPS addition (Fig. 8d). The KD efficiency reached in this case was 50%. The Knockdown of other cytoskeletal phosphoproteins like MTSS1 (KD ~ 90%), LSP1 (KD ~ 85%) and EPS8 (KD ~ 60%) did not alter LPS-induced macrophage spreading in such a severe manner indicating that these proteins do not participate in the cell spreading response but may support other cytoskeletal associated cell functions like e.g. endo- and exocytosis or migration processes (Fig. 12e-g).

These knockdown experiments serve as a starting point for a siRNA screen of further selected cytoskeletal proteins. Furthermore these techniques provide the possibility to get insight which phosphoproteins actually contribute in cytoskeletal rearrangement and adhesion processes.

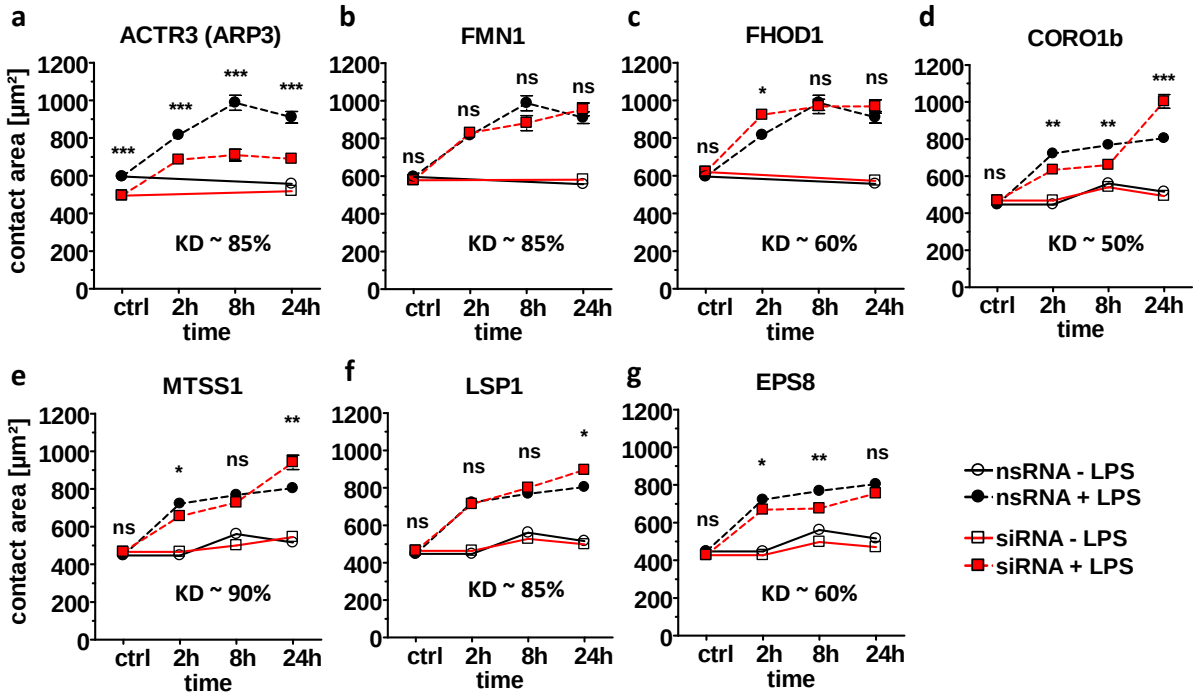

Figure 12. siRNA KD of selected cytoskeletal associated phosphoproteins. Spreading phenotype of siRNA treated macrophages. Differentiated primary macrophages were electroporated with specific siRNA for selected cytoskeletal proteins 48h prior LPS stimulation [100 ng/ml]. Contact area quantification of **(a)** ACTR3 (ARP3), **(b)** FMN1, **(c)** FHOD1, **(d)** CORO1b, **(e)** MTSS1, **(f)** LSP1 **(g)** EPS8 siRNA treated cells was measured by automatic segmentation software with subsequent manual correction. Shown are mean + SEM of at least 300 cells per condition. Media control (open symbols), LPS (closed symbols), non-silencing control RNA treated cells (circles), specific siRNA treated cells (red squares). Statistical significance refers to nsRNA treated LPS stimulated control cells compared to siRNA treated LPS stimulated cells. Knockdown efficiency was determined by qRT-PCR shown as KD within the graphs. ns=not significant; * p <0.05, ** p <0.001, *** p <0.0001 n=1-2.

4.2 Function of the Class I Myosins MYO1e and MYO1f in macrophages and DCs

Among the group of LPS-regulated cytoskeletal phosphoproteins, several class I myosins were identified. These proteins are able to interact simultaneously with actin filament and proteins or membranes and thus might play an important role as transport proteins regulating TLR4-driven macrophage immune response. Our research was aimed on the role of the two "long-tailed" motor proteins myosin1e (MYO1e) and myosin1f (MYO1f), because of their strong LPS-induced phosphorylation. In contrast to their other six family members they contain an additional SH3 domain at the N-terminus. The phosphosites detected in our phosphoproteome analysis were localized in the tail region of the proteins, mainly within the TH2 domain apart from a single one within the PH domain. Both myosins possess a similar phosphorylation pattern except of an additional phosphorylation at S1023 on MYO1f (Fig. 13a). A regulation of the motor proteins by this posttranslational modification occurs

very fast within the first 15 minutes after LPS stimulation and was still detectable after 4 h in our study of the macrophage phosphoproteome. Comparing both myosins MYO1e revealed a stronger phosphorylation within the TH2 domain compared to MYO1f (Fig. 13b). The functions of the single phosphorylation sites are still unknown and remain to be clarified.

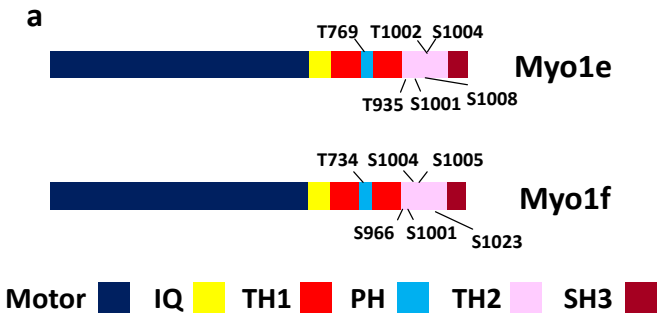

b

Myo1e	15min	4h
T769	0,74	-
T935	-	3,96
S1001	10,74	8
T1002	7,78	8,56
S1004	9,74	8
S1008	7,21	8

Myo1f	15min	4h
S734	1,34	2,39
S966	3,04	3,37
S1001	2,04	1,68
S1004	2,12	1,67
T1005	2,12	1,67
S1023	1,24	1,41

Figure 13. TLR4 activation induces phosphorylation of Myosin 1e and 1f in primary MØ. (a) Schematic illustration of MYO1e and MYO1f with single protein domains. Highlighted are the LPS-induced phosphorylation sites detected in our own phosphoproteome analysis. **(b)** Intensity of single phosphosites regulated in response to 15 min and 4 h LPS stimulation. Intensities are calculated by the ratio of stimulated to unstimulated condition.

4.2.1 Essential role of MYO1f in macrophage spreading

To test for a possible contribution of the motor protein MYO1f to TLR4-driven macrophage spreading and adhesion, specific siRNA knockdown was performed. Targeting MYO1f by a pool of four specific siRNAs, a knockdown efficiency of around 60% compared to control cells could be detected in primary macrophages. Macrophages not treated with any siRNA exhibited only a weak regulation of *Myo1f* mRNA expression in response to LPS. A slight decrease 2 h after stimulation followed by a subsequent modest increase until 24 h was detected. Transfecting siRNA into the cells did not influence the mRNA expression of *Myo1f* confirmed by the use of nsRNA (Fig. 14a). Macrophages expressing lower *Myo1f* mRNA levels showed a significantly decreased basal contact area. While the initial spreading occurred, MYO1f KD macrophages failed to increase their contact area throughout continuing LPS stimulation until 24h. Comparing the results to the spreading behavior of control cells indicated a requirement of MYO1f in this context (Fig. 14b).

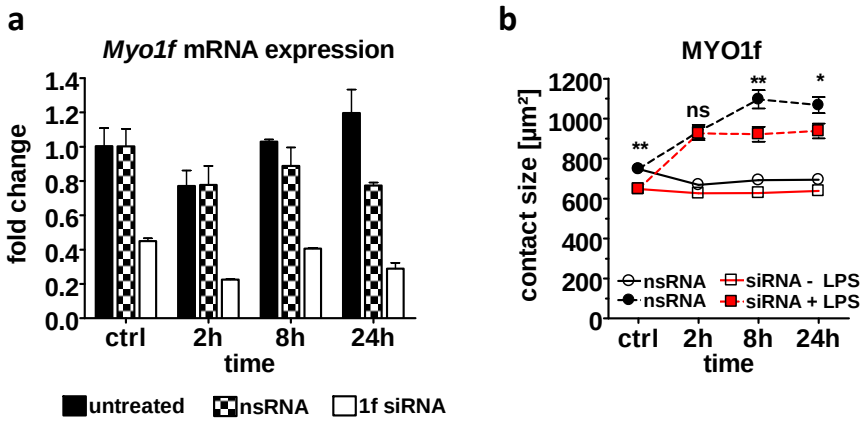

Figure 14 A role of phosphorylated MYO1f in MØ spreading. Spreading behavior of primary macrophages treated with specific siRNA for MYO1f KD in response to LPS [100 ng/ml]. **(a)** Differentiated primary macrophages were electroporated with specific siRNA for *Myo1f* 48 h prior LPS stimulation. mRNA expression levels and KD efficiency was determined by qRT-PCR. Gene expression was normalized to the expression of the "house-keeping gene" HPRT and fold changes were calculated to the unstimulated WT condition. In case of *Myo1f* KD the fold changes were calculated to the nsRNA treated unstimulated control cells. **(b)** Macrophage spreading was measured by automatic segmentation software with subsequent manual correction. Shown are mean + SEM of at least 300 cells per condition. Media control (open symbols), LPS (closed symbols), non-silencing control RNA treated cells (circles), *Myo1f* siRNA treated cells (red squares). Statistical significance refers to nsRNA treated LPS stimulated control cells compared to siRNA treated LPS stimulated cells. ns=not significant; * p <0.05, ** p <0.001 n=3.

Primary macrophages differentiated from bone marrow of mice with a genetic deletion in *Myo1e* were employed to continue our investigation on how these motor proteins contribute to macrophage spreading. Western blot analysis from lysates of *Myo1e* deficient macrophages confirmed the knockout (Fig. 15a). Quantifying the change in contact area *Myo1e* KO macrophages exposed a significant but modest reduction in TLR4-driven cell spreading compared to WT cells (Fig. 15b). The protein sequence homology of 71% and the presumably similar structure of both murine "long-tailed" class I myosins, redundancy effects could not be excluded. Therefore, we applied a *Myo1f* siRNA knockdown in primary *Myo1e* knockout macrophages to generate "double-deficient" cells. Determination of *Myo1e* and *Myo1f* mRNA expression by qRT-PCR under this condition did not show a compensatory up-regulation of *Myo1e* and *Myo1f*, respectively (Fig. 15c). A significant reduction in the basal contact area was measured under both conditions. Single-deficient *Myo1e* KO macrophages induced to spread, reaching a contact size similar to the control cells 8 h and 24 h after LPS stimulation. However, additional knockdown of *Myo1f* in *Myo1e*-deficient bone marrow macrophages resulted again in a significantly decreased phenotype throughout LPS stimulation, indicating that MYO1f is the major "long-tailed" class I myosin required in TLR4-driven macrophage spreading (Fig. 15d).

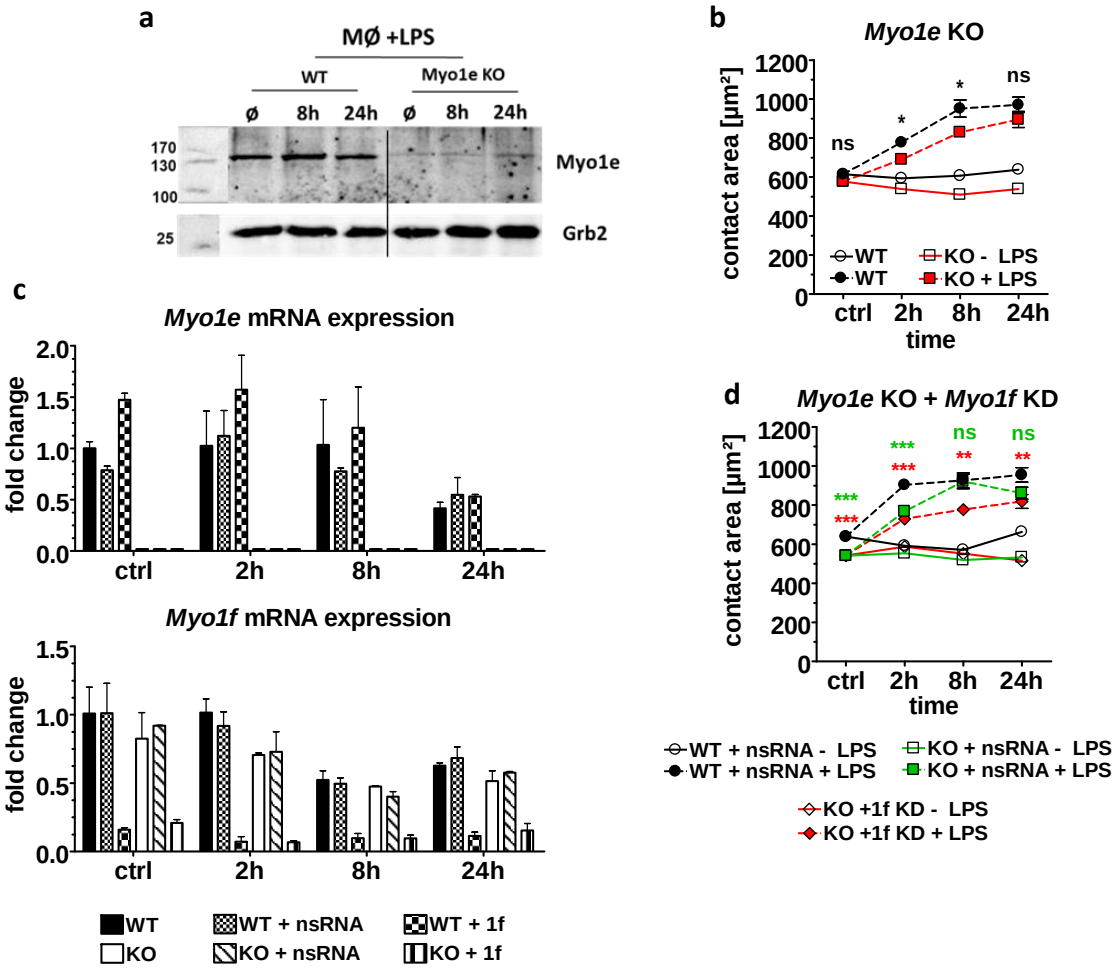

Figure 15. Differential role of Myosin 1e and 1f in MØ spreading. (a) Western blot control for *Myo1e* KO. Cell lysates taken at indicated time points after LPS stimulation [100 ng/ml]. Grb2: loading control. **(b)** Spreading behavior of primary *Myo1e* KO MØ in response to LPS. **(c)** Generation of "double-deficient" cells by *Myo1f* siRNA KD in *Myo1e* KO macrophages. Expression of mRNA levels and KD efficiency was determined by qRT-PCR. Fold changes were calculated to the unstimulated WT condition and in case of *Myo1f* KD to the nsRNA treated unstimulated control cells. **(d)** Spreading behavior of MYO1e single- (green) and MYO1e and 1f double-deficient macrophages (red). Spreading was measured by automatic segmentation software with subsequent manual correction. Shown are mean+SEM of at least 300 cells per condition. Statistical significance refers to WT or nsRNA treated LPS stimulated control cells compared to KO or siRNA treated LPS stimulated cells. ns=not significant; * p <0.05, ** p <0.001, *** p <0.001 n=3.

The spreading process is not exclusively dependent on the actin network. Regulation of this mechanism is simultaneously mediated by integrins, building a bridge between the extracellular matrix (ECM) and the actin cytoskeleton. Analysis of integrin expression on *Myo1e* KO MØ was performed to identify a possible contribution in this context, as it is known for example from MYO1f in β2-integrin surface expression on neutrophils [118]. Functional integrins are assembled by interaction of a α- and β-subunit whereas the β-subunit constitutes the essential domain. Thus expression of the MØ relevant β-integrins CD18, CD29 and CD61 was analyzed in response to LPS. CD29 and CD18 expression was up-regulated

after TLR4 activation while CD61 were even slightly down regulated. An increase of 40% compared to basal condition in CD18 expression was already observed after 8 h and remained at this level throughout LPS stimulation. Alterations in β-integrin expression caused by the lack of MYO1e were not observed (Fig. 16a). Hence, the expression of the α-integrins CD11a, CD11b and CD11c was determined and revealed only a modest TLR4-driven increase. All α-integrin subunits were already expressed in remarkable amounts on macrophages (Fig. 16b). These results indicate no contribution of MYO1e in surface expression of the integrin on primary LPS-stimulated macrophages.

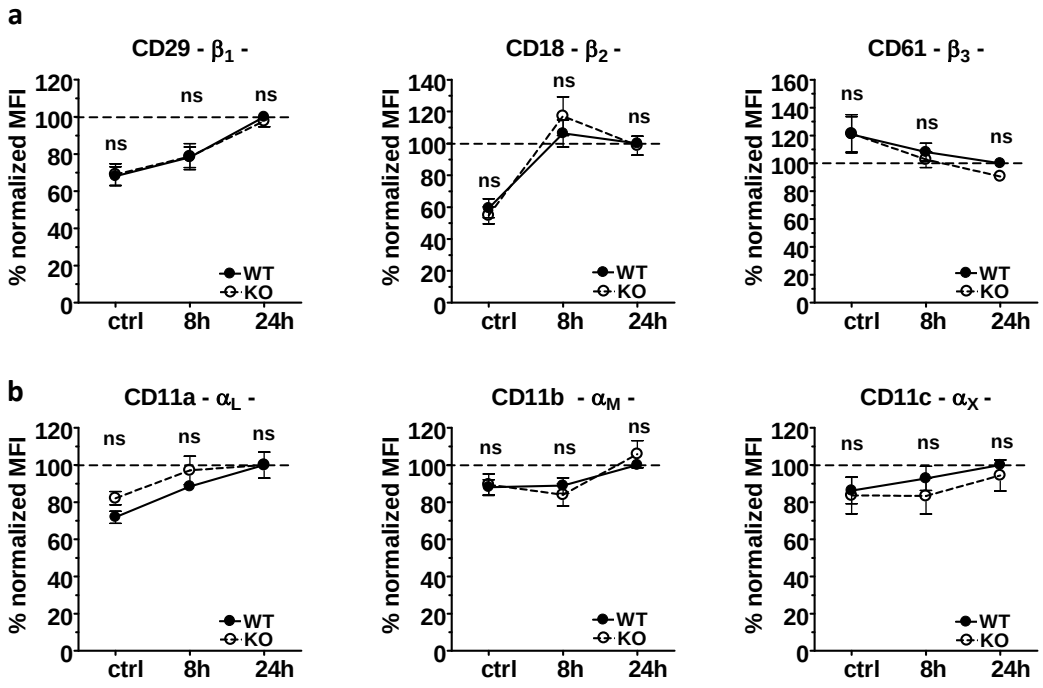

Figure 16. LPS induced integrin expression on *Myo1e* KO MØ. FACS analysis of integrin expression on primary WT (closed circles) or *Myo1e* KO (open circles) macrophages. Cells were stimulated with LPS [100 ng/ml] for indicated time points. **(a)** Expression of $\beta_{1\text{-}3}$-integrin subunits CD29, CD18 and CD61. **(b)** Expression of $\alpha_{L,M,X}$-integrin subunits CD11a, CD11b and CD11c. To normalize for differences between experiments in the absolute MFI, the 24 h time point of WT condition in each experiment was set to 100%. Shown are mean + SEM. n=3 ns = not significant

4.2.2 MYO1e in *in vivo* immune cell recruitment

Based on our observed class I myosin dependent spreading phenotype and the published evidence of migration abnormality in *Myo1f* KO neutrophils, we addressed the question whether the *Myo1e* KO affects the recruitment of immune cells to the site of heat killed *E. coli* injection. *Myo1e* KO or C57BL/6 control bone marrow cells were used to generate radiation chimeras. The CD45.1/2 congenic markers allowed to determine reconstitution efficiency and to gate on CD45.1-negative donor-derived cells. As a source of LPS, $4*10^7$

heat inactivated *E.coli* were injected intraperitoneally into mice and immune cells in the peritoneal lavage fluid were analyzed by FACS 24 h post injection. Determination of the total cell number revealed a significant increase within the peritoneum of *E.coli* challenged KO chimeras although a difference in untreated mice was not observed (Fig. 17a). Identification of cell subsets was done to determine whether the recruitment of specific populations was regulated by MYO1e. The major population found at the site of infection after 24h were PMNs followed by B-cells and macrophages (Fig. 17b). However, the previously observed increase in the total cell number was not caused by a specific immune cell population, because the mean numbers of all analyzed cell types were higher in *Myo1e* KO chimeras, even though this difference was significant only for NK cells.

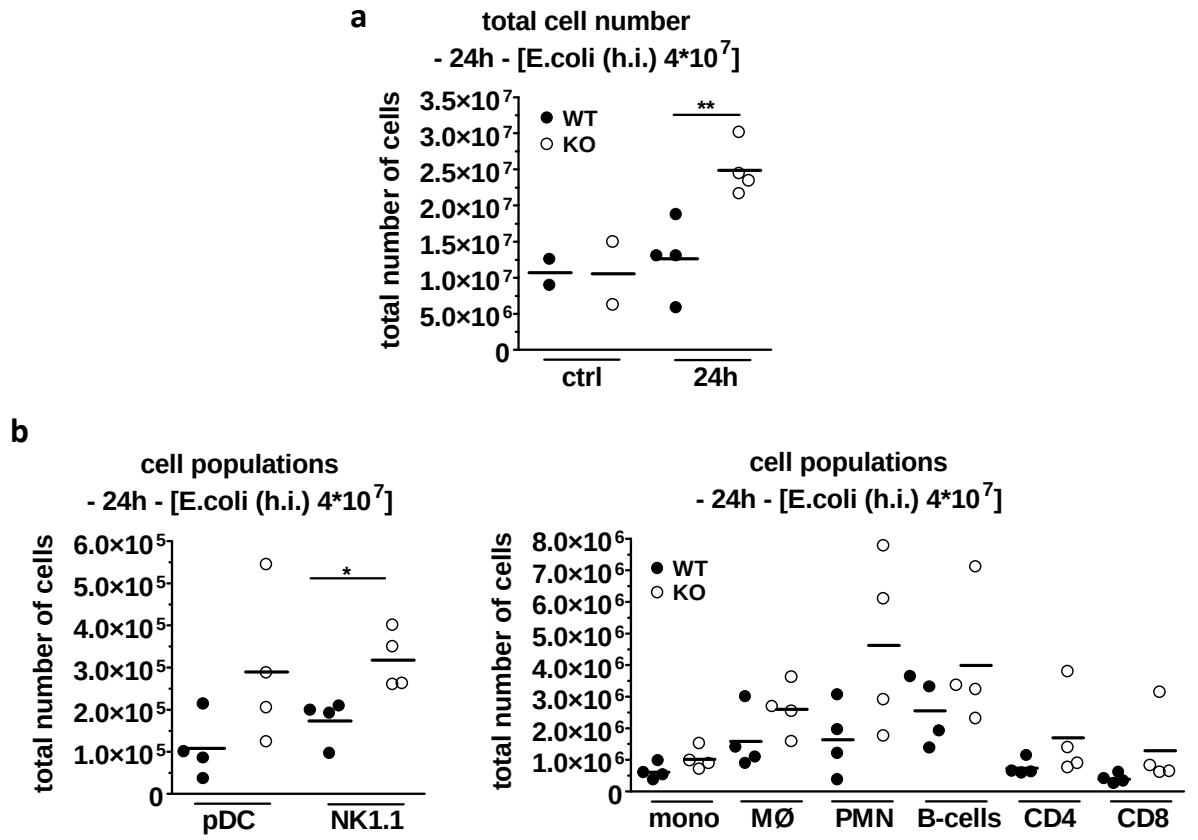

Figure 17. Enhanced immune cell recruitment to site of infection (*in vivo*). Lethally irradiated PTPRC mice were reconstituted with WT (closed circles) or *Myo1e* KO (open circles) BM. $4*10^7$ h.i. *E.coli* were injected i.p. and immune cell population in peritoneal lavage fluid 24h after mice treatment analyzed by FACS.**(a)** Total cell counts in untreated and *E.coli* treated WT and *Myo1e* KO chimeras. **(b)** Counts of immune cell populations analyzed by FACS after 24h *E.coli* challenge. Gated on CD45.1 negative cells for pDCs, NK-cells, monocytes, macrophages, PMNs, B-cells, CD4 and CD8 T-cells (used cell markers see in material and methods). Dots represent one mouse (4 treated mice per genotype). Bars represent MEAN. Statistical significance was determined by student's t-test. * p <0.05,** p <0.001

4.2.3 Selectively increased CCL2 secretion in primary *Myo1e* deficient macrophages

The cytokine response of activated macrophages is strongly regulated and controlled at various levels, starting from the induced mRNA transcription until the point of release from the cell surface. Cytokines synthesized in response to TLR4 activation need to be guided from the nuclear periphery through the cytoplasm towards the cell membrane where they finally get secreted in an organized manner. The cytoskeleton is one important cell organelle which allows such an active transport. To address the possible contribution of the motor protein MYO1e in this dynamic process, cytokine and chemokine secretion in the supernatants of LPS stimulated primary macrophages were analyzed. The pro- and anti-inflammatory cytokines TNF and IL-10 were both again secreted rapidly after LPS-stimulation while the release of IL-6 and IL-12p40 (data not shown) was first measurable 8 and 24 hours upon macrophage activation. The deficiency of MYO1e did not affect their release (Fig. 18a). However, extension of the supernatant analysis to the spectrum of chemokines revealed a contribution of MYO1e in the secretion system. Primary macrophages of both genotypes secreted a constitutive amount of CCL2 in a range of 200 to 800 pg/ml under basal culture condition which accounts for approximately 10% of the maximum released in response to LPS. Already 8 h after stimulation an increased CCL2 secretion of 50% in *Myo1e* KO macrophages was detected compared to WT cells. Up to 14 ng/ml of CCL2 were detected in TLR4-activated *Myo1e* KO macrophage cultures. The chemoattractant CCL4 was also measurable under basal conditions in a magnitude of 300 to 500 pg/ml and already peaked at 8 h post stimulation with concentrations of 45 to 50 ng/ml, keeping this level constant until 24 h under WT conditions. In contrast, macrophages lacking the motor protein MYO1e were also able to secret high amounts of CCL4 but compared to WT cells in a delayed manner. Differences of 25% reduction were detected at 8 h time points whereas 24 h after LPS addition KO cells aligned to concentrations detected in WT situations. A significant divergence in the secretion of other chemotactic agents like IP-10 (data not shown) was not detected in TLR4-activated primary macrophages (Fig. 18b).

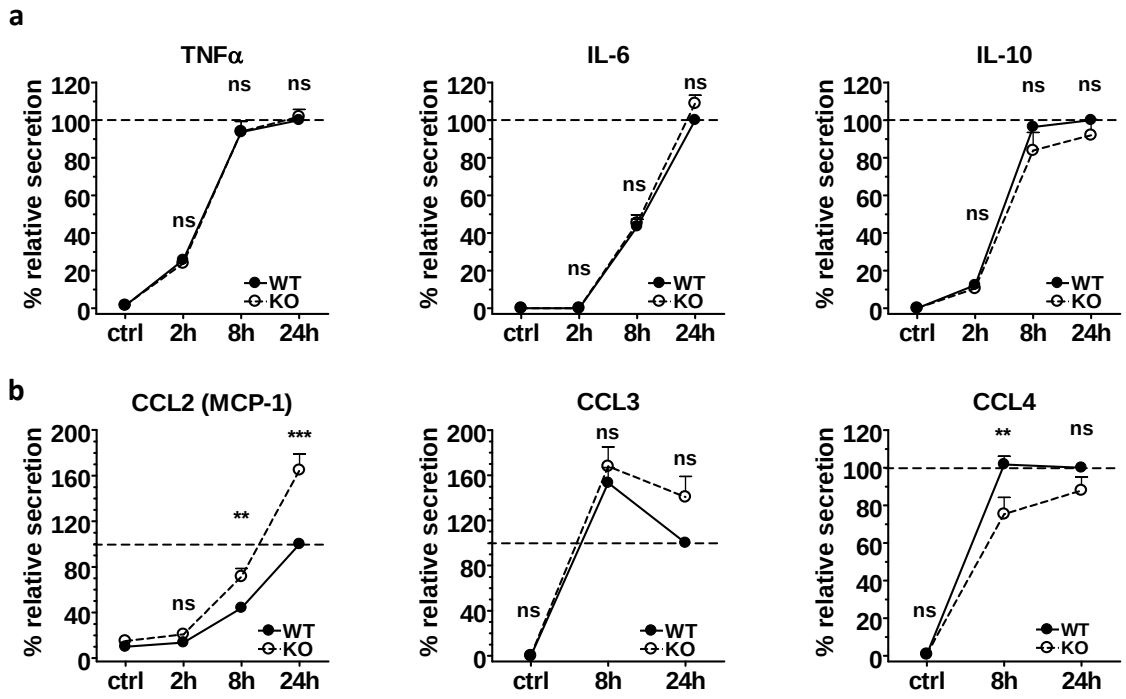

Figure 18. Alteration of chemokine secretion in activated *Myo1e* KO macrophages. Supernatants of the cultures were analyzed by ELISA for the presence of **(a)** cytokines and **(b)** chemokines. To normalize for differences between experiments in the absolute amount, the 24h time point of the LPS-treated control cells in each experiment was set to 100% (shown as - - - -). Shown are mean + SEM. ns=not significant; ** p <0.001,*** p <0.0001 n=5-7.

Induction of cytokine and chemokine biosynthesis as well as their release from immune cells is controlled by a variety of signaling cascades triggered by the activation of expressed receptors. The most prominent and fast-acting TLR4-driven pathways are mediated by MAPK like p38 and ERK1/2. Whether the observed change in CCL2 and CCL4 secretion was due to an aberrant MAPK signaling as an effect of the *Myo1e* KO was examined by Western blot analysis. Both kinases were constitutively expressed in comparable amounts in WT and KO macrophages. Stimulation with LPS induced a typical rapid ERK1/2 and p38 phosphorylation within the first 30 min which attenuated already after 1 h until the later time points except of p38 which showed re-phosphorylation 24 h post stimulation. Independent from the genotype both MAPK pathways were activated to the same extent (Fig. 19).

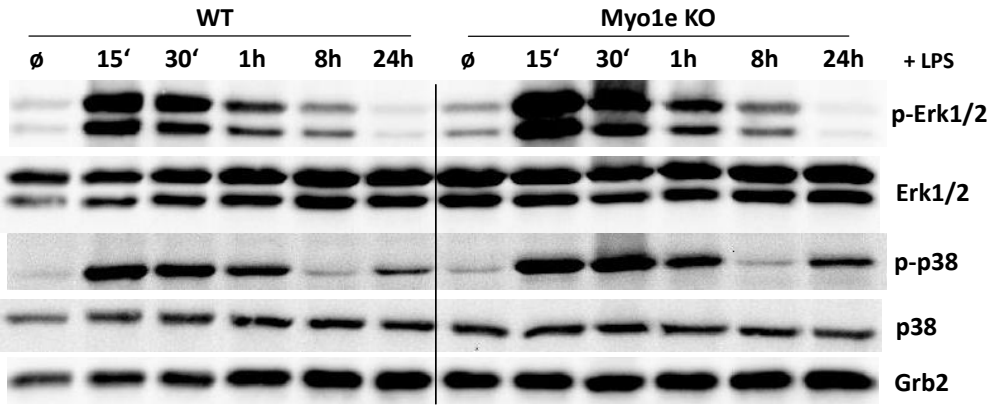

Figure 19. MAPK signaling in activated *Myo1e* KO macrophages. Western blot for ERK1/2 and p38 phosphorylation. Cell lysates were taken at indicated time points (15 min to 24 h) after LPS stimulation (100 ng/ml). Grb2: loading control

Furthermore, to investigate whether the increased CCL2 secretion resulted from a change in transcriptional levels, we determined its mRNA expression in TLR4 activated macrophages by quantitative RT-PCR. Primary macrophages already expressed *Ccl2* mRNA in comparable amounts to the "house-keeping" gene HPRT, acting as control expression gene independent of LPS stimulation. Activation of cultured macrophages induced a 90 - 130 fold increase in the mRNA expression of this chemoattractant 8 h post stimulation. This peak of mRNA induction was subsequently reduced to a 60 – 70 fold change 24 h after LPS addition compared to media control (Fig. 20). The regulation of *Ccl2* expression on the transcriptional level was not altered by the *Myo1e* KO, indicating that MYO1e does not participate in signal transduction from the activated TLR4 receptor to the nucleus but in transport and secretion processes of synthesized chemokines in primary macrophages.

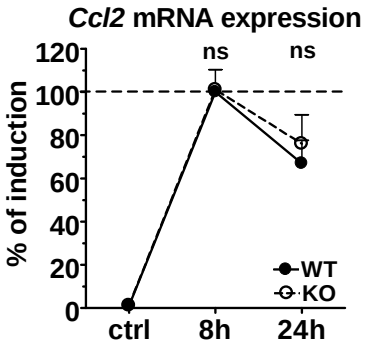

Figure 20. *Myo1e* KO does not influence *Ccl2* mRNA expression. WT and *Myo1e* KO MØ were stimulated with LPS [100 ng/ml] and *Ccl2* mRNA expression was determined by qRT-PCR. To normalize for differences between experiments in the fold changes, the maximum fold change of LPS-treated WT cells in each experiment was set to 100% (shown as - - - -). Detection of the house-keeping gene HPRT occurs at C_T values of 22-23 while basal *Ccl2* expression was measured at C_T = 23-24. Shown are mean + SEM. ns = not significant; n=6.

4.2.4 Increased CCL2 secretion phenotype in *Myo1e* KO dendritic cells

Aside from macrophages a highly important cell type of the innate immune system are dendritic cells. Based on the literature, describing the expression of MYO1e also in DCs [118] further investigations should identify a possible contribution of the motor protein to

chemokine secretion by this cell type. Comparable to primary macrophages, supernatants of GM-CSF derived bone marrow DC were analyzed for cytokine and chemokine secretion in response to LPS. Dendritic cells were also a very potent source of TLR4-induced cytokines. TNF was the only detected cytokine that peaked already 8 h after cell activation in a range of 4-6 ng/ml which was slightly reduced until 24 h time points. Compared to primary macrophages dendritic cells displayed a non-simultaneous release of IL-10 and TNF. Only 40% of the maximum amount (1,0 - 1,5 ng/ml) was reached after 8 h of the anti-inflammatory cytokine IL-10. Interestingly DCs lacking the class I myosin secreted almost doubled amounts of IL-6 compared to WT cells; although there were high variations between single experiments this difference was still significant indicating an engagement of MYO1e in cytokine release by this cell type (Fig. 21a). The CCL2 phenotype detected in MYO1e KO macrophages was also observed in DCs with a genetic deletion in *Myo1e*. LPS stimulated WT DCs secreted increasing amounts of the chemokine with prolonged stimulation. However, KO DC released constantly almost doubled amounts of CCL2 throughout LPS stimulation at a magnitude of 6 ng/ml at 24 h post stimulation. In our experiments MYO1e further affected the late CCL3 response to TLR4 activation. Secretion of this chemoattractant was strongly induced within the first 8 h upon LPS addition. Up to 8,5 ng/ml under WT condition was measurable and subsequently dropped down to 2 ng/ml at 24 h time points. DCs lacking MYO1e were not as efficient in down regulation of CCL3 release to the same extent as WT cells, because at later time points concentration of 5 ng/ml were still detectable. A contribution of MYO1e in CCL4 secretion was not detected in our hands (Fig. 21b).

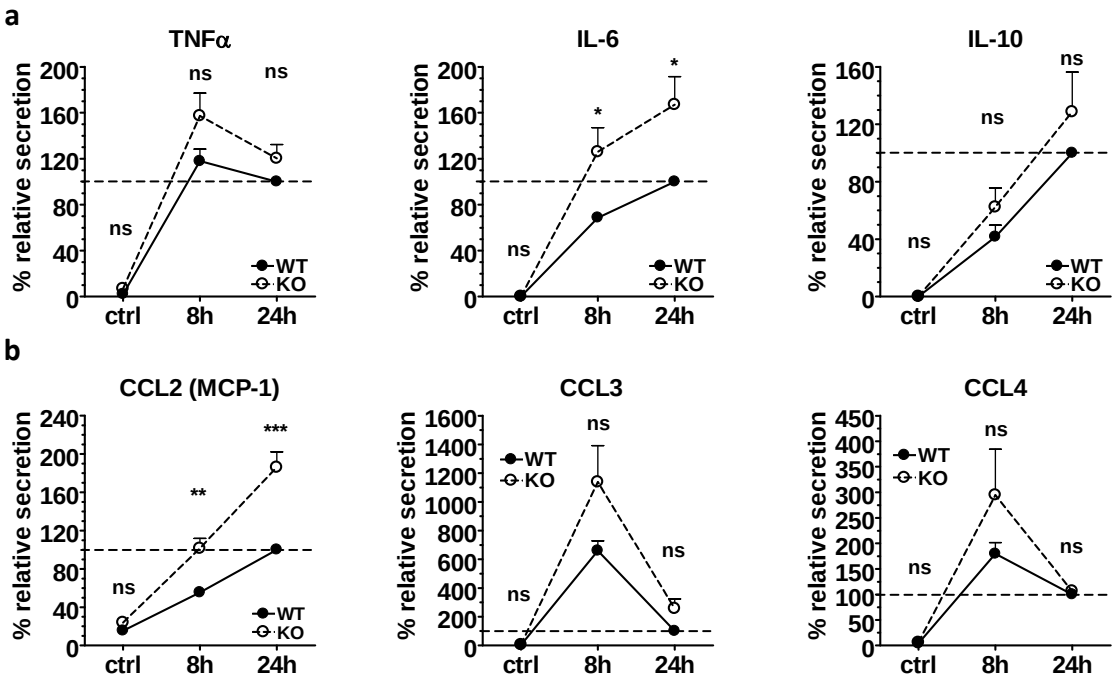

Figure 21. A role of MYO1e in chemokine secretion of activated dendritic cells. . Supernatants of the cultures were analyzed by ELISA for the presence of **(a)** cytokines and **(b)** chemokines. To normalize for differences between experiments in the absolute amount, the 24h time point of the LPS-treated control cells in each experiment was set to 100% (shown as - - - -). Shown are mean + SEM. ns=not significant; * p <0.05, *** p <0.0001; n=3-6.

Comparable to experiments with primary macrophages we next addressed the question whether the altered secretion phenotype of TLR4 activated dendritic cells resulted from a *Myo1e* KO caused change in signal transduction. We therefore determined the expression and activation of the MAPK ERK1/2 and p38 by immunoblot analysis. Both kinases were expressed in comparable amounts in WT and KO DCs. Phosphorylation of ERK1/2 and p38 in response to LPS stimulation occurs very rapidly already 15 – 30 min after addition of the TLR4 ligand and were diminished after 1h until the later time points. Independent from the genotype both MAPK pathways were activated to the same extent in DCs (Fig. 22).

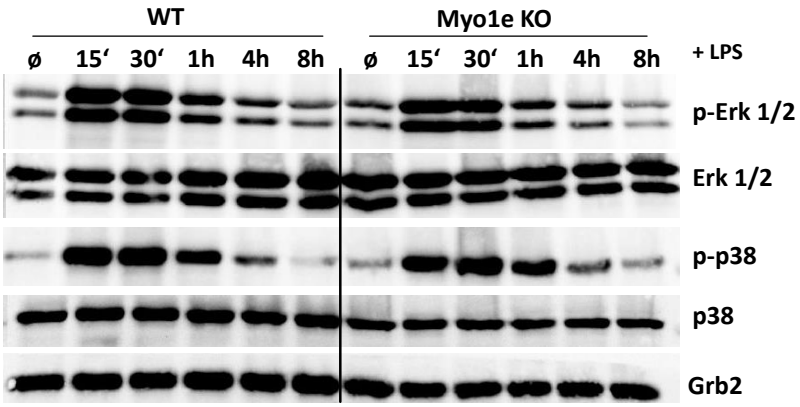

Figure 22. MAPK signaling in activated *Myo1e* KO DC. Western blot for ERK1/2 and p38 phosphorylation. Cell lysates were taken at indicated time points (15 min to 24 h) after LPS stimulation (100 ng/ml). Grb2: loading control

Furthermore, to investigate whether the increased CCL2 secretion resulted from a change on transcriptional levels we determined its mRNA expression in TLR4 activated DCs by quantitative RT-PCR. GM-CSF derived DC already expressed *Ccl2* mRNA in higher basal amounts compared to the "house-keeping" gene HPRT, acting as control expression gene independent of LPS stimulation. Activation of cultured WT DCs induced only a 1.4 - 2 fold increase in the mRNA expression of this chemoattractant 8 h post stimulation which was strongly down regulated at later time points. The control of *Ccl2* expression on transcriptional level in *Myo1e* KO cells displayed a significantly enhanced up-regulation of mRNA to the extent of 1.9-3 fold followed again by a subsequent down-regulation (Fig. 23). These experiments indicate a possible role of MYO1e not only in transport and secretion processes of cytokines and chemokines in DC but also a cell type specific contribution in regulation on the transcriptional level.

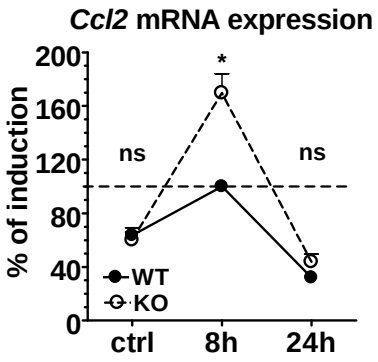

Figure 23. Increased CCL2 mRNA expression in *Myo1e* KO DC. WT and *Myo1e* KO DC were stimulated with LPS [100 ng/ml] and *Ccl2* mRNA expression was determined by qRT-PCR. To normalize for differences between experiments in the fold changes, the maximum fold change of LPS-treated WT cells in each experiment was set to 100% (shown as - - - -). Detection of the house-keeping gene HPRT occurs at C_T values of 24-25 while basal CCL2 expression was measured at C_T = 21-22. Shown are mean+SEM. ns = not significant; * p <0.05; n=4.

4.2.5 Reduced MHC-II surface expression on *Myo1e* deficient antigen presenting cells

Activation of adaptive immunity in response to invading pathogens is an essential task of the innate immune system. To mediate the response macrophages process phagocytozed extracellular material into peptides and subsequently present these antigenic structures via the MHC-II complex to $CD4^+$ T-cells. With respect to the important function and its intracellular localization in a membrane engulfed compartment we asked whether MYO1e may contribute to MHC-II surface expression on antigen presenting cells. Primary KO macrophages analyzed by FACS displayed a significantly reduced 15% lower basal MHC-II surface expression if compared to WT cells. Stimulation with LPS induced an increase of surface MHC-II with a maximum intensity 8 h after addition and a reduction back to initial expression levels measured at later time points. Interestingly, an impaired TLR4-driven up-regulation was observed in macrophages lacking MYO1e (Fig. 24a). In contrast, this defect was compensated by IFNγ stimulation, resulting in a continuously increased MHC-II expression throughout stimulation (Fig. 24b). Investigation on MHC-II mRNA expression argued against the notion that the observed phenotype results from a change on the transcriptional level. In qRT-PCR analysis both genotypes revealed similar amounts of MHC-II mRNA (C_T =21-23) under basal conditions. Activation of cultured macrophages induced a 1.5 - 2 fold increase in the mRNA expression 8 h post stimulation which was down regulated after 24 hours. Expression of *CIIT*a mRNA, the master regulator of MHC-II transcription, was decreased for the duration of TLR4 activation without differences between WT and KO condition (Fig. 24c). The results indicated that the reduced MHC-II surface expression is due to an intracellular transport defect caused by the *Myo1e* KO and not because of alterations in its biosynthesis.

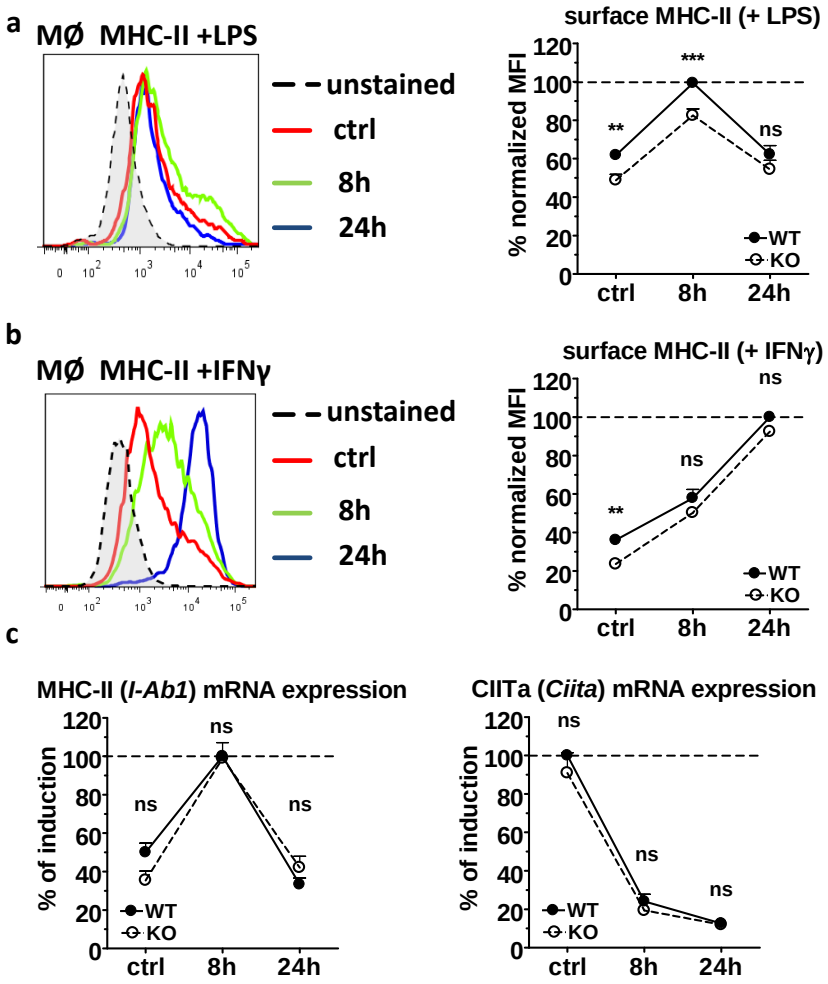

Figure 24. Decreased MHC-II surface expression on activated Myo1e KO MØ. (a, b) WT and *Myo1e* KO MØ were stimulated with LPS [100 ng/ml] or IFNγ [50 ng/ml] and MHC-II surface expression was determined by FACS. *Left:* Histogram overlay of WT cells. *Right:* MFI normalized for differences between experiments, the maximum MFI of treated WT cells in each experiment was set to 100% (shown as - - -). **(c)** MHC-II and CIITa mRNA expression of LPS treated MØ. Fold changes normalized for differences between experiments, the maximum fold change of LPS-treated WT cells in each experiment was set to 100% (shown as - - -). ns = not significant; ** p <0.001, *** p <0.0001.

In addition to antigen presentation the surface expression of co-stimulatory molecules is required to activate T-cells. For this reason, the surface expression of CD40, CD80 and CD86 was examined by FACS analysis on WT and *Myo1e* KO primary macrophages. In contrary to CD80 and CD86 which were already expressed in substantial amounts under basal condition, CD40 was detected at low levels on the cell surface. Activation of TLR4 induced only a 25-30% increase in CD86 expression while CD40 and CD80 were strongly up-regulated in response to LPS with a maximum in detection level 24 h after stimulation. However, a modest but significant decrease in CD80 expression on *Myo1e* KO cells was detected at the latest time point (Fig. 25a). The stimulation of macrophages with IFNγ also induced a regulation in

surface expression of all three co-stimulatory molecules. The decreased amount in CD80 at 24 h in response to LPS could be restored in *Myo1e* KO cells activated by IFNγ (Fig. 25b). The motor protein not only contributes in LPS-induced MHC-II up-regulation, it also seems to be involved in a full CD80 surface expression.

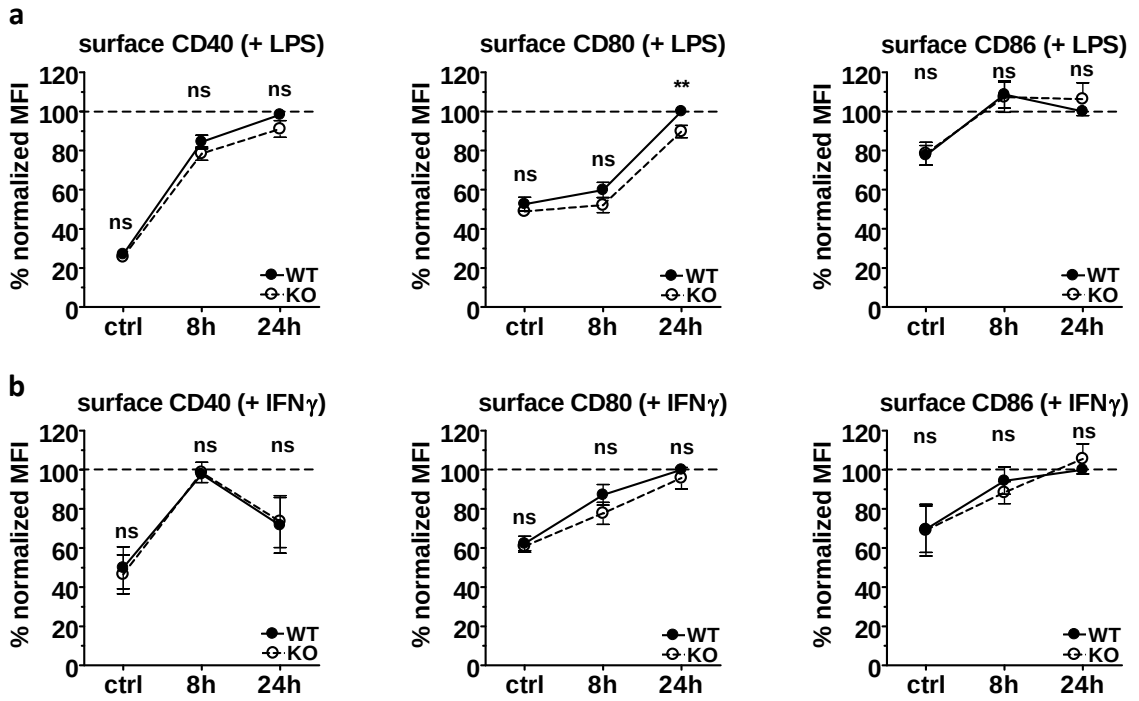

Figure 25. Co-stimulatory molecule expression on *Myo1e* KO MØ. Surface expression of co-stimulatory molecules CD40, CD80 and CD86 on **(a)** LPS [100 ng/ml] or **(b)** IFNγ [50 ng/ml] treated WT or *Myo1e* KO MØ detected by FACS analysis. MFI normalized for differences between experiments, the maximum MFI of treated WT cells in each experiment was set to 100% (shown as - - -). Shown are mean + SEM. ns = not significant. ** p <0.001, *** p <0.0001, n=4-7.

The most potent antigen presenting cell type of the innate immune system expressing TLR4 and MYO1e are dendritic cells. These cells already showed strikingly high amounts of surface MHC-II under basal conditions and were able to up-regulate the molecule roughly 1.5 fold in response to 24 h of TLR4 activation. Although *Myo1e* KO DCs did not show a difference in basal expression and early up-regulation after LPS stimulation, a continuing activation over 24 h resulted in a significant 20% reduction in MHC-II expression on KO cells (Fig. 26a, b). Stimulation of DCs with IFNγ did not affect the surface expression and also did not show an altered *Myo1e* KO phenotype (Fig. 26c). Analysis of the *Mhc-II* and *Ciita* mRNA production identified an altered expression pattern in response to LPS. DCs lacking MYO1e showed a significantly reduced *Ciita* and a corresponding *Mhc-II* mRNA expression 8 h after LPS stimulation (Fig. 26d), indicating that the *Myo1e* KO might interfere with the synthesis of the

MHC-II master regulator CIITa leading to a reduced *Mhc-II* mRNA production, which subsequently results in the diminished MHC-II surface expression on murine DCs at the later time points. Simultaneous measurements of co-stimulatory molecules showed a strong TLR4-driven up-regulation of CD40, CD80 and CD86 up to a 6-fold increase compared to initial condition. *Myo1e* KO DCs displayed no difference in surface expression patterns of these molecules with exception of CD40 with a weak but significant reduction in KO DCs 24 h after LPS stimulation (Fig. 26e).

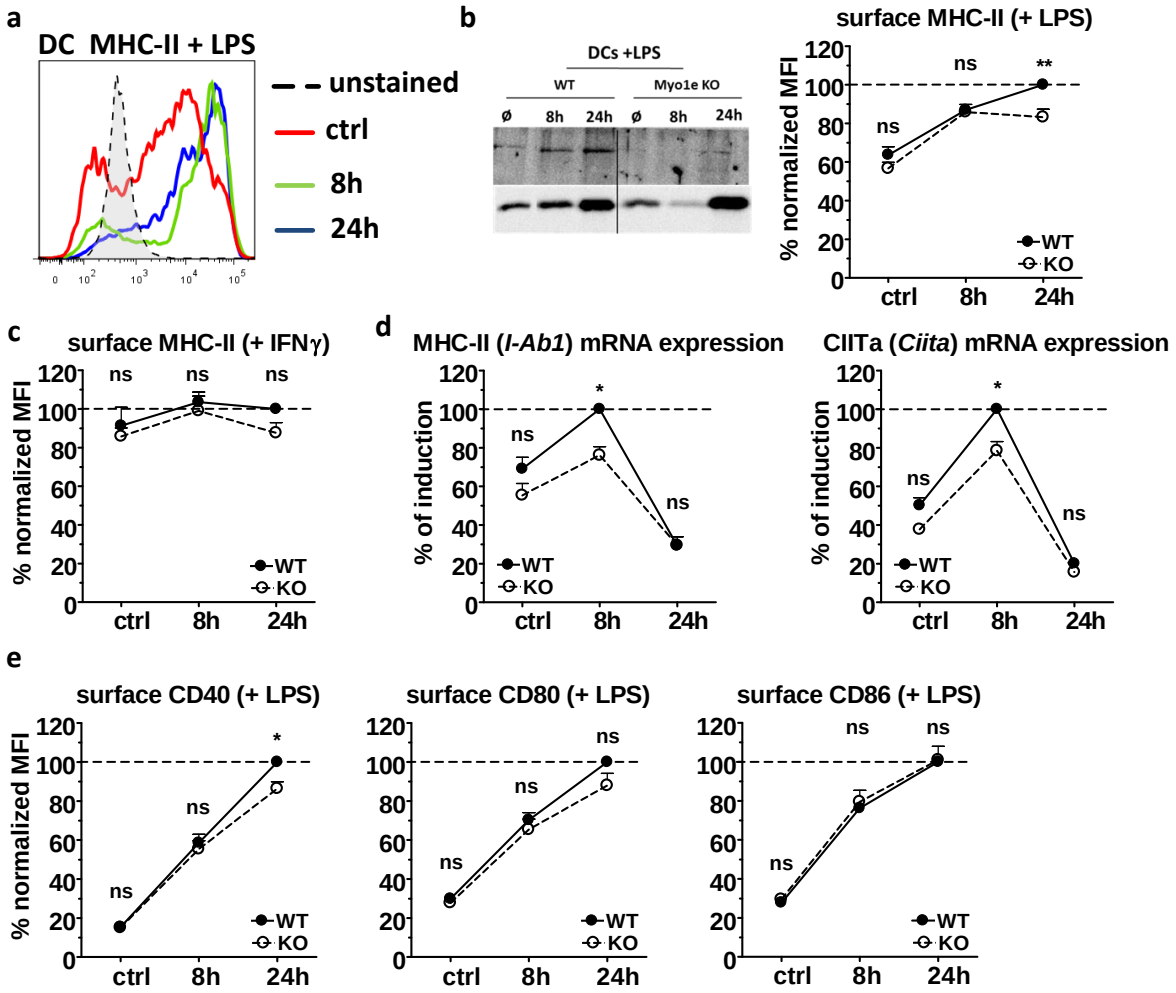

Figure 26. Reduced MHC-II mRNA and surface expression in Myo1e KO dendritic cells. **(a)** MHC-II histogram overlay of LPS activated WT DCs. **(b)** WT and *Myo1e* KO DCs stimulated with LPS [100 ng/ml]. *Myo1e* KO was confirmed by western blot and surface expression of MHC-II analyzed by FACS. n= 5 **(c)** MHC-II surface expression of IFNγ [50 ng/ml] stimulated DCs. n= 4 **(d)** *Mhc-II* and *Ciita* mRNA expression of LPS treated DCs. Fold changes normalized for differences between experiments, the maximum fold change of LPS-treated WT cells in each was set to 100%(shown as - - -). Shown are mean + SEM. n= 6 **(e)** Surface expression of co-stimulatory molecules CD40, CD80 and CD86 on LPS treated DCs. MFI were normalized for differences between experiments, the maximum MFI of treated WT cells in each experiment was set to 100% (shown as - - -). n=5; ns = not significant; * p <0.05, ** p <0.001.

4.2.6 Altered CD4 T-cell activation by *Myo1e* deficient APCs

The MHC-II phenotype of *Myo1e* KO MØ and DCs observed here raised the question whether this moderate reduction in surface expression has an impact on T-cell activation. To address this issue, we employed an *in vitro* T-cell stimulation assay where CD4 T-cells specific for OVA peptide were isolated from spleen and lymph nodes of OT-II mice and were subsequently co-cultured with OVA pre-incubated WT or KO MØ. The MHC-II mediated OVA peptide presentation by APCs and its recognition by T-cells expressing the specific transgenic TCR induces the activation of CD4 T helper cells. Hence, T-cell proliferation was examined by a ^{3}H-thymidine incorporation assay. Titrating the number of APCs revealed a significantly reduced T-cell proliferation under KO conditions at lower MØ counts. However, higher numbers of *Myo1e* KO MØ were able to induce comparable T-cell proliferation, indicating that macrophages lacking MYO1e may have an impaired capacity to activate T helper cells (Fig. 27a). FACS analysis of CD25 levels on $CD4^{+}$ cells within the culture confirmed the impaired activation after 72 h. T-cells co-incubated with a low number of KO MØ up-regulated CD25 to a less extent compared to WT condition (Fig. 27b). Furthermore significantly decreased IFNγ levels were measured under KO conditions independent of the MØ cell numbers (Fig. 27c).

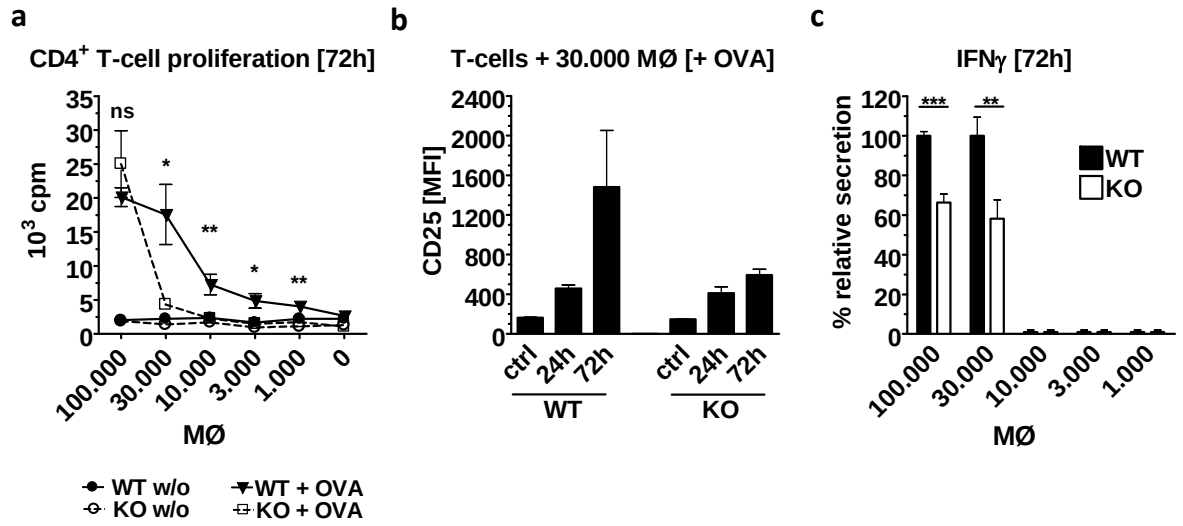

Figure 27. Impaired T helper cell activation through *Myo1e* KO MØ. *In vitro* OT-II assay to determine MØ MHC-II specific activation of CD4 T-cells. **(a)** T-cell proliferation measured by ^{3}H-thymidine incorporation assay. MØ were pre-incubated with 2 mg/ml OVA over night and intensively washed in cRPMI before addition of MACS isolated CD4^{+} T-cells from spleen and LN of OT-II mice. MØ numbers were titrated as indicated above and always 3*10^{5} T-cells were added. After 72 h of co-culture 1µCi of ^{3}H-thymidine was added and incubated overnight at 37°C before measuring. Shown are MEAN+SEM. n=3 **(b)** OT-II cells were incubated with 3*10^{4} MØ. Gated on CD4^{+} cells CD25 expression was determined by FACS at indicated time points. Shown are MEAN+SD. **(c)** Supernatants were analyzed for IFNγ production by ELISA. To normalize for differences between experiments in the absolute amounts, the mean of WT condition in each experiment was set to 100%. Shown are mean + SEM. n=3; ns = not significant; * p <0.05, ** p <0.001, *** p <0.001.

The more professional APCs mainly responsible for T-cell activation are dendritic cells. The OT-II approach was also utilized to investigate the contribution of MYO1e in MHC-II specific T-cell activation mediated by DCs. Low numbers of DCs (1.000 – 10.000) independent of the genotype were comparable in their T-cell activation capacity. However, a striking change in T–cell proliferation was detected under conditions with high numbers of DCs (30.000 – 100.000) which ended up in a significantly decreased T-cell proliferation under KO conditions (Fig. 28a). Comparable observations were obtained by CFSE labeling of T-cells. *Myo1e* KO DCs induced a reduced or delayed T-cell proliferation. Started from the point of co-incubation each T-cell division cycle can be determined by each peak. Under KO conditions the majority of activated T-cells divided two times and a third and fourth cycle were detectable. In contrast, under WT condition most of the T-cells were within the third division cycle and even a fourth and fifth were measured (Fig. 28b). Activation of CD4^{+} T-cells dramatically increased until 72 h of co-culturing with DCs measured by up-regulation of CD25. However, no difference between WT and *Myo1e* KO conditions was observed (Fig.

28c). Investigation of the T-cell cytokine response revealed an altered IFNγ secretion after co-incubation with OVA-loaded KO DCs in the majority of the different DC doses (Fig. 28d).

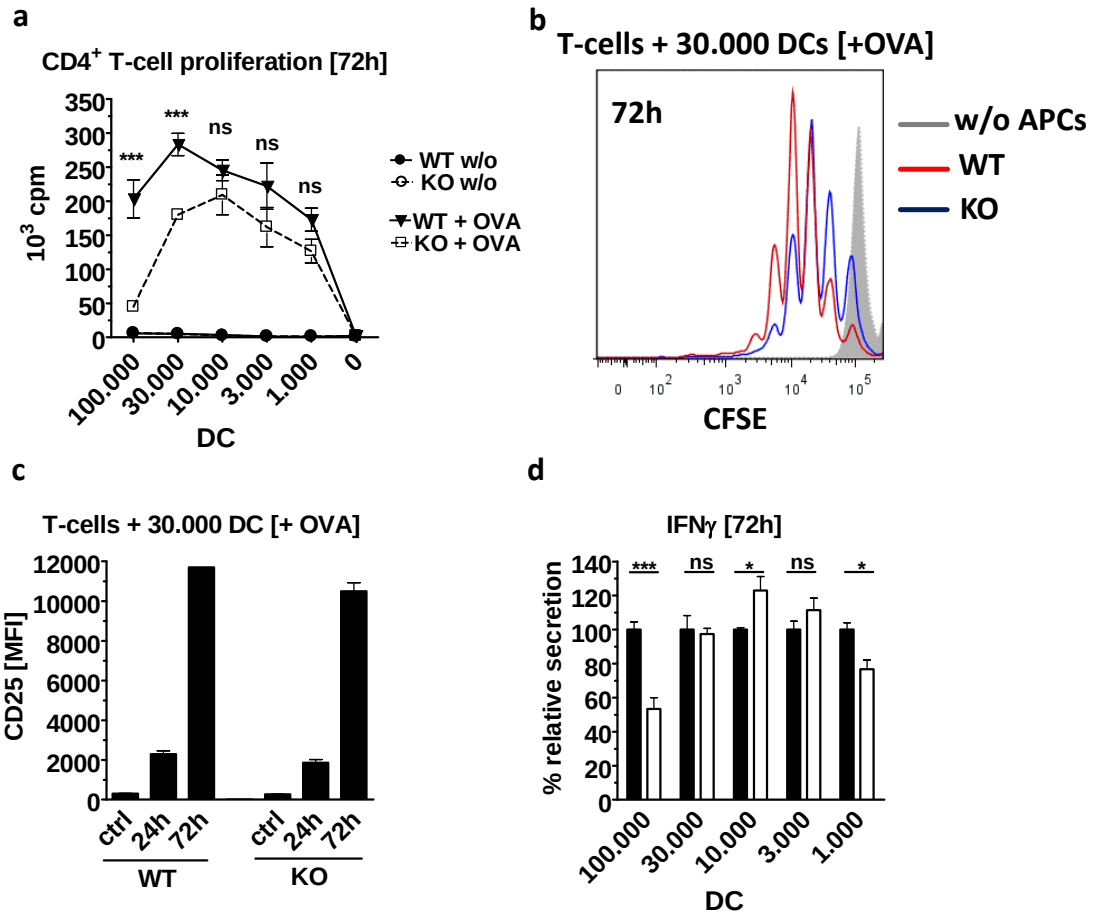

Figure 28. *Myo1e* KO DCs induced alteration in CD4$^+$ T helper cell activation. *In vitro* OT-II assay to determine DC MHC-II specific activation of CD4 T-cells. **(a)** T-cell proliferation measured by ^{3}H-thymidine incorporation assay. DCs were pre-incubated with 2 mg/ml OVA over night and intensively washed in cRPMI before addition of MACS isolated CD4$^+$ T-cells from spleen and LN of OT-II mice. DC numbers were titrated as indicated above and always 3*10^5 T-cells were added. After 72 h of co-culture 1µCi of ^{3}H-thymidine was added and incubated overnight at 37°C before measuring. Shown are MEAN+SEM. n=3 **(b)** T-cells were labeled with CFSE before co-incubation with 3*10^4 DCs. After 72h samples were analyzed by FACS. n=1 **(c)** T helper cells were incubated with 3*10^4 DCs. Gated on CD4$^+$ cells CD25 expression was determined by FACS at indicated time points. Shown are MEAN+SD. n=1**(d)** Supernatants were analyzed for IFNγ production by ELISA. To normalize for differences between experiments in the absolute amounts, the mean of WT condition was set to 100%. Shown are mean + SEM. n=3; ns = not significant; * p <0.05, *** p <0.0001.

Due to the fact that T-cell activation and antigen presentation requires a previous processing of the up-taken protein into small peptides and there loading on MHC-II molecules, we finally examined whether the altered T-cell activation by *Myo1e* KO APCs may result from change in antigen processing. Thus we applied DQ-OVA on WT and KO MØ as well as DCs. This fluorophore labeled OVA with self-quenching capacity can be visualized by increased

fluorescence upon its proteolytical cleavage. FACS analysis of MØ incubated with DQ-OVA revealed a very potent processing of the protein, indicated by the fast and strong increase in fluorescence signals. Throughout DQ-OVA incubation almost no difference between WT and KO MØ was detectable except at the 24h time point (Fig. 29a). Interestingly DCs lacking MYO1e showed a significantly enhanced OVA processing during the whole kinetic. Although the initial processing does not occur to such an extent as in MØ, after 24h *Myo1e* KO DCs processed relatively equal amounts of OVA compared to WT MØ (Fig. 29b). These results indicated contribution of MYO1e in antigen processing events in DCs.

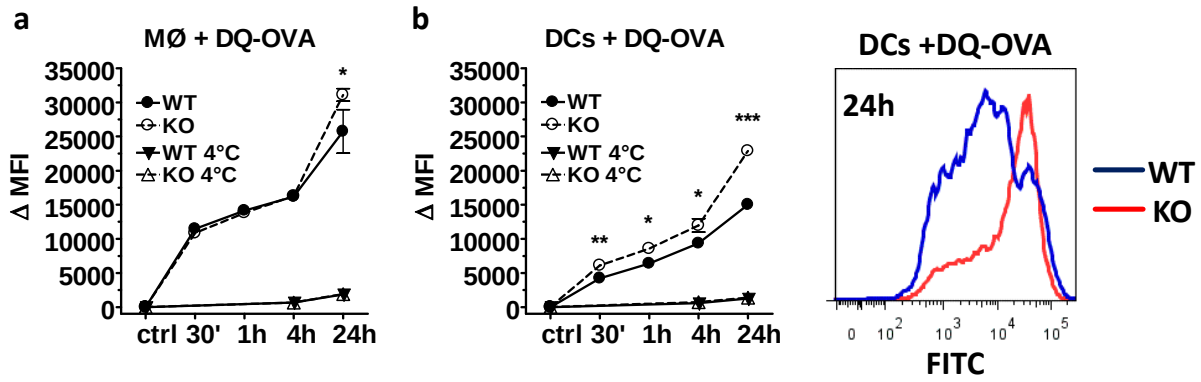

Figure 29. **Contribution of MYO1e in antigen processing by APCs. (a)** MØ and **(b)** DCs were incubate with DQ-OVA (20 µg/ml) for indicated time points at 37°C or 4°C as control. Cells were fixed with 2%PFA/PBS to stop processing and subsequently analyzed by FACS. Shown are MEAN+SD of biological triplicates as ΔMFI (MFI of untreated cells subtracted from MFI of treated cells). Histogram overlay of DCs + DQ-OVA at 24h. WT DCs (blue line); *Myo1e* KO DCs (red line); n=1. * p <0.05, ** p <0.001, *** p <0.0001.

4.2.7 MYO1e in MHC-II surface expression on B-cells

The third immune cell type expressing MHC-II and TLR4 are B-cells. Known from literature these cells only express MYO1e as a class I "long-tailed" myosin [118, 162] depending on their maturation stage [116]. Based on our previous findings regarding MØ and DCs, B-cells were an interesting target to investigate the contribution of MYO1e in MHC-II expression. Due to the fact that only bone marrow of WT and *Myo1e* KO mice was available to us, we generated bone marrow chimeras by reconstitution of RAG KO mice with WT or *Myo1e* KO bone marrow to finally obtain B-cells lacking MYO1e (Fig.30).

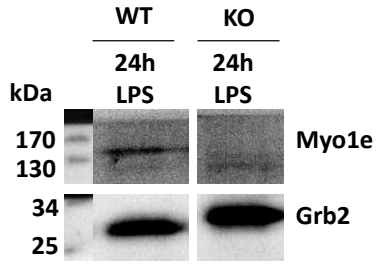

Figure 30. Confirmation of *Myo1e* KO in B-cells of RAG KO mice reconstituted with WT or *Myo1e* KO BM. $B220^+$ B-cells were isolated via MACS from spleen of BM chimera mice. Cells were incubated with 10 µg/ml LPS and lysates were taken at indicated time points. Grb2: loading control.

To simultaneously investigate whether the lack of MYO1e caused a change in B-cell distribution within the mice under basal condition we analyzed the ratio of $CD19^+$ $B220^+$ cells in different organs accompanied by analysis of their basal MHC-II expression. Started our analysis from bone marrow (BM) over blood (Bl) to the spleen (Sp) and the peritoneum (Pe) the ratio of CD19+B220+ cells strongly increase with highest amounts around 45-50% detected in spleen. The bone marrow harbored only 5-10% of already differentiated $CD19^+$ $B220^+$ B-cells but an equal, coexistent and clearly distinguishable population of $CD19^+B220^{dim}$ cells. Possibly caused by the high variance in B-cell ratios between reconstituted mice, a difference in cell distribution between the two genotypes could not be detected under basal conditions (Fig. 31a). Analysis of MHC-II revealed an already high expression on $B220^+$ B-cells in all examined organs except of the $CD19^+$ $B220^{dim}$ population of the BM whereas highest amounts were measured on B-cells within the peritoneum (Fig.31b). To investigate whether B-cells are able to up-regulate MHC-II in response to LPS and if this is influenced by MYO1e, cell suspensions from the organs were stimulated and subsequently examined for MHC-II expression on $CD19^+$ $B220^+$ cells. B-cells of the bone marrow, spleen and peritoneum weakly elevated the expression of surface MHC-II after 24 h of LPS treatment but independent from the *Myo1e* KO (Fig. 31c-e). These results indicated that MYO1e does not contribute to MHC-II surface expression in B-cells.

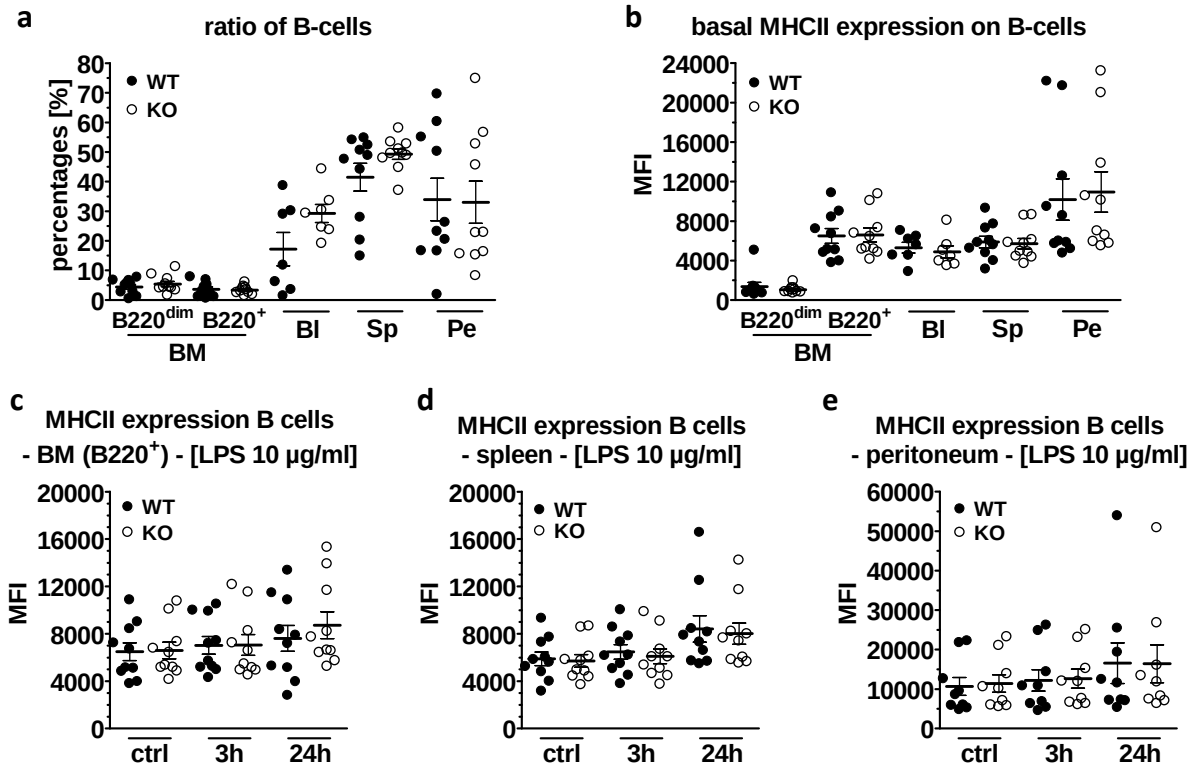

Figure 31. MYO1e in organ specific MHC-II expression on B-cells. RAG KO mice reconstituted with either WT (black circles) or *Myo1e* KO (clear circles) bone marrow were analyzed for basal B-cell distribution and MHC-II expression. Dots represents MEAN of technical replicates from one mouse (7-10 mice per genotype) **(a)** Percentages of $CD19^{+}$ $B220^{+}$ or ^{dim} (intermediate) cells in bone marrow (BM), blood (Bl), spleen (Sp) and peritoneum (Pe) analyzed by FACS. **(b)** Basal MHC-II surface expression on B-cells from different organs. **(c-e)** Cell suspensions of BM, Sp and Pe were stimulated with LPS [10 µg/ml] for indicated time points. MHC-II expression on $CD19^{+}$ $B220^{+}$ cells was analyzed by FACS. Bars represents MEAN+SEM.

5 Discussion

A global and quantitative phosphoproteome analysis of LPS-activated MØ, performed in our lab, identified 1800 phosphoproteins with around 7000 regulated phosphosites. Among these, bioinformatic analysis revealed the cytoskeleton as a hotspot of TLR4-driven protein phosphorylation [30]. Quantitative analysis of MØ spreading was validated and utilized as a measurable and cytoskeleton-dependent readout to investigate the impact of genetic or pharmacological inhibition of known TLR signaling components. We identified an essential but time-dependent requirement for MYD88 and the MAPK p38 and ERK1/2 in early and late TRL4-driven spreading. A siRNA knock down (KD) screen for selected cytoskeletal phosphoproteins identified the two class I myosins MYO1e and MYO1f as important contributors to LPS-triggered macrophage spreading. Further investigations on primary MØ and DC lacking MYO1e showed a selectively increased secretion of the chemokine CCL2 as well as a reduced basal and LPS-induced MHC-II surface expression on both antigen presenting cell types. The capacity of macrophages and DC lacking MYO1e to stimulate antigen-specific CD4+ T cell proliferation was remarkably impaired. Our results provide evidence for a non-redundant function of the motor protein MYO1e in the regulation of TLR4-controlled, cytoskeleton-associated functional properties of macrophages and DC, and in the induction of a full MHC-II restricted adaptive immune response.

5.1 Quantitative analysis of cell spreading

In order to better understand the contribution of the cytoskeleton in the control of TLR4 induced immune cell response, we validated macrophage spreading as measurable readout. This important cell function is strongly dependent on actin dynamics regulated by signaling molecules and cytoskeletal associated proteins, and reflects the adherence process at the site of infection. To measure TLR4-driven spreading *in vitro,* BMM were stimulated with LPS in a kinetic manner up to 24 h and finally visualized by fluorescence microscopy. The change in contact area between cell and surface material was determined, compared to unstimulated control conditions and defined as spreading. A manual quantification of the spreading response was possible by using ImageJ [163, 164] or tools provided by the fluorescence microscope software AxioVision 4.8.2 from Carl Zeiss MicroImaging. However, these approaches had the disadvantage of being labor-intensive and time consuming. In addition the manual delineation of the cell borders potentially introduces bias. Hence, analysis of multiple

images within an acceptable time frame and a constantly accurate annotation quality was infeasible. Utilization of automatic image analysis software provided the possibility to circumvent these drawbacks. To this end, freeware software packages like CellProfiler [165, 166] are available which can be adapted to the image content by adjusting several parameters, e.g. minimum and maximum cell diameter, threshold selection methods or pre-processing methods. However, adjustment of all these parameters to obtain sufficient results is as well very time-consuming for researchers not familiar with image processing. Thus, in cooperation with the group of PD Dr. Wittenberg from the Fraunhofer-Institut in Erlangen, we developed and optimized a two-step algorithm to segment nuclei and subsequently to determine cell size and contact area [154, 167]. This automated segmentation routine gave us the opportunity for a rapid acquisition of quantitative and reliable data from microscopy images without pre-processing procedures done by the user. Comparison of automated to manual annotation demonstrated a good concordance in resting macrophages and early after stimulation. The observed increase in variation at later time points resulted from overlapping cells based on the spreading behavior of macrophages. An occasional manual editing of the contact area annotation was required at the late time points. Overall very similar results were obtained in several experiments investigating the cell spreading (Fig 7). Thus, our two-step algorithm was used in a semi-automated procedure, combining automated annotation with manual correction, to quantify TLR4 induced macrophage spreading with a tremendous reduction in time and labor [147]. To improve the performance of the automatic annotation tool the quality of the input data is very critical. The quality of fluorescence microscopy pictures, in terms of staining intensity and signal-to-noise ratio of the cells versus slide background is one of the pivotal parameters. In our hands staining of the macrophage surface marker CD11b with APC-labeled antibodies reached the best signal, compared to cytosolic CFSE or membrane lipid PKH staining. The reduced accuracy of the annotation tool at later time points after stimulation might be explained by the localization of CD11b. Continuing LPS stimulation can cause changes in redistribution or clustering of CD11b in different cellular compartments, creating local maxima that are falsely recognized as cell boarders. Hence, staining of surface markers like MHC-I, CD45 or Fc receptor which are also highly expressed independent of the activation status or the use of antibodies labeled with stronger fluorescent dyes could improve the tool performance. In the future, the development of automatic segmentation algorithms the annotation of overlapping cells remains an issue that must be solved by computer scientists.

5.2 Contribution of TLR4 signaling in macrophage spreading

Convinced by the potential of our quantitative readout system and the advantage to interfere by utilization of specific pharmacological inhibitors and selected knockout (KO) cells, we further analyzed the contribution of TLR4 signaling molecules in the control of macrophage spreading. The LPS-triggered spreading observed first after 1 h and increasing continuously until 8-24 h (Fig. 6) could be caused by direct TLR4-driven signaling inducing actin polymerization or cytoskeleton rearrangement, or it could depend on indirect effects of TLR-driven cytokine release, e.g. TNF. Compared to the cytokines IL-6 and IL-12p40, TNF is the only pro-inflammatory cytokine secreted early enough to potentially cause initial spreading (Fig. 8). In our experiments we have not excluded this possibility. Feasible experiments to address this issue will require the use of selected KO macrophages or application of inhibitors off protein biosynthesis (e.g. Cycloheximide), transport and secretion (e.g. Brefeldin A) or specific inhibitors of the metalloprotease ADAM17 (TACE) responsible for TNF shedding and release. Strong evidence that LPS directly induces a rapid actin rearrangement in macrophages was already described in peritoneal macrophages of C3H/HeN mice, where an assembling and disassembling within the first 6 minutes after LPS stimulation was observed in contrast to macrophages of LPS non-responder C3H/HeJ mice [69]. Comparable observations were made on the macrophage cell line J774, where TLR4 activation induced a rapid morphological change within 20 minutes accompanied by an enrichment of actin filaments in ruffles at the leading edge [73]. To address this issue in murine bone marrow macrophages, shorter LPS stimulation time points are required to observe initial changes in actin dynamics. To determine the cytoskeletal rearrangement processes, fluorescence microscopy or FACS analysis of cells stained with phalloidin for polymerized actin filaments would be necessary. Furthermore, the fractionation of the actin cytoskeleton by high-speed centrifugation from cell lysates of activated MØ can give information on dynamic changes. This method allows the densitometric quantification of separated monomeric G-actin and filamentous F-actin. The ratio of G- to F-actin indicates alterations in assembling or disassembling dynamics [73].

An essential adapter protein of TLR4 signaling is MYD88, required for transduction of intracellular signaling. The use of KO macrophages confirmed its crucial role in LPS-induced cytokine production. Thus, cells lacking the molecule entirely failed to produce TNF, IL-6 or IL-10. Interestingly *Myd88* KO macrophages, compared to *Myd88* heterozygous control cells, exhibited a normal spreading response to LPS during the initial phase until 2 h. Only under longer lasting LPS stimulation from 8 – 24 h, *Myd88* KO macrophages showed a

reduced spreading, indicating a crucial role of MYD88 mediated signaling during late phase adherence (Fig. 8). To our knowledge, a role of MYD88 in LPS-induced actin rearrangement has not been described before. The normal TLR4-driven initial spreading of *Myd88* KO MØ is supposed to be mediated via the MYD88 independent pathway, including the second adaptor protein TRIF. To examine this assumption, the use of macrophages lacking TRIF or both adaptors MYD88/TRIF will be useful. Furthermore, to distinguish between direct effects of MYD88 on macrophage spreading and secondary effects mediated by secreted cytokines, transfer of supernatant from WT MØ onto *Myd88* KO was performed. Macrophages lacking the TLR4 adaptor protein did not increase their contact area in response to the supernatants (data not shown). The results suggested a direct induction of macrophage spreading and cytoskeleton rearrangement by LPS and less through the secreted cytokines.

Central mediators regulated in response to TLR4 activation are the MAPK p38 and ERK1/2 and thus became focus of our following investigations. Both MAPKs were necessary for a full cytokine production of primary macrophages in response to TLR4 activation. Interestingly a time-dependent requirement for p38 and ERK1/2 for early and late spreading responses, respectively, was found (Fig. 9 and 10). In the absence of p38 a significantly reduced early, but intact late spreading was observed. *P38*-deficient macrophages, compared to cells lacking *Myd88*, exhibited a slightly reduced basal contact area, which could also indicate differences in differentiation caused by the lack of these molecules (Fig. 8 and 9). The use of specific pharmacological inhibitors for p38 would be helpful to confirm the p38-dependent early LPS-induced spreading. The approach was used to reveal the contribution of the MAPK ERK1/2 in this context. Macrophages treated with the MEK1 inhibitor PD184352 showed a similar spreading response to *Myd88* KO cells, with intact early spreading but a strongly reduced response after 8 h and 24 h (Fig. 8 und 10). Thus, ERK1/2 appears to be the main kinase of the MYD88-dependent spreading response. However, the utilization of this pharmacological inhibitor entailed some limitations. First, a strongly diminished basal and LPS-induced phosphorylation of ERK1/2 was observed, but a complete suppression was not obtained. Second, the PD184352 treatment may have additional effects aside MEK1 inhibition, which can contribute to the observed spreading phenotype although a variation in p38 activation could not be observed (Fig. 10). To definitively confirm the role of ERK1/2 in the TLR4-driven late spreading response, experiments with respective KO macrophages are necessary. With these experiments we revealed a dichotomy of p38 and ERK1/2 in TLR4-induced spreading, where the late spreading response is mediated by MYD88 and ERK1/2, while early spreading in contrast is dependent on p38 signaling. With respect to the normal

early spreading of *Myd88* KO MØ, the early activation of p38 should be MYD88 independent. In fact, the LPS-induced phosphorylation of both MAPK is only delayed in *Myd88*-deficient macrophages [28]. Experiments performed in the macrophage cell line J774 also showed a contribution of p38 in early LPS-induced spreading by activation of β_2-integrins via the Ras-like GTPase RAP1 [140].

The regulation of MAPK activity is crucial to control the response of innate immune cells. Endogenous regulators expressed by macrophages are dual-specificity phosphatases (DUSPs), known to be involved in p38 and ERK1/2 regulation [37, 168]. The use of specific KO macrophages for DUSP1 and DUSP16 confirmed their differential role in the regulation of LPS-induced production of IL-10 and IL-12p40 (Fig. 11). A contribution of DUSP1 to cytoskeleton-dependent cell functions has been described. Macrophages lacking DUSP1 showed an impaired spreading under resting conditions [38] and monocytes of diabetic mice express only low levels of DUSP1, leading to a hyperactivation of p38 and ERK1/2 in response to CCL2 and an increased chemotaxis and adhesion [168]. Interestingly, we observed that macrophages lacking either DUSP1 or DUSP16 showed a similar reduction in spreading at 8-24 h. Mechanisms behind the DUSP depend spreading phenotype are currently unknown. However, it is worth noting that 18 of 44 cytoskeletal phosphoproteins detected in our phosphoproteome analysis contains a MAPK binding motif, corroborating their importance as potential cytoskeleton regulators (Fig. 5).

Furthermore, the expression and activation of integrins controlled by MAPK [139, 140] and possibly regulated through DUSPs, might be involved in TLR4-induced macrophage spreading. To address this question, inhibitor-treated or specific MAPK and DUSP KO macrophages can be screened for basal and LPS-induced integrin surface expression by FACS analysis. In addition to macrophage spreading on plastic slides, in this context it would be informative to determine the spreading response on slides coated with integrin ligands, e.g. fibronectin, collagen or ICAM-1. Aside surface expression, MYD88, MAPK and DUSPs might be involved in activation of integrins by controlling the inside-out signal. For the β_2-integrin CD18, the most prominent subunit on innate immune cells, specific antibodies exist which recognize epitopes formed during the activation process by conformational changes. Their application allows to distinguish between the “bent, inactive”, “extended, intermediate affinity” and “extended, high affinity” conformation of the integrin and whether this process is influenced by TLR4 activation and signaling components [138].

One established pathway from TLR4 to integrin activation is transmitted by the focal-adhesion kinase-related PYK2 and the adaptor protein paxillin (PXN) [169]. The

phosphorylation of paxillin on Ser130, mediated by ERK1/2 in response to LPS, is required for GSK3-dependent phosphorylation of Ser126 [170]. All members of the described ERK1/2-GSK3-PYK2-PXN pathway were found strongly phosphorylated after LPS at several sites in our phosphoproteome analysis [30]. Interestingly, in *Myd88* KO macrophages the activation of PXN and PYK2 were just weakly reduced [171], which might explain the intact initial spreading in *Myd88*-deficient cells observed in our experiments. Another potential mechanism involved in MYD88-independent macrophage spreading is provided by an early activation of the small GTPases CDC42 and RAC in response to LPS, known to be important in actin rearrangements [81].

5.3 Cytoskeletal phosphoproteins in LPS-induced macrophage spreading

Although some of the molecules in macrophage spreading are well described, the fact that 44 cytoskeletal proteins were regulated by TLR4-driven phosphorylation in our phosphoproteome analysis [30] indicates that multiple proteins contribute to the changes in macrophage spreading, motility or other cytoskeletal cell functions. To elucidate the functional role of chosen candidate proteins we established a siRNA knock down (KD) in primary mouse macrophages, based on a protocol developed by the group of Jonathan Jantsch [146]. The delivery of small interference RNA (siRNA) into the cells for selective gene silencing occurs via electroporation. Compared to other transfection methods with DEAE-dextran, calcium phosphate or lipofectamine, this procedure possesses a high efficiency with more than 95% transfected cells. Importantly, the electroporation did not impair the viability and immunological functions of macrophages, e.g. phagocytosis, expression of cytokines and NO production. To avoid cell stress by accutase treatment or mechanical detachment from plates in advance to electroporation, the differentiation of primary MØ was performed in hydrophobic teflon bags, yielded more than 90% macrophages ($CD11b^{high}$ $F4/80^{high}$) within the culture population after 8 days [146]. This culture condition was critical for the survival rate of macrophages after electroporation and siRNA treatment. The development of macrophages under non-adherent conditions seemed normal, however the surface attachment and activation of integrins is required for a complementary and optimal TLR4 response, leading to a full ERK1/2 and JNK activation and induction of an entire TNFα production [136]. In respect to cytokine secretion and up-regulation of surface molecules, MØ differentiated in teflon bags and petri dishes respond in similar kinetics and in same extent to LPS, in our hands. However, cells derived from the two differentiation approaches showed occasional differences in their spreading response. For this reason it was indispensable to

compare control and treated cells differentiated under same conditions. Cells treated with siRNA were rested 48 h to develop the full siRNA effect before LPS stimulation. The KD efficiencies measured on mRNA level by quantitative real-time PCR showed a high variability from 50-90% (Fig. 12). This high variability depends on the amount of the target mRNA expressed under basal condition and the inducibility of the respective gene expression in response to the stimulus. Target mRNAs available in larger quantity require enough time to get eliminated by the RNAi machinery, while mRNAs with low basal expression provide less possibility for target interaction. Thus, the cells get cleared from free siRNA molecules by nucleases [172]. Furthermore, the KD success depends on the dose of the delivered siRNA as well as its stability. The best results for the majority of the cytoskeletal proteins were obtained 48 h after siRNA treatment. In case of proteins with low KD efficiency a shorter siRNA incubation period of 24 h may obtain better results. To confirm the KD also on protein level, Western blot analysis of cell lysates for the respective proteins are necessary in future experiments.

Measurements on TLR4-induced spreading indeed revealed a contribution for some of the selected proteins in primary macrophages (Fig. 12). The most striking effects were observed in response to the KD of the actin polymerization factor (APF) ARP3 and its antagonist CORO1b. ARP3 is part of the multi protein complex ARP2/3, which is composed of seven subunits including ARP2 and ARPC1-5. It is the best described APF in lower and higher eukaryotes and its activity is essential to form branch-ends on existing actin filaments required for lamellipodia formation [88]. Furthermore, it plays a central role in macrophage chemotaxis and receptor-mediated phagocytosis [14]. First studies linking specific phosphorylation events of this protein complex to its functional control were done in lysates of human neutrophils. Here, the phosphorylation of ARPC5 was mediated by the MAPK p38 and thus the authors speculate that it activates the ARP2/3 complex [92]. Furthermore, the phosphorylation of the subunit ARP2 in *Dictyostelium* was also shown to regulate the multi-protein complex activity [89, 90]. In our phosphoproteome studies of TLR4 activated primary macrophages a strong and consistent phosphorylation of the ARP3 subunit was identified, whose function is still unknown. However, biochemical studies identified a crucial role for the ARP3 subunit in actin polymerization, linking the whole complex to the site of actin filaments [173]. For these reasons we expected to observe a change in the LPS-induced spreading phenotype in macrophages treated with the specific ARP3 siRNA. Indeed, an initially reduced contact area as well as a strong impaired spreading response throughout LPS stimulation was measured. Macrophages manipulated in the synthesis of ARP3 protein

presumably failed to form the functional ARP2/3 complex and thus lose their ability to increase the contact area. The initial early spreading upon stimulation might be due to a high protein expression of all ARP2/3 subunits under basal conditions and enables the cells to rapidly adapt its morphology in response to a trigger. These results indicated an essential role for ARP3 in formation of a functional ARP2/3 complex, required in primary macrophage spreading.

Although the KD efficiency for CORO1b was only 50%, its down regulation on mRNA level resulted in a strong alteration in macrophage spreading. Cells treated with specific siRNA showed a similar initial contact size but a significantly reduced early spreading up to 8 h upon stimulation. However, these cells subsequently enhanced their spreading until 24 h and ended up in a significantly strong increase in contact size compared to control cells. This cytoskeletal protein inhibits ARP2/3 activity by replacing it from actin filaments and additionally coordinates the activity of the actin depolymerization factor cofilin [160, 174]. In fibroblasts the CORO1b/ARP2/3 interaction is regulated by phosphorylation of CORO1b by the protein kinase C (PKC) in response to PMA [175]. PKC isoforms are well known to be activated in response to TLR4 activation [176] and a modest but consistent phosphorylation of PKC-β and PKC-δ was also detected in our phosphoproteome analysis. This might provide evidence for a PKC/CORO1b regulation of actin dynamics in response to TLR4 activation in primary macrophages. The down regulation of CORO1b by siRNA treatment might cause a hyperactive ARP2/3 complex dissipating the majority of monomeric G-actin for F-actin formation. It is possible that the disruption in disassembling processes inhibits the constant supply with G-actin and thus results in a reduced early spreading. To compensate or overwhelm the defect, macrophages might then activate additional depolymerization factors or increase the expression of actin, resulting in a stronger increase in contact area until 24 h, caused by the hyperactive ARP2/3 complex.

The KD of other phosphorylated actin polymerization factors FMN1 and FHOD1, which belong to the formin family, did not show a change in the spreading behavior of macrophages. A possible explanation might be the difference in the procedure of actin polymerization. While ARP2/3 activation induces actin branching to build a dense network required in lamellipodia formation, formins interact with the tip of actin filaments and elongate them linear to form filopodia structures [84, 88, 177]. In contrast to ARP2/3, macrophages express several types of formins [178], which might be able to act redundantly. In further experiments a simultaneous double or multiple siRNA KD of selected formins can reduce this risk and might reveal a possible role of these APF in TLR4 induced macrophage spreading.

Furthermore, fluorescence microscopy can be utilized to focus on morphological changes caused by the formin KD. Their down regulation might reveal a contribution in TLR4-driven filopodia formation. These finger-like structures of macrophages are known to be critical in phagocytosis processes [179] and thus FMN1 and FHOD1 should be examined in uptake processes.

The KD of the cytoskeletal adaptor protein missing-in-metastasis 1 (MTSS1) revealed a minor but biphasic alteration in spreading, with a significantly reduced early spreading and increased late spreading in response to LPS. The protein contains independent F- and G-actin binding domains and is thus believed to recruit actin monomers or other proteins to specific cytoskeletal networks [180]. Furthermore, redistribution in fibroblasts from the cytoplasm to membrane ruffles, dependent on Tyr-397 and Tyr-398 phosphorylation, is described in response to platelet-derived growth factor (PDGF) [181]. Interestingly, MTSS1 KO fibroblasts display a reduced spreading within 2 h in response to adherence as well as a distinct morphology and altered cytoskeleton reorganization after PDGF stimulation. The cell motility and endocytosis is also impaired [182]. The strong phosphorylation of MTSS1 in LPS-stimulated macrophages was detected on several serine residues from position 348 to 355, the approximate position compared to fibroblasts. Our results together with observations on murine fibroblasts indicate an important role for the phosphorylation within this range, and thus might be essential to control murine MTSS1 function.

The siRNA KD of LSP1 and EPS8 caused only minor changes in macrophage spreading; although the respective mRNA in challenged MØ was reduced from 60-85 %. LSP1 is expressed in all human and murine leukocytes [93] and described to be involved in regulation of the actin cytoskeleton structure and motile function of neutrophils by mediating MAPK signaling to the cytoskeleton [93-95, 183, 184]. Its activity is regulated by p38/MK2-mediated phosphorylation on Ser243 within its C-terminal F-actin binding region and thus stabilizing F-actin polymerization during neutrophils chemotaxis [94, 183, 184]. Furthermore, confocal microscopy analysis showed that LSP1 targets MEK1 and ERK2 to peripheral actin filaments in a B-lymphoma cell line [95]. TLR4-driven phosphorylation of several residues within the C-terminal region of LSP1, even Ser242, was detected in LPS-activated macrophages; some of them identified within a MAPK substrate motif [30]. The obtained results suppose that LSP1 does not contribute to LPS-induced macrophage spreading, but it may be involved in chemotaxis as described for neutrophils. The same might be true for the signal adaptor EPS8, also functional as capping protein and described to be essential in DC migration [185]. Recent studies identified a contribution of EPS8 in macrophage phagocytosis and bacterial killing.

Here, LPS induced EPS8 expression followed by its interaction with TLR4-MYD88 in the cytosol and at the phagosomes, and is necessary to fully activate SRC, focal adhesion kinase (FAK), and p38 MAPK [186]. A requirement of MTSS1, LSP1and EPS8 in TLR4-driven macrophage spreading is not as obvious as in case of ARP3 and CORO1b. Thus, macrophage spreading seems not to be the main cell function controlled by these proteins. Investigations of further cytoskeleton-associated cell functions are necessary to rule out an essential function for the respective phosphoproteins. Phagocytosis assays with fluorescent labeled beads or pathogens such as *E.coli* can be used to identify a possible contribution in uptake processes. To examine the pathogen killing capacity of the macrophages, a gentamicin protection assay can be utilized. Fluorescence microscopy in combination with phalloidin staining for F-actin filaments might be a feasible approach to determine the polarization potential of the cells in response to the trigger. Leading edge formation accompanied with F-actin enrichment might also be useful. To clearly identify the leading edge, an additional paxillin, talin or vinculin staining would be necessary to visualize podosomes. These short lived, punctate structures are concurrently formed and recruited to membrane protrusions of motile cells, and are thought to be involved in tissue invasion and matrix remodeling, but also can be found *ex vivo* [187]. Utilization of wound healing and trans-well assays can be used to determine the role of selected cytoskeletal phosphoproteins in LPS-induced motility or respectively migration towards stimuli gradients. Altogether, the technique of specific siRNA KD in combination with the automated annotation software proved to be a promising approach to screen for phosphoproteins involved in TLR4-driven cytoskeletal rearrangements and select candidate proteins for further investigations.

5.4 Class I myosins MYO1e and MYO1f are required for efficient MØ spreading

MYO1e and MYO1f belong to the group of class I myosins composed of eight members, who are able to interact with actin filaments and lipid membranes through distinct regions in their C-terminal tail domain. Both proteins are so-called long-tailed class I myosins based on the presence of three tail homology domains (TH1, TH2 and a SH3 domain termed TH3) [99]. A strong and consistent phosphorylation of both motor proteins was found in TLR4-activated primary macrophages (Fig. 13). The majority of the identified LPS-regulated phosphosites are located within the TH2 domain and one threonine within the pleckstrin homology (PH) domain. The TH2 domain of long-tailed myosin is required for microtubule – F-actin

interaction [188, 189] and as well mediates an ATP-independent actin binding of the myosins [108]. Furthermore, the prolin-rich TH2-domain allows the oligomerization of long-tailed myosins critical for movement and cargo binding [130]. The PH domain is necessary for anionic phospholipid binding and membrane localization [125]. In previous studies a motility defect of murine neutrophils lacking MYO1f was described. This phenotype results from an abnormal increase in exocytosis of β_2-integrin containing granules, leading to an enhanced adherence [118].

The specific siRNA KD for *Myo1f* in primary macrophages resulted in a reduced basal contact area and an impaired LPS-induced spreading (Fig. 14). Given the observed MYO1f effect, we also examined the contribution of MYO1e, which showed considerably stronger phosphorylation after LPS stimulation (Fig. 13). In *Myo1e* KO macrophages, qRT-PCR analysis confirmed the lack of *Myo1e* transcripts, but in Western blots a faint band of the expected molecular weight (MW) was still observed (Fig. 15). We assume that this band is caused by cross reactivity of the antibody with MYO1f of the same MW of 125kDa. However, *Myo1e* KO MØ showed only a moderately reduced spreading response to LPS after 2 h and 8 h. Due to the high structural homology of both class I myosins we performed siRNA KD of *Myo1f* in *Myo1e* KO macrophages to generate "double-deficient" macrophages. MYO1e and MYO1f collaborated for efficient LPS-induced spreading in macrophages, as demonstrated by our experiment. FACS analysis of *Myo1f* KD macrophages should reveal whether the change in spreading phenotype is also caused by an altered integrin surface expression, as already described for neutrophils [118]. The expression of adhesion molecules on *Myo1e* KO macrophages was not influenced by the genetic deletion of the protein. All analyzed integrins were expressed comparable to WT control cells (Fig. 16).

However, recent studies provide evidence that MYO1e contributes in cytoskeleton rearrangement and cell adhesion. MYO1e in human umbilical vein endothelial cells (HUVEC) was identified to co-localize with CARMIL, FHOD1, ARP3 and β_3-intergins in early adhesion sites, suggested to transport the actin polymerization proteins to these structures and additionally be involved in its stabilization. The localization of MYO1e depends on its SH3 domain, which is not present in short tailed class I myosin isoforms [130]. Furthermore, proteomic studies identified MYO1e as a component of macrophage podosomes [190] and fibroblast integrin adhesome [191]. In fibroblasts the invadosome localization of MYO1e was identified to be dependent on its TH1 and TH2 domain [192] and in renal podocytes colocalizes with actin filaments at the site of newly established cell-cell contacts [135]. Fluorescence microscopy analysis of MYO1e in primary macrophages can be used to

examine the localization or TLR4-driven redistribution of the motor protein. The observation of an altered spreading phenotype of *Myo1e* KO macrophages led us to the question whether the migration of immune cells *in vivo* is influenced by the deletion of the motor protein. An *in vivo* model was utilized, where *Myo1e*-deficient immune cell recruitment in response to intraperitoneally injected, heat killed *E. coli* (as source of LPS) was studied (Fig. 17). Interestingly, analysis of the total cell influx at the site of injection revealed a significantly elevated cell number. The increased total cell number was not caused by the enhanced recruitment of a specific immune cell subset. Even cell types, such as neutrophils which do not express MYO1e under WT condition [118] were found enriched in the peritoneum. This indicates that MYO1e contributes in an immune response, which alters cell migration in a secondary way, leading to general enhanced immune cell recruitment. To further address this issue the distribution of immune cell subsets in different organs such as bone marrow, blood or spleen should be analyzed to determine a possible difference already under basal conditions in the utilized mouse model. Furthermore, the measurement of cytokines and chemokines in the peritoneum and in serum of mice can give a hint whether a possible alteration in their content is responsible for the increased cell influx in response to heat killed *E. coli*.

Since MYO1e and its SH3 domain was reported to be involved in receptor-mediated endocytosis [121], we investigated the contribution of MYO1e and MYO1f in TLR4-driven macrophage phagocytosis (data not shown). Application of an unspecific bead and *E. coli* phagocytosis assay showed a comparable uptake of particles or pathogens independent on the KO or siRNA KD of the motor proteins. In our hands, the uptake of fluorescent latex beads and GFP-expressing *E. coli* similarly increased over the time, even in *Myo1e* KO macrophages additionally treated with *Myo1f* siRNA. These results indicate that MYO1e and MYO1f are not involved in macrophage phagocytosis. *Myo1e*-deficient macrophages were utilized in a gentamicin protection assay to examine a possible role of the protein in pathogen killing. Incubation of macrophages with *E. coli*, *S. aureus* or *Salmonella* up to 20 h upon antibiotic treatment revealed no difference in pathogen killing dependent on the macrophage genotype. Thus, MYO1e also did not contribute in intracellular pathogen killing (data not shown).

5.5 MYO1e selectively regulates the release of the chemokine CCL2 from macrophages and DCs

Activation of TLR4 by LPS induces rapid and massive induction of pro-inflammatory gene expression as well as secretion of cytokines and chemokines known from quantitative proteome, transcriptome and secretome analysis, which are involved in cellular communication, adhesion and migration [193, 194]. An example is TNF, which may induce a spreading response in leukocytes [195]. Thus we examined whether the reduced spreading phenotype observed in *Myo1e* KO macrophages was related to TLR4-driven cytokines release (Fig. 18). The kinetic and amounts of TNF, IL-6, IL-12p40 and IL-10 were unaltered in macrophages lacking MYO1e. However, a significantly increased release of the chemokine CCL2/MCP-1 was detected in the supernatant of LPS-stimulated KO macrophages compared to WT cells at the 8 h and 24 h time points. This effect was specific for CCL2, as alterations in the secretion of other chemokines like IP-10 and CCL3 was not detected. A transiently higher release for CCL4 was observed in WT macrophages. Interestingly, an increased secretion of CCL2 was also measured when *Myo1e*$^{-/-}$ bone marrow-derived dendritic cells were stimulated with LPS (Fig. 21). Thus MYO1e, which is expressed in MØ and DCs [118], regulates TLR4-driven CCL2 release in both cell types. Recent studies showed that CCL2 causes cytoskeletal rearrangements and morphological changes in macrophages [196]. Blocking the CCL2 receptor CCR2 on macrophages with specific antibodies prior to LPS stimulation might reveal whether the reduced spreading observed in KO cells results from the elevated CCL2 in the supernatant or occurs as direct effect of the motor protein KO. The increased secretion of CCL2 is presumably caused by altered transport and release from the cells, because the downstream signaling measured by MAPK phosphorylation of p38 and ERK1/2 (Fig. 19 and 22) and expression on mRNA level (Fig. 20) was not altered in MYO1e MØ. A regulatory role of MYO1e in vesicular trafficking of the chemokine CCL2 seems therefore likely. Interestingly an involvement of the long-tailed class I myosins and their regulatory function in exocytosis processes was already observed. MYO1e is involved in granule release in *Xenopus oocytes* [127] and granulocytes deficient in MYO1f showed an increased CD18 surface expression [118]. To confirm the contribution of class I myosins in this context, the application of the pharmacological myosin 1 inhibitor PCIP can be useful [130]. These results indicate a conserved mechanism for the long-tailed myosins MYO1e in vesicle trafficking and exocytosis processes. Intracellular staining of CCL2 combined with FACS analysis can give additional information. Thus, cells lacking MYO1e should harbor

less intracellular CCL2 in response to LPS, on grounds of the increased release and unaltered biosynthesis of the chemokine. Due to the fact that no interaction partner for class I myosins in response to TLR4 activation is identified to explain this mechanism, immunoprecipitation experiments with a subsequent mass spectrometry analysis for co-precipitated proteins might be helpful.

5.6 MYO1e is required for optimal MHC-II surface expression on macrophages and DCs

Previous studies on *Myo1f*-deficient neutrophils demonstrated an increased surface expression of β_2-integrins, and thus the functional regulation of an endocytosis processes by a long-tailed myosin [118]. Therefore, we addressed the question whether MYO1e also contributes in expression of surface molecules on TLR4-activated MØ. FACS analysis of LPS-stimulated macrophages for surface molecules including integrins and co-stimulatory molecules revealed no obvious alterations in that expression, except of CD80, which was weakly but significantly reduced on LPS-activated MØ (Fig. 16 and 25). A surprising finding in *Myo1e*-deficient macrophages was the selective reduction in MHC-II surface expression levels under basal and LPS-induced conditions. Suggestions that MYO1e regulates the intracellular transport of MHC-II were corroborated by the unchanged mRNA transcription of the molecule in Myo1e KO cells (Fig. 24). Also in DCs, which expressed much higher levels of MHC-II, a MYO1e-dependent reduction of MHC-II 24h after LPS stimulation was observed (Fig. 26). A contribution of the motor protein in MHC-II expression on B-cells, which exclusively express MYO1e [118], was not detected in our hands (Fig. 31). Interestingly, recent system biology studies of pathways controlling antigen presentation described a function for MYO1e in the regulation of intracellular MHC-II transport to the plasma membrane [132, 197]. In a genome-wide RNAi screen the authors found the GTPase ARL14/ARF7 to be involved in MHC-II expression, followed by yeast-2-hybrid-based identification of its effector protein ARF7EP. Subsequent pulldown experiments with GST-tagged ARF7EP in cytosolic extracts of human PBMCs identified MYO1e by mass spectrometry analysis and finally confirmed this interaction by co-immunoprecipitation. Based on their findings the researchers postulated that ARF7 connects to the actin network by ARF7-MYO1e interaction and thus controls the redistribution of MHC-II [132, 197]. Whether the same or comparable interactions in murine macrophages or DCs are responsible in regulation of MYO1e-dependent MHC-II surface expression is currently unknown. Specific siRNA KD experiments in murine MØ and DC for the GTPase ARF7 or its effector protein ARF7EP can give first indications, if resulting in

comparable MHC-II surface expression patterns as observed in *Myo1e* KO cells. Furthermore, co-localization studies by fluorescence microscopy for intracellular MHC-II and MYO1e in WT and KO cells can be used to visualize the interaction and motor protein-dependent redistribution in response to LPS. In addition to the *Myo1e* KO, the global class I myosin inhibitor PCIP [130, 198, 199] can be utilized to reveal a possible contribution of other class I myosins such as MYO1f in MHC-II surface expression. To examine the role of MYO1f in this context we already applied MYO1f KD in MYO1e KO MØ (data not shown). However, cells treated either with specific or non-targeting control siRNA showed an increase in MHC-II surface expression throughout TLR4 activation, comparable to IFNγ stimulation. This indicates that siRNA treatment may activate oligonucleotide recognition receptors, induce an IFN response and thus may influence the sensible and IFN-dependent MHC expression. To address this issue the employment of *Myo1e*/*Myo1f* double KO cells will be essential.

5.7 *Myo1e*-deficient antigen-presenting cells are impaired in eliciting T-cell activation

The surprising finding that MYO1e selectively regulates MHC-II surface protein in murine macrophages and DCs indicated a possible effect on antigen presentation and elicitation of T-cell responses. Whether the MYO1e-dependent MHC-II phenotype is functional relevant was analyzed in an OT-II system. Hence, purified CD4 T-cells from OT-II transgenic mice which carry a T-cell receptor (TCR) specific for MHC-II-bound ovalbumin (OVA) peptide were co-cultured with APCs pre-incubated with whole OVA protein, and antigen-specific T-cell activation was analyzed (Fig. 27 and 28). In case of macrophages only a high number of *Myo1e* KO cells within the co-culture results in the same T-cell proliferation comparable to WT conditions, although T-cells still produced significantly less amounts of IFNγ (Fig. 27). DCs lacking MYO1e showed an impaired activation capacity under high DC-OT-II ratio observed by reduced antigen-specific T-cell proliferation, and IFNγ production (Fig. 28). This indicates that the absence of MYO1e in macrophages and DC led to a significant reduction in the capacity of APCs to induce an antigen-specific cytokine-production and CD4 T-cell proliferation. Interestingly, a participation of a class I myosin in MHC-II mediated T-cell activation has also been described in B-cells. Here the short-tailed myosin MYO1c was shown to interact with MHC-II and contribute in antigen-specific CD4 T-cell stimulation. Overexpression of a dominant-negative MYO1c version or specific siRNA knockdown led to

reduced T-cell activation and IL-2 secretion induced by B lymphocytes [162]. Our results showed that MYO1e in MØ and DC is essential to induce a full MHC-II response.

However, the OT-II approach used in our experiments did not offer the information whether the impaired T-cell activation was directly caused by the decrease in MHC-II surface expression or additionally through an alteration in endocytosis or antigen processing. To address this issue, a possible change in antigen processing caused by the *Myo1e* KO was analyzed by utilization of DQ-OVA, a fluorescently labeled OVA which illuminates upon proteolytical cleavage. To simulate conditions comparable to the OT-II assay, the DQ-OVA was kept within the APC culture until 24 h instead of a short pulse period (Fig. 29). In MØ the antigen processing throughout the whole kinetic was not influenced by the *Myo1e*-deficiency, and thus also an alteration in endocytosis can be excluded. Hence, the impaired T-cell activation capacity of *Myo1e* KO macrophages most likely derived from the reduced MHC-II surface expression in combination with a weak reduction in CD80. DCs are not as fast in antigen processing as MØ, caused by the lower protease content within their lysosomes [200, 201]. This behavior was also observed in our experiments, confirming the properness of the applied DQ-OVA assay. However, DC lacking MYO1e showed a constantly enhanced antigen processing compared to WT cells. This raises the question whether MYO1e contributes in the regulation of antigen processing in murine DC or whether it influences endocytosis. A contribution of MYO1e in endocytosis processes was already described in fibroblasts [121, 122] Application of fluorescently labeled OVA, able to illuminate without previous cleavage, additionally to DQ-OVA should dissect the role for MYO1e in the different processes.

To investigate the issue in the OT-II system it is necessary to use the $OVA_{323-339}$ peptide [202] instead of whole OVA protein to circumvent the need for intracellular antigen processing. The slow antigen processing capacity of DC under WT conditions is advantageous for a better T-cell activation. In contrast, the rapid proteolytical cleavage in MØ causes an excess of antigens followed by degradation for the majority of the processed peptides. This characteristic prevents a strong T-cell activation by macrophages. The enhanced antigen processing in *Myo1e* KO DC might cause a comparable effect, and thus, additionally to a reduced MHC-II surface expression, lead to the impaired T-cell activation.

Since in this thesis exclusively MYO1e-dependent phenotypes were described, the challenge for future experiments will be to determine the mechanisms by which the motor protein controls spreading, chemokine secretion and MHC-II presentation in macrophages and DC. In

addition to the analysis of the cell biology of MYO1e, the regulation of its localization and interaction with binding partners by site-specific phosphorylation needs to be studied in detail. The involvement of Myo1e in several key functional aspects of macrophage and DC biology (such as cell spreading and motility, chemokine secretion and antigen presentation), shown here in vitro, suggests that this motor protein may also play an important role in innate immune cell recruitment and function during inflammatory and infectious disease processes *in vivo*.

References

1. Belkaid, Y. and D. Artis, *Immunity at the Barriers.* European Journal of Immunology, 2013. **43**(12): p. 3096-3097.
2. Janeway, C.A., Jr.; Murphy, K.; Travers, P.; Walport, M., *Janeway Immunologie*. Vol. 7. 2009: Spektrum Akademischer verlag Heidelberg.
3. Metchnikoff, E., *On the Present State of the Question of Immunity in Infectious Diseases.* Scandinavian Journal of Immunology, 1989. **30**(4): p. 387-398.
4. Weidenbusch, M. and H.J. Anders, *Tissue Microenvironments Define and Get Reinforced by Macrophage Phenotypes in Homeostasis or during Inflammation, Repair and Fibrosis.* Journal of Innate Immunity, 2012. **4**(5-6): p. 463-477.
5. Lech, M., et al., *Tissues use resident dendritic cells and macrophages to maintain homeostasis and to regain homeostasis upon tissue injury: the immunoregulatory role of changing tissue environments.* Mediators Inflamm, 2012. **951390**(10): p. 3.
6. Karcher, R.L., S.W. Deacon, and V.I. Gelfand, *Motor–cargo interactions: the key to transport specificity.* Trends in Cell Biology, 2002. **12**(1): p. 21-27.
7. Moqbel, R. and J.J. Coughlin, *Differential secretion of cytokines.* Sci STKE, 2006. **2006**(338): p. pe26.
8. Stow, J.L., et al., *Cytokine secretion in macrophages and other cells: pathways and mediators.* Immunobiology, 2009. **214**(7): p. 601-12.
9. Akhmanova, A. and J.A. Hammer Iii, *Linking molecular motors to membrane cargo.* Current Opinion in Cell Biology, 2010. **22**(4): p. 479-487.
10. Stow, J.L. and R.Z. Murray, *Intracellular trafficking and secretion of inflammatory cytokines.* Cytokine & growth factor reviews, 2013. **24**(3): p. 227-39.
11. Lucas, M., et al., *Apoptotic Cells and Innate Immune Stimuli Combine to Regulate Macrophage Cytokine Secretion.* The Journal of Immunology, 2003. **171**(5): p. 2610-2615.
12. Stoy, N., *Macrophage Biology and Pathobiology in the Evolution of Immune Responses: A Functional Analysis.* Pathobiology, 2001. **69**(4): p. 179-211.
13. Greenberg, S. and S. Grinstein, *Phagocytosis and innate immunity.* Current Opinion in Immunology, 2002. **14**(1): p. 136-145.
14. Rougerie, P., V. Miskolci, and D. Cox, *Generation of membrane structures during phagocytosis and chemotaxis of macrophages: role and regulation of the actin cytoskeleton.* Immunological Reviews, 2013. **256**(1): p. 222-239.
15. Yeo, J.C., et al., *High-throughput quantification of early stages of phagocytosis.* Biotechniques, 2013. **55**(3): p. 115-24.
16. Saftig, P. and J. Klumperman, *Lysosome biogenesis and lysosomal membrane proteins: trafficking meets function.* Nat Rev Mol Cell Biol, 2009. **10**(9): p. 623-635.
17. Flannagan, R.S., G. Cosio, and S. Grinstein, *Antimicrobial mechanisms of phagocytes and bacterial evasion strategies.* Nat Rev Micro, 2009. **7**(5): p. 355-366.
18. Mantegazza, A.R., et al., *Presentation of Phagocytosed Antigens by MHC Class I and II.* Traffic, 2013. **14**(2): p. 135-52.
19. Neefjes, J., et al., *Towards a systems understanding of MHC class I and MHC class II antigen presentation.* Nat Rev Immunol, 2011. **11**(12): p. 823-36.
20. Janeway, C.A. and R. Medzhitov, *INNATE IMMUNE RECOGNITION.* Annual Review of Immunology, 2002. **20**(1): p. 197-216.
21. Suresh, R. and D.M. Mosser, *Pattern recognition receptors in innate immunity, host defense, and immunopathology.* Advances in physiology education, 2013. **37**(4): p. 284-91.
22. Lemaitre, B., et al., *The Dorsoventral Regulatory Gene Cassette spätzle/Toll/cactus Controls the Potent Antifungal Response in Drosophila Adults.* Cell, 1996. **86**(6): p. 973-983.
23. Kawai, T. and S. Akira, *The role of pattern-recognition receptors in innate immunity: update on Toll-like receptors.* Nat Immunol, 2010. **11**(5): p. 373-384.

24. Akira, S. and K. Takeda, *Toll-like receptor signalling.* Nat Rev Immunol, 2004. **4**(7): p. 499-511.
25. Akira, S., S. Uematsu, and O. Takeuchi, *Pathogen recognition and innate immunity.* Cell, 2006. **124**(4): p. 783-801.
26. Kawai, T. and S. Akira, *TLR signaling.* Cell Death Differ, 2006. **13**(5): p. 816-825.
27. Lu, Y.-C., W.-C. Yeh, and P.S. Ohashi, *LPS/TLR4 signal transduction pathway.* Cytokine, 2008. **42**(2): p. 145-151.
28. Kawai, T., et al., *Unresponsiveness of MyD88-Deficient Mice to Endotoxin.* Immunity, 1999. **11**(1): p. 115-122.
29. Hiroaki Hemmi, S.A., *TLR Signalling and the Function of Dendritic Cells.* Chem Immunol Allergy, 2005. **86**: p. 120-135.
30. Weintz, G., et al., *The phosphoproteome of toll-like receptor-activated macrophages.* Molecular systems biology, 2010. **6**: p. 371.
31. Martinez-Lopez, N. and R. Singh, *ATGs: Scaffolds for MAPK/ERK signaling.* Autophagy, 2014. **10**(3): p. 123-125.
32. Rousseau, S., et al., *p38 MAP kinase activation by vascular endothelial growth factor mediates actin reorganization and cell migration in human endothelial cells.* Oncogene, 1997. **15**(18): p. 2169-77.
33. Ono, K. and J. Han, *The p38 signal transduction pathway Activation and function.* Cellular Signalling, 2000. **12**(1): p. 1-13.
34. Kondoh, K. and E. Nishida, *Regulation of MAP kinases by MAP kinase phosphatases.* Biochimica et Biophysica Acta (BBA) - Molecular Cell Research, 2007. **1773**(8): p. 1227-1237.
35. Farooq, A. and M.-M. Zhou, *Structure and regulation of MAPK phosphatases.* Cellular Signalling, 2004. **16**(7): p. 769-779.
36. Hammer, M., et al., *Control of dual-specificity phosphatase-1 expression in activated macrophages by IL-10.* European Journal of Immunology, 2005. **35**(10): p. 2991-3001.
37. Lang, R., M. Hammer, and J. Mages, *DUSP meet immunology: dual specificity MAPK phosphatases in control of the inflammatory response.* Journal of immunology, 2006. **177**(11): p. 7497-504.
38. Shen, J., et al., *Lack of Mitogen-Activated Protein Kinase Phosphatase-1 Protects ApoE-Null Mice Against Atherosclerosis.* Circulation Research, 2010. **106**(5): p. 902-910.
39. Tanoue, T., et al., *A Novel MAPK Phosphatase MKP-7 Acts Preferentially on JNK/SAPK and p38α and β MAPKs.* Journal of Biological Chemistry, 2001. **276**(28): p. 26629-26639.
40. Katagiri, C., et al., *Phosphorylation of Ser-446 Determines Stability of MKP-7.* Journal of Biological Chemistry, 2005. **280**(15): p. 14716-14722.
41. Niedzielska, M., et al., *Gene Trap Mice Reveal an Essential Function of Dual Specificity Phosphatase Dusp16/MKP-7 in Perinatal Survival and Regulation of Toll-like Receptor (TLR)-induced Cytokine Production.* Journal of Biological Chemistry, 2014. **289**(4): p. 2112-2126.
42. Wickstead, B. and K. Gull, *The evolution of the cytoskeleton.* The Journal of Cell Biology, 2011. **194**(4): p. 513-525.
43. Moulding, D.A., et al., *Actin cytoskeletal defects in immunodeficiency.* Immunological Reviews, 2013. **256**(1): p. 282-299.
44. Burkhardt, J.K., *Cytoskeletal function in the immune system.* Immunological Reviews, 2013. **256**(1): p. 5-9.
45. Hsieh, M.J., P.J. White, and C.W. Pouton, *Interaction of viruses with host cell molecular motors.* Current Opinion in Biotechnology, 2010. **21**(5): p. 633-639.
46. Gruenheid, S. and B.B. Finlay, *Microbial pathogenesis and cytoskeletal function.* Nature, 2003. **422**(6933): p. 775-781.
47. Gaudin, R., et al., *HIV trafficking in host cells: motors wanted!* Trends in cell biology, 2013. **23**(12): p. 652-662.

48. Nogales, E., *STRUCTURAL INSIGHTS INTO MICROTUBULE FUNCTION.* Annual Review of Biochemistry, 2000. **69**(1): p. 277-302.
49. Wade, R., *On and Around Microtubules: An Overview.* Molecular Biotechnology, 2009. **43**(2): p. 177-191.
50. Westermann, S. and K. Weber, *Post-translational modifications regulate microtubule function.* Nat Rev Mol Cell Biol, 2003. **4**(12): p. 938-948.
51. Binker, M.G., et al., *Cytoplasmic Linker Protein-170 Enhances Spreading and Phagocytosis in Activated Macrophages by Stabilizing Microtubules.* The Journal of Immunology, 2007. **179**(6): p. 3780-3791.
52. Hanania, R., et al., *Classically Activated Macrophages Use Stable Microtubules for Matrix Metalloproteinase-9 (MMP-9) Secretion.* Journal of Biological Chemistry, 2012. **287**(11): p. 8468-8483.
53. Roberts, A.J., et al., *Functions and mechanics of dynein motor proteins.* Nat Rev Mol Cell Biol, 2013.
54. Goldman, R.D., et al., *The function of intermediate filaments in cell shape and cytoskeletal integrity.* The Journal of Cell Biology, 1996. **134**(4): p. 971-983.
55. Herrmann, H. and U. Aebi, *INTERMEDIATE FILAMENTS: Molecular Structure, Assembly Mechanism, and Integration Into Functionally Distinct Intracellular Scaffolds.* Annual Review of Biochemistry, 2004. **73**(1): p. 749-789.
56. Herrmann, H., et al., *Intermediate filaments: from cell architecture to nanomechanics.* Nat Rev Mol Cell Biol, 2007. **8**(7): p. 562-573.
57. Chung, B.-M., J.D. Rotty, and P.A. Coulombe, *Networking galore: intermediate filaments and cell migration.* Current Opinion in Cell Biology, 2013. **25**(5): p. 600-612.
58. Brown, M.J., et al., *Rigidity of Circulating Lymphocytes Is Primarily Conferred by Vimentin Intermediate Filaments.* The Journal of Immunology, 2001. **166**(11): p. 6640-6646.
59. Beneš, P., et al., *Role of vimentin in regulation of monocyte/macrophage differentiation.* Differentiation, 2006. **74**(6): p. 265-276.
60. de Lanerolle, P. and L. Serebryannyy, *Nuclear actin and myosins: Life without filaments.* Nat Cell Biol, 2011. **13**(11): p. 1282-1288.
61. Biro, M., et al., *Cell cortex composition and homeostasis resolved by integrating proteomics and quantitative imaging.* Cytoskeleton (Hoboken), 2013.
62. Aunis, D. and M.F. Bader, *The cytoskeleton as a barrier to exocytosis in secretory cells.* J Exp Biol, 1988. **139**: p. 253-66.
63. Nakaseko, Y. and M. Yanagida, *Cell biology: Cytoskeleton in the cell cycle.* Nature, 2001. **412**(6844): p. 291-292.
64. Pollard, T.D. and G.G. Borisy, *Cellular Motility Driven by Assembly and Disassembly of Actin Filaments.* Cell, 2003. **112**(4): p. 453-465.
65. Pollard, T.D. and J.A. Cooper, *Actin, a central player in cell shape and movement.* Science, 2009. **326**(5957): p. 1208-12.
66. Fletcher, D.A. and R.D. Mullins, *Cell mechanics and the cytoskeleton.* Nature, 2010. **463**(7280): p. 485-492.
67. Li, R. and G.G. Gundersen, *Beyond polymer polarity: how the cytoskeleton builds a polarized cell.* Nat Rev Mol Cell Biol, 2008. **9**(11): p. 860-873.
68. Amann, K.J. and T.D. Pollard, *Cellular regulation of actin network assembly.* Current Biology, 2000. **10**(20): p. R728-R730.
69. Shinji, H., et al., *Reorganization of microfilaments in macrophages after LPS stimulation.* Exp Cell Res, 1991. **193**(1): p. 127-33.
70. Terman, J.R. and A. Kashina, *Post-translational modification and regulation of actin.* Current Opinion in Cell Biology, 2013. **25**(1): p. 30-38.
71. Aberle, H., *Redox switch for actin.* Nat Cell Biol, 2013. **15**(12): p. 1403-1404.
72. Hung, R.-J., et al., *SelR reverses Mical-mediated oxidation of actin to regulate F-actin dynamics.* Nat Cell Biol, 2013. **15**(12): p. 1445-1454.

73. Kleveta, G., et al., *LPS induces phosphorylation of actin-regulatory proteins leading to actin reassembly and macrophage motility.* Journal of Cellular Biochemistry, 2012. **113**(1): p. 80-92.
74. Dai, Q. and S.B. Pruett, *Ethanol suppresses LPS-induced Toll-like receptor 4 clustering, reorganization of the actin cytoskeleton, and associated TNF-alpha production.* Alcohol Clin Exp Res, 2006. **30**(8): p. 1436-44.
75. Kustermans, G., et al., *Perturbation of actin dynamics induces NF-kappaB activation in myelomonocytic cells through an NADPH oxidase-dependent pathway.* Biochem. J., 2005. **387**(2): p. 531-540.
76. Legrand-Poels, S., et al., *Modulation of Nod2-dependent NF-κB signaling by the actin cytoskeleton.* Journal of Cell Science, 2007. **120**(7): p. 1299-1310.
77. Eswarappa, S.M., V. Pareek, and D. Chakravortty, *Role of actin cytoskeleton in LPS-induced NF-kappaB activation and nitric oxide production in murine macrophages.* Innate Immun, 2008. **14**(5): p. 309-18.
78. Burridge, K. and K. Wennerberg, *Rho and Rac Take Center Stage.* Cell, 2004. **116**(2): p. 167-179.
79. Barrio, L., J. Saez de Guinoa, and Y.R. Carrasco, *TLR4 Signaling Shapes B Cell Dynamics via MyD88-Dependent Pathways and Rac GTPases.* The Journal of Immunology, 2013. **191**(7): p. 3867-3875.
80. Stanley, A.C., et al., *The Rho GTPase Rac1 is required for recycling endosome-mediated secretion of TNF in macrophages.* Immunol Cell Biol, 2013.
81. Kong, L. and B.X. Ge, *MyD88-independent activation of a novel actin-Cdc42/Rac pathway is required for Toll-like receptor-stimulated phagocytosis.* Cell Res, 2008. **18**(7): p. 745-55.
82. Smith, S.D., et al., *PAK1-mediated activation of ERK1/2 regulates lamellipodial dynamics.* J Cell Sci, 2008. **121**(Pt 22): p. 3729-36.
83. Pichon, S., M. Bryckaert, and E. Berrou, *Control of actin dynamics by p38 MAP kinase – Hsp27 distribution in the lamellipodium of smooth muscle cells.* Journal of Cell Science, 2004. **117**(12): p. 2569-2577.
84. Faix, J., *Formine und Aktinzytoskelett.* BIOSpektrum, 2006. **01**: p. 19.
85. Pollard, T.D., *Regulation of Actin Filament Assembly by Arp2/3 Complex and Formins.* Annual Review of Biophysics and Biomolecular Structure, 2007. **36**(1): p. 451-477.
86. Boehm, M.B., et al., *The mammalian formin FHOD1 interacts with the ERK MAP kinase pathway.* Biochemical and Biophysical Research Communications, 2005. **335**(4): p. 1090-1094.
87. Takeya, R., et al., *The mammalian formin FHOD1 is activated through phosphorylation by ROCK and mediates thrombin-induced stress fibre formation in endothelial cells.* The EMBO Journal, 2008. **27**(4): p. 618-628.
88. Insall, R.H. and L.M. Machesky, *Actin Dynamics at the Leading Edge: From Simple Machinery to Complex Networks.* Developmental Cell, 2009. **17**(3): p. 310-322.
89. LeClaire, L.L., et al., *Phosphorylation of the Arp2/3 complex is necessary to nucleate actin filaments.* The Journal of Cell Biology, 2008. **182**(4): p. 647-654.
90. Choi, C.H., et al., *Phosphorylation of actin-related protein 2 (Arp2) is required for normal development and cAMP chemotaxis in Dictyostelium.* The Journal of biological chemistry, 2013. **288**(4): p. 2464-74.
91. Mendoza, Michelle C., et al., *ERK-MAPK Drives Lamellipodia Protrusion by Activating the WAVE2 Regulatory Complex.* Molecular Cell, 2011. **41**(6): p. 661-671.
92. Singh, S., et al., *Identification of the p16-Arc Subunit of the Arp 2/3 Complex as a Substrate of MAPK-activated Protein Kinase 2 by Proteomic Analysis.* Journal of Biological Chemistry, 2003. **278**(38): p. 36410-36417.
93. Li, Y., A. Guerrero, and T.H. Howard, *The actin-binding protein, lymphocyte-specific protein 1, is expressed in human leukocytes and human myeloid and lymphoid cell lines.* The Journal of Immunology, 1995. **155**(7): p. 3563-9.

94. Huang, C.-K., et al., *LSP1 Is the Major Substrate for Mitogen-activated Protein Kinase-activated Protein Kinase 2 in Human Neutrophils.* Journal of Biological Chemistry, 1997. **272**(1): p. 17-19.
95. Harrison, R.E., B.A. Sikorski, and J. Jongstra, *Leukocyte-specific protein 1 targets the ERK/MAP kinase scaffold protein KSR and MEK1 and ERK2 to the actin cytoskeleton.* Journal of Cell Science, 2004. **117**(10): p. 2151-2157.
96. Krendel, M. and M.S. Mooseker, *Myosins: Tails (and Heads) of Functional Diversity.* Physiology, 2005. **20**(4): p. 239-251.
97. Sladewski, T.E., et al., *Single-molecule reconstitution of mRNA transport by a class V myosin.* Nat Struct Mol Biol, 2013. **20**(8): p. 952-957.
98. Maravillas-Montero, J.L. and L. Santos-Argumedo, *The myosin family: unconventional roles of actin-dependent molecular motors in immune cells.* J Leukoc Biol, 2012. **91**(1): p. 35-46.
99. McConnell, R.E. and M.J. Tyska, *Leveraging the membrane - cytoskeleton interface with myosin-1.* Trends Cell Biol, 2010. **20**(7): p. 418-26.
100. Mermall, V., P.L. Post, and M.S. Mooseker, *Unconventional Myosins in Cell Movement, Membrane Traffic, and Signal Transduction.* Science, 1998. **279**(5350): p. 527-533.
101. Kumar, C.C., et al., *Characterization and differential expression of human vascular smooth muscle myosin light chain 2 isoform in nonmuscle cells.* Biochemistry, 1989. **28**(9): p. 4027-4035.
102. Taylor, K.A., et al., *Role of the essential light chain in the activation of smooth muscle myosin by regulatory light chain phosphorylation.* Journal of Structural Biology, 2013(0).
103. Barylko, B., D.D. Binns, and J.P. Albanesi, *Regulation of the enzymatic and motor activities of myosin I.* Biochimica et Biophysica Acta (BBA) - Molecular Cell Research, 2000. **1496**(1): p. 23-35.
104. Jurado, L.A., P.S. Chockalingam, and H.W. Jarrett, *Apocalmodulin.* Physiological Reviews, 1999. **79**(3): p. 661-682.
105. Leibler, S. and D.A. Huse, *Porters versus rowers: a unified stochastic model of motor proteins.* The Journal of Cell Biology, 1993. **121**(6): p. 1357-1368.
106. O'Connell, C.B., M.J. Tyska, and M.S. Mooseker, *Myosin at work: Motor adaptations for a variety of cellular functions.* Biochimica et Biophysica Acta (BBA) - Molecular Cell Research, 2007. **1773**(5): p. 615-630.
107. Kim, S.V. and R.A. Flavell, *Myosin I: From yeast to human.* Cellular and Molecular Life Sciences, 2008. **65**(14): p. 2128-2137.
108. Coluccio, L.M., *Myosin I.* Am J Physiol, 1997. **273**(2 Pt 1): p. C347-59.
109. Greenberg, M.J. and E.M. Ostap, *Regulation and control of myosin-I by the motor and light chain-binding domains.* Trends Cell Biol, 2013. **23**(2): p. 81-9.
110. Fujita-Becker, S., et al., *Changes in Mg2+ ion concentration and heavy chain phosphorylation regulate the motor activity of a class I myosin.* J Biol Chem, 2005. **280**(7): p. 6064-71.
111. Osherov, N. and G.S. May, *In vivo function of class I myosins.* Cell Motility and the Cytoskeleton, 2000. **47**(3): p. 163-173.
112. Houdusse, A., M. Silver, and C. Cohen, *A model of Ca(2+)-free calmodulin binding to unconventional myosins reveals how calmodulin acts as a regulatory switch.* Structure, 1996. **4**(12): p. 1475-90.
113. Diakonova, M., G. Bokoch, and J.A. Swanson, *Dynamics of Cytoskeletal Proteins during Fcγ Receptor-mediated Phagocytosis in Macrophages.* Molecular Biology of the Cell, 2002. **13**(2): p. 402-411.
114. Dart, A.E., et al., *The motor protein myosin 1G functions in FcgammaR-mediated phagocytosis.* Journal of cell science, 2012. **125**(Pt 24): p. 6020-9.
115. Maravillas-Montero, J.L., et al., *Myosin 1c Participates in B Cell Cytoskeleton Rearrangements, Is Recruited to the Immunologic Synapse, and Contributes to Antigen Presentation.* The Journal of Immunology, 2011. **187**(6): p. 3053-3063.

116. Santos-Argumedo, L., J.L. Maravillas-Montero, and O. López-Ortega, *Class I myosins in B-cell physiology: functions in spreading, immune synapses, motility, and vesicular traffic.* Immunological Reviews, 2013. **256**(1): p. 190-202.
117. Maravillas-Montero, J.L., et al., *Myosin 1g regulates cytoskeleton plasticity, cell migration, exocytosis and endocytosis in B lymphocytes.* European Journal of Immunology, 2013: p. n/a-n/a.
118. Kim, S.V., et al., *Modulation of cell adhesion and motility in the immune system by Myo1f.* Science, 2006. **314**(5796): p. 136-9.
119. Tsiavaliaris, G., et al., *Mechanism, regulation, and functional properties of Dictyostelium myosin-1B.* J Biol Chem, 2008. **283**(8): p. 4520-7.
120. Stöffler, H.-E. and M. Bähler, *The ATPase Activity of Myr3, a Rat Myosin I, Is Allosterically Inhibited by Its Own Tail Domain and by Ca2+ Binding to Its Light Chain Calmodulin.* Journal of Biological Chemistry, 1998. **273**(23): p. 14605-14611.
121. Krendel, M., E.K. Osterweil, and M.S. Mooseker, *Myosin 1E interacts with synaptojanin-1 and dynamin and is involved in endocytosis.* FEBS Lett, 2007. **581**(4): p. 644-50.
122. Cheng, J., A. Grassart, and D.G. Drubin, *Myosin 1E coordinates actin assembly and cargo trafficking during clathrin-mediated endocytosis.* Mol Biol Cell, 2012.
123. Chen, C.L., et al., *Myosin I links PIP3 signaling to remodeling of the actin cytoskeleton in chemotaxis.* Sci Signal, 2012. **5**(209): p. ra10.
124. Patino-Lopez, G., et al., *Myosin 1G Is an Abundant Class I Myosin in Lymphocytes Whose Localization at the Plasma Membrane Depends on Its Ancient Divergent Pleckstrin Homology (PH) Domain (Myo1PH).* Journal of Biological Chemistry, 2010. **285**(12): p. 8675-8686.
125. Feeser, E.A., et al., *Myo1e binds anionic phospholipids with high affinity.* Biochemistry, 2010. **49**(43): p. 9353-60.
126. Taylor, M.J., D. Perrais, and C.J. Merrifield, *A high precision survey of the molecular dynamics of mammalian clathrin-mediated endocytosis.* PLoS Biol, 2011. **9**(3): p. e1000604.
127. Schietroma, C., et al., *A role for myosin 1e in cortical granule exocytosis in Xenopus oocytes.* J Biol Chem, 2007. **282**(40): p. 29504-13.
128. Bond, L.M., et al., *Myosin motor proteins are involved in the final stages of the secretory pathways.* Biochem Soc Trans, 2011. **39**(5): p. 1115-9.
129. Papadopulos, A., et al., *The cortical acto-myosin network: from diffusion barrier to functional gateway in the transport of neurosecretory vesicles to the plasma membrane.* Frontiers in Endocrinology, 2013. **4**.
130. Gupta, P., et al., *Myosin 1E localizes to actin polymerization sites in lamellipodia, affecting actin dynamics and adhesion formation.* Biology Open, 2013. **2**(12): p. 1288-1299.
131. Lindvall, J.M., et al., *Differential expression and molecular characterisation of Lmo7, Myo1e, Sash1, and Mcoln2 genes in Btk-defective B-cells.* Cell Immunol, 2005. **235**(1): p. 46-55.
132. Paul, P., et al., *A Genome-wide multidimensional RNAi screen reveals pathways controlling MHC class II antigen presentation.* Cell, 2011. **145**(2): p. 268-83.
133. Krendel, M., et al., *Disruption of Myosin 1e promotes podocyte injury.* J Am Soc Nephrol, 2009. **20**(1): p. 86-94.
134. Chase, S.E., et al., *Podocyte-specific knockout of myosin 1e disrupts glomerular filtration.* Am J Physiol Renal Physiol, 2012.
135. Bi, J., et al., *Myosin 1e is a component of the glomerular slit diaphragm complex that regulates actin reorganization during cell-cell contact formation in podocytes.* American Journal of Physiology - Renal Physiology, 2013.
136. Monick, M.M., et al., *Interaction of matrix with integrin receptors is required for optimal LPS-induced MAP kinase activation.* Am J Physiol Lung Cell Mol Physiol, 2002. **283**(2): p. L390-402.

137. Zhang, Y. and H. Wang, *Integrin signalling and function in immune cells.* Immunology, 2012. **135**(4): p. 268-275.
138. Evans, R., et al., *Integrins in immunity.* J Cell Sci, 2009. **122**(Pt 2): p. 215-25.
139. Caron, E., A.J. Self, and A. Hall, *The GTPase Rap1 controls functional activation of macrophage integrin alphaMbeta2 by LPS and other inflammatory mediators.* Curr Biol, 2000. **10**(16): p. 974-8.
140. Schmidt, A., E. Caron, and A. Hall, *Lipopolysaccharide-induced activation of beta2-integrin function in macrophages requires Irak kinase activity, p38 mitogen- activated protein kinase, and the Rap1 GTPase.* Mol Cell Biol, 2001. **21**(2): p. 438-48.
141. Han, C., et al., *Integrin CD11b negatively regulates TLR-triggered inflammatory responses by activating Syk and promoting degradation of MyD88 and TRIF via Cbl-b.* Nat Immunol, 2010. **11**(8): p. 734-42.
142. Böhm, C., et al., *The α-Isoform of p38 MAPK Specifically Regulates Arthritic Bone Loss.* The Journal of Immunology, 2009. **183**(9): p. 5938-5947.
143. Livak, K.J. and T.D. Schmittgen, *Analysis of Relative Gene Expression Data Using Real-Time Quantitative PCR and the 2−ΔΔCT Method.* Methods, 2001. **25**(4): p. 402-408.
144. Towbin, H., T. Staehelin, and J. Gordon, *Electrophoretic transfer of proteins from polyacrylamide gels to nitrocellulose sheets: procedure and some applications.* Proc Natl Acad Sci U S A, 1979. **76**(9): p. 4350-4.
145. Stockinger, B., et al., *B cells solicit their own help from T cells.* J Exp Med, 1996. **183**(3): p. 891-9.
146. Wiese, M., et al., *Small interfering RNA (siRNA) delivery into murine bone marrow-derived macrophages by electroporation.* Journal of Immunological Methods, 2010. **353**(1–2): p. 102-110.
147. Wenzel, J., et al., *Measurement of TLR-Induced Macrophage Spreading by Automated Image Analysis: Differential Role of Myd88 and MAPK in Early and Late Responses.* Front Physiol, 2011. **2**: p. 71.
148. Adachi, O., et al., *Targeted Disruption of the MyD88 Gene Results in Loss of IL-1- and IL-18-Mediated Function.* Immunity, 1998. **9**(1): p. 143-150.
149. Dorfman, K., et al., *Disruption of the erp/mkp-1 gene does not affect mouse development: normal MAP kinase activity in ERP/MKP-1-deficient fibroblasts.* Oncogene, 1996. **13**(5): p. 925-31.
150. Hammer, M., et al., *Dual specificity phosphatase 1 (DUSP1) regulates a subset of LPS-induced genes and protects mice from lethal endotoxin shock.* The Journal of Experimental Medicine, 2006. **203**(1): p. 15-20.
151. Weintz, G., et al., *The phosphoproteome of toll-like receptor-activated macrophages.* Mol Syst Biol, 2010. **6**: p. 371.
152. Held, C., et al., *Using multimodal information for the segmentation of fluorescent micrographs with application to virology and microbiology.* Conf Proc IEEE Eng Med Biol Soc, 2011. **2011**: p. 6487-90.
153. Roerdink, J. and A. Meijster, *The watershed transform: definitions, algorithms and parallelization strategies.* Math. Morphol., 2000. **41**: p. 187-228.
154. Held, C., et al. *Using multimodal information for the segmentation of fluorescent micrographs with application to Virology and microbiology*. in *Engineering in Medicine and Biology Society,EMBC, 2011 Annual International Conference of the IEEE*. 2011.
155. Sethian, J., *Level Set Methods and Fast Marching Methods.* Cambridge: Cambridge University Press, 1999.
156. Grill, C., et al., *Analysis of the ERK1,2 transcriptome in mammary epithelial cells.* The Biochemical journal, 2004. **381**(Pt 3): p. 635-44.
157. Patterson, K.I., et al., *Dual-specificity phosphatases: critical regulators with diverse cellular targets.* The Biochemical journal, 2009. **418**(3): p. 475-89.
158. Foger, N., et al., *Differential regulation of mast cell degranulation versus cytokine secretion by the actin regulatory proteins Coronin1a and Coronin1b.* The Journal of experimental medicine, 2011. **208**(9): p. 1777-87.

159. Humphries, C.L., et al., *Direct regulation of Arp2/3 complex activity and function by the actin binding protein coronin.* The Journal of cell biology, 2002. **159**(6): p. 993-1004.
160. Cai, L., et al., *Coronin 1B coordinates Arp2/3 complex and cofilin activities at the leading edge.* Cell, 2007. **128**(5): p. 915-29.
161. Gandhi, M., et al., *Coronin switches roles in actin disassembly depending on the nucleotide state of actin.* Molecular cell, 2009. **34**(3): p. 364-74.
162. Maravillas-Montero, J.L., et al., *Myosin 1c participates in B cell cytoskeleton rearrangements, is recruited to the immunologic synapse, and contributes to antigen presentation.* J Immunol, 2011. **187**(6): p. 3053-63.
163. Girish, V. and A. Vijayalakshmi, *Affordable image analysis using NIH Image/ImageJ*: Indian J Cancer. 2004 Jan-Mar;41(1):47.
164. Schneider, C.A., W.S. Rasband, and K.W. Eliceiri, *NIH Image to ImageJ: 25 years of image analysis.* Nat Methods, 2012. **9**(7): p. 671-5.
165. Carpenter, A.E., et al., *CellProfiler: image analysis software for identifying and quantifying cell phenotypes.* Genome Biol, 2006. **7**(10): p. 31.
166. Lamprecht, M.R., D.M. Sabatini, and A.E. Carpenter, *CellProfiler: free, versatile software for automated biological image analysis.* Biotechniques, 2007. **42**(1): p. 71-5.
167. Held, C., et al., *Enhancing automated micrograph-based evaluation of LPS-stimulated macrophage spreading.* Cytometry A, 2013. **83**(4): p. 409-18.
168. Kim, H.S., et al., *Redox regulation of MAPK phosphatase 1 controls monocyte migration and macrophage recruitment.* Proc Natl Acad Sci U S A, 2012. **109**(41): p. E2803-12.
169. Williams, L.M. and A.J. Ridley, *Lipopolysaccharide Induces Actin Reorganization and Tyrosine Phosphorylation of Pyk2 and Paxillin in Monocytes and Macrophages.* The Journal of Immunology, 2000. **164**(4): p. 2028-2036.
170. Cai, X., et al., *Glycogen Synthase Kinase 3- and Extracellular Signal-Regulated Kinase-Dependent Phosphorylation of Paxillin Regulates Cytoskeletal Rearrangement.* Molecular and Cellular Biology, 2006. **26**(7): p. 2857-2868.
171. Hazeki, K., et al., *Toll-like receptor-mediated tyrosine phosphorylation of paxillin via MyD88-dependent and -independent pathways.* European Journal of Immunology, 2003. **33**(3): p. 740-747.
172. Bartlett, D.W. and M.E. Davis, *Effect of siRNA nuclease stability on the in vitro and in vivo kinetics of siRNA-mediated gene silencing.* Biotechnology and Bioengineering, 2007. **97**(4): p. 909-921.
173. Liu, S.L., et al., *Insertions within the actin core of actin-related protein 3 (Arp3) modulate branching nucleation by Arp2/3 complex.* The Journal of biological chemistry, 2013. **288**(1): p. 487-97.
174. Cai, L., et al., *Coronin 1B Antagonizes Cortactin and Remodels Arp2/3-Containing Actin Branches in Lamellipodia.* Cell, 2008. **134**(5): p. 828-842.
175. Cai, L., et al., *Phosphorylation of Coronin 1B by Protein Kinase C Regulates Interaction with Arp2/3 and Cell Motility.* Journal of Biological Chemistry, 2005. **280**(36): p. 31913-31923.
176. Loegering, D.J. and M.R. Lennartz, *Protein kinase C and toll-like receptor signaling.* Enzyme Res, 2011. **537821**(10): p. 23.
177. Chhabra, E.S. and H.N. Higgs, *The many faces of actin: matching assembly factors with cellular structures.* Nat Cell Biol, 2007. **9**(10): p. 1110-1121.
178. Krainer, E.C., et al., *The multiplicity of human formins: Expression patterns in cells and tissues.* Cytoskeleton, 2013. **70**(8): p. 424-438.
179. Kress, H., et al., *Filopodia act as phagocytic tentacles and pull with discrete steps and a load-dependent velocity.* Proceedings of the National Academy of Sciences, 2007. **104**(28): p. 11633-11638.
180. Lee, S.H., et al., *Structural Basis for the Actin-Binding Function of Missing-in-Metastasis.* Structure, 2007. **15**(2): p. 145-155.

181. Wang, Y., et al., *Tyrosine Phosphorylation of Missing in Metastasis Protein Is Implicated in Platelet-derived Growth Factor-mediated Cell Shape Changes.* Journal of Biological Chemistry, 2007. **282**(10): p. 7624-7631.
182. Yu, D., et al., *Murine Missing in Metastasis (MIM) Mediates Cell Polarity and Regulates the Motility Response to Growth Factors.* PLoS One, 2011. **6**(6): p. e20845.
183. Wu, Y., et al., *MAPKAPK2-mediated LSP1 phosphorylation and FMLP-induced neutrophil polarization.* Biochemical and Biophysical Research Communications, 2007. **358**(1): p. 170-175.
184. Kahle, N.A., et al., *Bacterial quorum sensing molecule induces chemotaxis of human neutrophils via induction of p38 and leukocyte specific protein 1 (LSP1).* Immunobiology, 2013. **218**(2): p. 145-151.
185. Frittoli, E., et al., *The Signaling Adaptor Eps8 Is an Essential Actin Capping Protein for Dendritic Cell Migration.* Immunity, 2011.
186. Chen, Y.-J., et al., *Eps8 Protein Facilitates Phagocytosis by Increasing TLR4-MyD88 Protein Interaction in Lipopolysaccharide-stimulated Macrophages.* Journal of Biological Chemistry, 2012. **287**(22): p. 18806-18819.
187. Linder, S. and M. Aepfelbacher, *Podosomes: adhesion hot-spots of invasive cells.* Trends in cell biology, 2003. **13**(7): p. 376-385.
188. Jung, G. and J.A. Hammer, 3rd, *The actin binding site in the tail domain of Dictyostelium myosin IC (myoC) resides within the glycine- and proline-rich sequence (tail homology region 2).* FEBS Lett, 1994. **342**(2): p. 197-202.
189. Rump, A., et al., *Myosin-1C associates with microtubules and stabilizes the mitotic spindle during cell division.* Journal of Cell Science, 2011. **124**(15): p. 2521-2528.
190. Cervero, P., et al., *Proteomic analysis of podosome fractions from macrophages reveals similarities to spreading initiation centres.* European Journal of Cell Biology, 2012. **91**(11-12): p. 908-922.
191. Schiller, H.B., et al., *Quantitative proteomics of the integrin adhesome show a myosin II-dependent recruitment of LIM domain proteins.* EMBO reports, 2011. **12**(3): p. 259-266.
192. Ouderkirk, J.L. and M. Krendel, *Myosin 1e is a component of the invadosome core that contributes to regulation of invadosome dynamics.* Experimental Cell Research, 2014(0).
193. Eichelbaum, K., et al., *Selective enrichment of newly synthesized proteins for quantitative secretome analysis.* Nat Biotech, 2012. **30**(10): p. 984-990.
194. Eichelbaum, K. and J. Krijgsveld, *Rapid temporal dynamics of transcription, protein synthesis and secretion during macrophage activation.* Molecular & Cellular Proteomics, 2014.
195. Menegazzi, R., et al., *Chloride ion efflux regulates adherence, spreading, and respiratory burst of neutrophils stimulated by tumor necrosis factor-alpha (TNF) on biologic surfaces.* The Journal of Cell Biology, 1996. **135**(2): p. 511-522.
196. Vogel, D.Y., et al., *Macrophages migrate in an activation-dependent manner to chemokines involved in neuroinflammation.* J Neuroinflammation, 2014. **11**(1): p. 23.
197. Paul, P. and J. Neefjes, *Studying MHC Class II Transport in Dendritic Cells.* Methods Mol Biol, 2013. **960**: p. 489-507.
198. Martin, R., et al., *Total Synthesis of Pentabromo- and Pentachloropseudilin, and Synthetic Analogues—Allosteric Inhibitors of Myosin ATPase.* Angewandte Chemie International Edition, 2009. **48**(43): p. 8042-8046.
199. Chinthalapudi, K., et al., *Mechanism and Specificity of Pentachloropseudilin-mediated Inhibition of Myosin Motor Activity.* Journal of Biological Chemistry, 2011. **286**(34): p. 29700-29708.
200. Hume, D.A., *Macrophages as APC and the Dendritic Cell Myth.* The Journal of Immunology, 2008. **181**(9): p. 5829-5835.
201. Delamarre, L., et al., *Differential Lysosomal Proteolysis in Antigen-Presenting Cells Determines Antigen Fate.* Science, 2005. **307**(5715): p. 1630-1634.

202. Robertson, J.M., P.E. Jensen, and B.D. Evavold, *DO11.10 and OT-II T Cells Recognize a C-Terminal Ovalbumin 323–339 Epitope.* The Journal of Immunology, 2000. **164**(9): p. 4706-4712.

Danksagung

Ich bedanke mich bei Thomas Rudel von der Julius-Maximilians-Universität Würzburg für die Betreuung meiner externen Arbeit im Labor von Roland Lang sowie bei Thomas Dandekar für die Genehmigung meiner externen Dissertation am Institut für klinische Mikrobiologie, Immunologie und Hygiene des Universitätsklinikums Erlangen.

Ich bedanke mich ganz herzlich bei meinem Doktorvater Roland Lang, der im Vorfeld alle Hebel in Bewegung gesetzt hat, um mir die Promotion in seinem Labor zu ermöglichen. Des Weiteren bedanke ich mich für die Vergabe des spannenden Themas und für die ausgezeichnete Unterstützung während der gesamten Zeit. Er hatte stets ein offenes Ohr für jegliche Probleme und stand mir jederzeit mit Rat und Tat zur Seite. Zusätzlich bedanke ich mich besonders für die Möglichkeit eines Forschungsaufenthaltes an der SUNY Upstate Medical University in Syracuse, NY, USA.

Ich danke Christian Bogdan, dass ich meine Doktorarbeit an seinem Institut anfertigen konnte sowie für seine konstruktiven Ratschläge in wissenschaftlichen Diskussionen.

Ich danke allen Kooperationspartnern, die zum Gelingen dieser Forschungsarbeit beigetragen haben. Für die Bereitstellung verschiedener Mausstämme danke ich Jean Pierre David (*p38*-/-), Elisabeth Zinser und Gerhard Krönke (OT-II), David Vöhringer (RAG1 KO) und Mira Krendel (Myo1e-/-).
Ich bedanke mich bei unseren Kooperationspartnern Thomas Wittenberg und Christian Held vom Fraunhofer Institut in Erlangen für die großartige und spannende Zusammenarbeit zur Entwicklung und Etablierung einer Zellannotationssoftware. Des Weiteren bedanke ich mich bei Ralf Palmisano für die professionelle und hervorragende Unterstützung in sämtlichen Angelegenheiten zur Fluoreszenzmikroskopie.

Ich bedanke mich bei Mira Krendel für die Möglichkeit einen Forschungsaufenthaltes in Ihrem Labor und die gute Betreuung. Ganz herzlich bedanke ich mich auch bei Jing Bi, Jess Ouderkirk, Chris Pellenz und vor allem Sharon Chase für die Unterstützung und lockere Atmosphäre im Labor, aber auch den Spaß nach getaner Arbeit. Ganz herzlich bedanke ich mich bei Naoko Michaela Sasaki für die Gastfreundschaft und die gute Bewirtung.

Vielen Dank an Gabriele Weintz, die mit Ihren Vorarbeiten den Grundstein für diese Forschungsarbeit gelegt hat.

Danke an Martin Hermann für die Leitung des GK/SFB643 sowie Andreas Bauer für dessen Engagement in meiner Betreuungskommission.

Ein ganz besonderer Dank geht an die Mitarbeiter der AG Lang, Barbara Bodendorfer, Katrin Jozefowski, Magdalena Niedzielska, Katharina Hofmann, Hanne Schoenen, Christiane Desel, Jenny Ostrop, Alexandra Huber, Madlen Wolf, Marcus Derigs und Thomas Hupfer für Ihre Unterstützung, wissenschaftliche Diskussionen und den Spaß bei der Arbeit. Vielen Dank an die Arbeitsgruppen Mattner und Lührmann für die lustige Stimmung im Schreibraum.

Ganz herzlich bedanke ich mich bei meinen Eltern, meiner Familie und meinen Freunden für deren Unterstützung sowie Ablenkung vom Arbeitsalltag. Von ganzem Herzen danke ich Mandy Triemer die mir zusätzlich in stressigen Zeiten der Rücken freigehalten hat und mir immer liebevoll zur Seite stand.

List of publications

Wenzel J, Ouderkirk JL, Krendel M, Lang R. 2014

The class I myosin Myo1e regulates TLR4-triggered macrophage spreading, chemokine release and antigen presentation via MHC-II.

submitted

Held C, **Wenzel J**, Weismann V, Palmisano R, Lang R, Wittenberg T. 2013

Enhancing automated micrograph-based evaluation of LPS-stimulated macrophage spreading.

Cytometry A. 2013 Apr;83(4):409-18.

Desel C. Werninghaus K, Ritter M, Jozefowski K, **Wenzel J**, Russkamp N, Schleicher U, Christensen D, Wirtz S, Kirschning C, Agger EM, Prazeres da Costa C, Lang R. 2013

The Mincle-activating adjuvant TDB induces MyD88-dependent Th1 and Th17 responses through IL-1R signaling.

PLoS One. 2013;8(1):e53531.

Wenzel J, Held C, Palmisano R, Teufel S, David JP, Wittenberg T, Lang R. 2011

Measurement of TLR-Induced Macrophage Spreading by Automated Image Analysis: Differential Role of Myd88 and MAPK in Early and Late Responses.

Front Physiol. 2011;2:71.

Data base entry (2012)

Fluorescence images in Bioimage Benchmark Collection of Broad Instituts http://www.broadinstitute.org/bbbc/BBBC020/

Eidesstattliche Erklärung

Hiermit erkläre ich an Eides statt,

- die Dissertation eigenständig, d.h. insbesondere selbstständig und ohne Hilfe einer kommerziellen Promotionsberatung angefertigt und keine anderen als die angegebenen Quellen oder Hilfsmittel benutzt wurden,

- dass ich die Gelegenheit zum Promotionsvorhaben nicht kommerziell vermittelt bekommen habe und insbesondere nicht eine Person oder Organisation eingeschaltet habe, die gegen Entgelt Betreuer bzw. Betreuerinnen für die Anfertigung von Dissertation sucht,

- dass ich die Regeln der Universität Würzburg über gute wissenschaftliche Praxis eingehalten habe,

- dass ich mich bis zu diesem Tage noch keiner Doktorprüfung unterzogen habe. Ebenso hat die von mir vorgelegte Dissertation noch keiner anderen Fakultät oder einem ihrer Mitglieder vorgelegen.

Würzburg, den _____

Jens Wenzel